OXFORD BROOKES UNIVERSITY

DEPARTMENT OF BIOLOGICAL AND MEDICAL SCIENCES

Characterisation of the Arabidopsis mid-SUN proteins at the plant NE

Bisa Andov

SUPERVISORY TEAM:

Dr. Katja Graumann

Dr. Verena Kriechbaumer

Professor David Evans

A thesis submitted in partial fulfilment of the requirements for the degree of

Doctor of Philosophy

22nd April 2021

Abstract

The Sad1-Unc84 (SUN) proteins of *Arabidopsis thaliana* (Arabidopsis) consist of two sub-groups - the classical C-terminal (Cter) SUN domain proteins and the mid-SUN domain proteins. The mid-SUN domain proteins have been suggested to have a functional role in Linker of Nucleoskeleton and Cytoskeleton (LINC) complex formation at the nuclear envelope (NE), similarly to Cter-SUN domain proteins. In addition to interacting with LINC complex components, they have been reported to localise to both the NE and endoplasmic reticulum (ER). There is also evidence that they interact with the ER membrane transcription factor *At*maMyb based on results from membrane yeast two hybrid screens. This project aimed to further characterise the Arabidopsis mid-SUN proteins *At*SUN3 and *At*SUN4 and their function at the plant ER and NE.

Putative interactions between SUN domain proteins and *At*maMyb were tested using acceptor photobleaching Förster resonance energy transfer (apFRET). Interactions were detected between *At*SUN3 and *At*maMyb exclusively. Experiments using *At*SUN3 domain deletions indicated that the coiled coil domain of *At*SUN3 is required for homomeric interactions. FRET measured by fluorescence lifetime microscopy (FRET-FLIM) was also used to investigate mid-SUN homo- and heterodimerisation.

ER-enrichment of *At*SUN3 and *At*SUN4 was confirmed by calculating the ratio of fluorescence intensity between ER and nuclear periphery. Additionally, a high-resolution confocal imaging technique used to determine protein localisation at the nuclear periphery was further refined. This was used to show that fluorescent protein fusions of both mid-SUN proteins co-localised with the ER/outer nuclear membrane (ONM) marker mCherry and not the inner nuclear

membrane (INM) membrane marker *At*SUN2. These results indicate that *At*SUN3 and *At*SUN4 localise to the ONM/perinuclear ER and not to the INM.

Altogether, this work indicates that mid-SUNs have functional roles in addition to LINC complex formation based on protein-protein interactions they form due to their sub-cellular localisation.

Acknowledgments

Firstly, I must thank my supervisors Katja, Verena and David for their guidance and kindness throughout my PhD. I would of course like to thank Katja for giving me this opportunity, and for all her support over the years. Without it I would not have undertaken this endeavour, for which I shall always be grateful. I also thank Verena for her expertise and encouragement to pursue new ideas, as well as always finding time for a chat. I must also thank David for always being available for discussions regarding lab work and thesis writing; I particularly appreciated his support whilst Katja and Verena were on maternity leave. On that note, I highly enjoyed having tiny visitors join us in lab meetings from time to time. I am very grateful for all my supervisors' help, especially throughout unprecedented times.

I must thank our collaborators at the Université Clermont Auvergne, namely Christophe Tatout, for sharing data with our lab group that was key to this work. I would additionally like to thank Sarah Mermet for producing the *At*SUN3 domain deletion mutants that were used in this thesis during her lab placement at Brookes. I would also like to thank Charlotte Pain, Stefan Wojcik and Verena for the provision of the FRET-FLIM data used in this thesis, as well as the Central Laser Facility of the Rutherford Appleton Laboratory for permitting this work to be carried out.

For maintaining the greenhouse and its occupants, as well as keeping the lab equipped and in working order, I would like to thank Anna Frej and Alice Wingfield. It was also a pleasure chatting with you both whilst I resided in your corner of the office.

For providing me with a constant supply of laughter and snacks, I thank all members of the Sinclair Annex, past and present. Their intellectual input, supportive coffee trips and love of social bonding made my time at Brookes even more enjoyable. I want to additionally thank the members of the plant cell biology group, past and present, for patiently listening to me talk about my endeavours and

providing useful feedback, especially: Charlotte, Stefan, Tatiana Spatola Rossi, Alistair McGuinness, Joe McKenna, and Frances Tolmie.

I should also say a massive thank you to my friends outside of Brookes who have supported me from near and afar and have been so understanding throughout. I would especially like to thank Hollie and Sharna for sending me care packages and checking in on me, as well as helping me to have fun.

Lastly, I must thank my family for all their support. I would especially like to thank my parents for their continuous encouragement, care, and for always believing in me.

This work was funded by the Nigel Groome Scholarship

Waterperry Gardens, 21st August 2018

Sinclair Annex Christmas Party, 13th December 2018

International Botanical Microscopy Meeting, 19th April 2019

BMS Departmental Research Evening, 2nd May 2019

Contents

List of Presentations

The following oral presentation has been given on this work:

1. **Characterising the Arabidopsis mid-SUN proteins** – *Oxford Brookes University Annual Postgraduate Research Symposium 2020*

The following poster presentations have been given on this work:

1. **Investigating protein-protein interactions between Arabidopsis mid-SUN proteins and the transcription factor maMyb at the plant nuclear envelope** - *Oxford Brookes University Annual Postgraduate Research Symposium 2019, INDEPTH Annual Meeting 2019 and the International Botanical Microscopy Meeting 2019*

2. **Characterisation of the Arabidopsis mid-SUN proteins** - *Oxford Brookes University Graduate College Research Student Exhibition 2020*

3. **Characterising the Arabidopsis mid-SUN proteins** – *SEB Annual Conference 2021*

List of Abbreviations

ABA - Abscisic acid

apFRET - acceptor-photobleaching Förster Resonance Energy Transfer

AU - Airy Unit

Ca2+ - Calcium

CFP - Cyan Fluorescent Protein

CLSM - Confocal Laser Scanning Microscopy

CRWN - CROWDED NUCLEI Proteins

Cter-SUN – C-terminal SUN domain protein

CXN – Calnexin

DM1 - Doesn't Make Infection 1

DDR - DNA Damage Response

DNAPK - DNA-dependent kinase

dNTPs - Deoxyribonucleotide Triphosphates

dy - Desynaptic

EM - Electron Microscopy

EMD - Estimated Medial Distance

E_F - FRET efficiency

ER - Endoplasmic Reticulum

FG - Phenylalanine and Glycine Repeats

FI - Fluorescence Intensity

FLIM - Fluorescence Lifetime Imaging Microscopy

FRET - Förster Resonance Energy Transfer

FRET-FLIM - Förster Resonance Energy Transfer measured by Fluorescence Lifetime Imaging Microscopy

γ-TURC - γ-tubulin ring complex

GaAsp - Gallium Arsenide Phosphide

GCPs - γ-tubulin complex proteins

GFP- Green Fluorescent Protein

INM - Inner Nuclear Membrane

KASH - Klarsicht/Anc1/Syne1

LB - Lysogeny Broth

LBR - Lamin B Receptor

LCA - Lycopersicon Ca^{2+} ATPase

LECA - Last Eukaryotic Common Ancestor

LEM1 - Lamin–Emerin–Man1

LINC (a) - Linker of Nucleoskeleton and Cytoskeleton

LINC (b) - Little Nuclei Proteins

mRFP - monomeric-Red Fluorescent Protein

mRNPs - Messenger Ribonucleoproteins

MT – Microtubule

MTFs - Membrane-bound Transcription Factors

MTOC - Microtubule-Organizing Centre

MY2H - Membrane Yeast Two-Hybrid

NAC - NAM, ATAF1,2 and CUC2 proteins

NE - Nuclear Envelope

NEAPs - Nuclear Envelope Associated Proteins

NEBD - Nuclear Envelope Breakdown

NLI - Nuclear Localisation Indices

NLS - Nuclear Localisation Signal

NM – Nuclear Membrane

NMPC - Nuclear Matrix Constituent Protein

NPC - Nuclear Pore Complex

Nups – Nucleoporins

NTL9 - NAC WITH TRANSMEMBRANE MOTIF1-LIKE9

OD - Optical Density

ONM - Outer Nuclear Membrane

Ost - Osteopotentia

PCR- Polymerase Chain Reaction

PFAP - Proline-Phenylalanine-Alanine-Proline

PNER - Perinuclear ER

PNETs - Plant NE Transmembrane Proteins

PNS – Perinuclear Space

PICC - Pamp-Induced Coiled-Coil

PICL – PICC-Like

Poms – Pore Membrane Proteins

PMT - Photomultiplier Tube

PR1 - PATHOGENESIS-RELATED1

RanGAP - Ran GTPase-activating protein

rER - rough ER

RIP - regulated intramembrane proteolysis

Rpm-1 - Regulator of Presynaptic Morphology 1

ROI - Region of Interest

RTNL - Reticulon-Like Protein

RUP - Regulated Ubiquitin/proteasome-dependent Processing

SERCA - Sarcoplasmic Reticulum/Endoplasmic Reticulum

SEM - Scanning Electron Microscopy

S.E.M - Standard Error of the Mean

sER – Smooth ER

SINE - SUN-interacting nuclear envelope proteins

SNR - Signal-to-Noise Ratio

SOC - Super Optimal broth

SPB - Spindle Pole Body

SUN - Sad1-Unc84

SYNV - Sonchus Yellow Net Virus

TAE - Tris-Acetate-EDTA

TEM – Transmission Electron Microscopy

TF- Transcription Factor

TIK - TIR-KASH protein

TMD - Transmembrane Domain

UPR - Unfolded Protein Response

WGD - Whole Genome Duplication

WIPs - WPP domain– interacting proteins

WITs - WPP domain–interacting tail-anchored proteins

YFP- Yellow Fluorescent Protein

Y2H - Yeast Two-Hybrid

List of Figures

List of Tables

List of Equations

$$NLI = \frac{(NE_1 + NE_2)}{(ER_1 + ER_2)}$$

$$E_F = 100 \times ((I_{pre} - I_{post}) / I_{pre})$$

Chapter One | Introduction

The work described in this thesis was carried out to explore the location and interactions of a less well characterised family of proteins, the Arabidopsis mid-SUN proteins. Previously, these had been proposed to be part of the LINC complex and located at the NE (Murphy et al., 2010; Graumann et al., 2014). This introduction provides an overview of the NE and its constituents, before providing a detailed description of the LINC complex and the proteins studied in this thesis. Specifically, these proteins are *At*SUN3 and *At*SUN4, and their putative binding partner *At*maMyb. In order to carry out this work, a combination of techniques was used based on transient expression *in planta* (as described in Chapters 2&5). Firstly, protein-protein interactions were investigated at the NE; putative interactions between SUN proteins and *At*maMyb were tested. The homo- and hetero-oligomerisation of mid-SUN proteins were also explored. Additionally, domain deletion mutants were designed to explore the role of key domains in previously described protein-protein interactions. The results produced from these protein interaction studies are discussed in Chapter 3. Airyscan confocal microscopy was then developed and used in conjunction with a FI ratio method to study the localisation of the mid SUN proteins. This is discussed further in Chapters 4&5. The implications of the results produced in this thesis and how these contribute to our understanding of mid-SUN functionality is discussed in Chapter 6, concluding with avenues to explore in the future.

1.0 NE structure and function

1.1 The Nuclear Membranes

The NE consists of two lipid bilayers that encircle the nucleus to protect its genetic material, as well as providing a surface for specific molecules to anchor and interact with NE elements (Fig. 1). The two membranes are known as the Outer Nuclear Membrane (ONM), and the Inner Nuclear Membrane (INM; Fig. 1.1). The luminal space between these two membranes, referred to as the perinuclear space (PNS), and the ONM are contiguous with the ER (Fig. 1.1). Both possess membrane-associated proteins that are specific to each bilayer which interact to carry out various cellular and nuclear functions (Fig. 1.1; Crisp et al., 2006; Graumann et al., 2010; Morimoto et al., 2012; Wong et al., 2014; Thakar et al., 2017; Burke, 2018; Gumber et al., 2019). On the inside the INM lies a lattice-like structure called the nuclear lamina, which acts as a scaffolding network that helps to support the nucleus.

Together these components form a dynamic system required to mediate interactions between the nucleoplasm and cytoplasm by providing anchoring sites for chromatin or cytoskeletal components, such as actin (Terry et al., 2007; Schneider et al., 2011; Brohnstein et al., 2015). Through such activities, the NE mediates nuclear positioning and chromosome organisation within the nucleus, helping to regulate gene expression (Gunderson and Worman, 2013; Poulet et al., 2017).

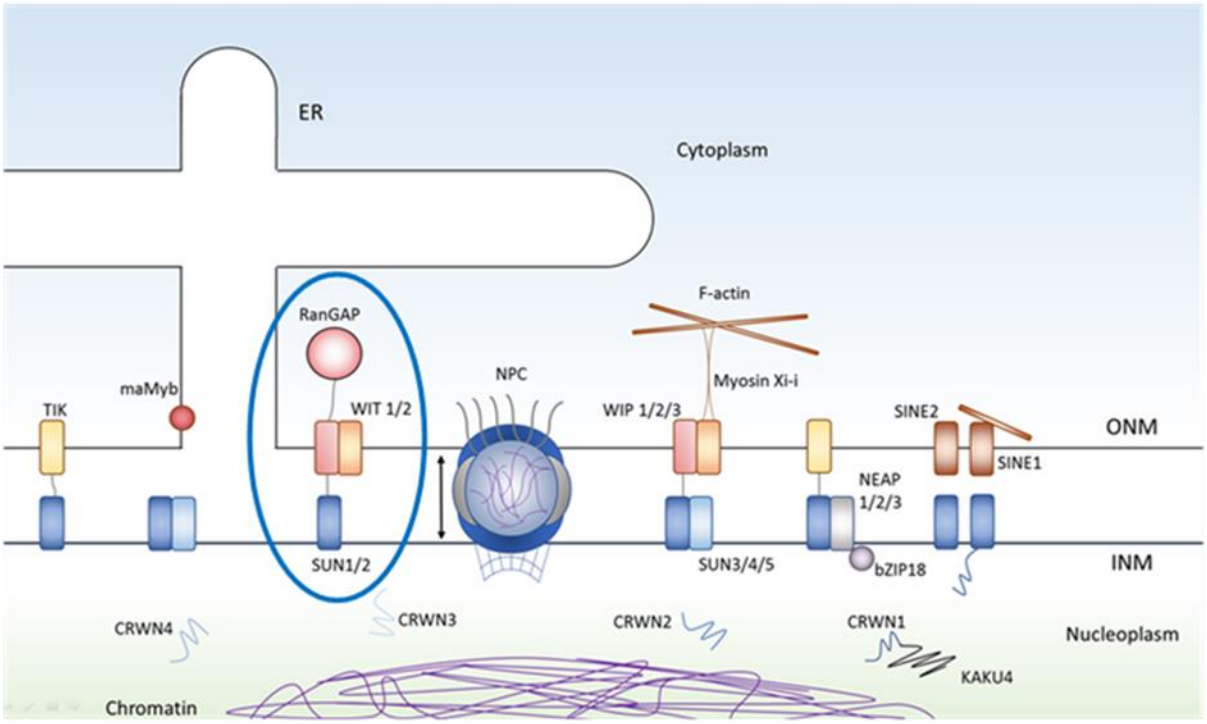

Figure 1.1 The known components of the plant nuclear envelope (NE), and how these contribute to nuclear bridging complexes. The NE is comprised of 2 lipid membranes: the outer nuclear membrane (ONM), which runs contiguously with the endoplasmic reticulum (ER), and the inner nuclear membrane (INM). Nuclear Pore Complexes (NPCs) are spanned across these two membranes to facilitate molecular transport across the NE (arrow indicates bi-directional movement). Membrane-associated proteins of both membranes interact with one another to carry out a variety of nuclear and cellular processes, which require Linker of Nucleoskeleton and Cytoskeleton (LINC) complexes to take place (outlined in a blue circle). These require ONM-localised KASH proteins and INM-localised SUN proteins to interact within the periplasm, forming bridging complexes that incorporate nucleo- and cytoskeletal components. KASH analogs that have been identified in plants are SINE, *At*TIK, *At*WIP and *At*WIPs. Potential plant lamin proteins that have been identified are the CRWN protein family and KAKU4. Plants have been found to have two highly conserved sub-groups of SUN protein; the Cter-SUNs which have a c-terminally located SUN domain, and the mid-SUNs which have an internal SUN domain. Cter-SUNs have been reported to interact with *At*WIP, which in turn interacts with *At*WIT and facilitates the anchorage of actin to the NE. Similar complexes are required to anchor *At*RanGAP to the NE. C-ter SUNs also interact with SINE proteins and CRWN1, as well as nuclear-envelope associated proteins (NEAPs), which interact with the putative transcription factor *At*bZIP18. Mid-SUNs have also been found to interact with Cter-SUNs, plant KASH proteins and the ER-localised transcription factor *At*maMyb in membrane yeast-two hybrid screens, but these latter interactions have yet to be confirmed *in planta* (putative interactions are highlighted with question marks). The multi-protein complexes shown above are based on reported interactions; what these putative complexes do demonstrate is the expansive and sophisticated layout of the plant NE.

1.1.2 Nuclear Pore Complexes

The NE also contains nuclear pore complexes (NPCs), which are large macromolecular complexes that span across the PNS to connect both membranes (Fig. 1.1). NPCs are made up of approximately

30 different, smaller proteins known as nucleoporins (Nups) throughout the eukaryotes, which vary in their respective molecular masses (Rout, 2000; Cronshaw, 2002; Schwartz, 2016). There are three different groups of Nups; firstly, there are the pore membrane proteins (Poms), that anchor NPCs to the NE due to possessing a transmembrane domain (TMD). Secondly there are core scaffold Nups which serve as structural components that can also interact with the NE and Poms. The core scaffold that they contribute to is comprised of three outer rings between which are sandwiched two inner rings, made up of proteins that possess only α-solenoids and β-propellers, or an N-terminal β-propeller preceding an α-solenoid (Devos et al., 2006). This scaffold is sandwiched between cytoplasmic filaments and the nuclear basket, a structure that extends into the nucleoplasm. This latter component has a variety of functions including the anchoring of chromatin to the NPC whilst also organising other nucleoplasmic components around the NPC entrance to ensure transport of messenger ribonucleoproteins (mRNPs) into the cytoplasm (Casolari et al., 2004; Dilworth et al., 2005; Kylberg et al., 2010; Strambio-De-Castillia et al., 2010). Lastly there are the FG-Nups which are so named for being enriched in phenylalanine and glycine (FG) repeats, which are required for selectively recruiting proteins to NPCs for transport. These are anchored by the core scaffold, and it has been observed that there is an asymmetric distribution of FG-Nups so that they are biased to be either nucleo- or cytoplasmic facing (Zeitler et al., 2004). As a result of this complex structure, the NPC fulfils multiple requirements. NPCs have been shown to be anchored by the pore membrane, specifically through pore membrane proteins interacting with NPC scaffold proteins (Mitchell et al., 2010). Additionally, they have also been indicated to be required for NPC assembly (Funakoshi et al., 2007; Mitchell et al., 2010).

NPC structure has generally been found to be very highly conserved throughout the eukaryotes, with many lineages sharing similar fold structures, amino acid composition, molecular mass and even Nups (DeGrasse et al., 2009). This has led to a proposal that NPCs from different species shares such similarity having evolved from the NPC present in the Last Eukaryotic Common Ancestor (LECA), from which species-specific NPC structures evolved (DeGrasse et al., 2009). It has been observed that the structure of plant NPCs is more similar to their vertebrate counterparts than yeast, but with

a number of different components (Tamura et al., 2010); some Nups are present in plants that are not in vertebrates, which may relate to a lineage-specific function.

NPCs serve as the main transport hubs that allow for the bi-directional exchange of molecules between the nucleus and cytoplasm (Hurt and Beck, 2015; Knockenhauer and Schwartz, 2016). Molecules smaller than 40 kDa, such as ions or proteins, can freely diffuse through NPCs whereas larger molecules require nuclear localisation signals/nuclear export sequences and interactions with transport proteins which themselves interact with FG-Nups across the NPC barrier (Obado et al., 2016). One such example is RanGTP/RanGDP for which a gradient exists at the NPC barrier to provide directionality, with RanGTP being more prominent in the nucleoplasm and RanGDP being more prominent in the cytoplasm (Kalab et al., 2002).

1.1.3. The Plant Nuclear Lamina

In animals, the nuclear lamina is a filamentous protein framework that sits beneath the INM (Aebi et al., 1986). These are made up of a family of type V intermediate filament proteins that are collectively known as lamins (Burke and Stewart, 2013). Numerous integral INM proteins serve as anchors that aid in the organisation of lamina proteins and mediate their attachment to the NE (Gerace and Tapia, 2018). These interactions between the INM and nuclear lamina proteins, as well as chromatin, help to form a nuclear lamina network that is necessary in providing the nucleus with structural integrity (Solovei et al., 2013; Gruenbaum and Medalia, 2015). In addition to this, animal lamina proteins have also been reported to regulate gene expression (Huber et al., 2009; Gomez-Cavazos and Hetzer, 2012), typically (but not always) resulting transcriptional repression (Kumaran et al., 2008; Reddy et al., 2008; Akhtar et al., 2013; Brunet et al., 2019).

It was previously thought that plants did not have nuclear lamina proteins as there are no sequence homologs of lamins in the plant genome (Fiserova et al., 2009; Ciska and Moreno Diaz de la Espina, 2014). However, a filamentous protein structure associated with the INM was observed in tobacco BY-2 cells and subsequently proposed to be a lamina consisting plant lamin-like proteins (Fiserova

et al., 2009). Currently, the primary protein candidates for plant lamin-like proteins are members of the nuclear matrix constituent protein family (NMCPs; Ciska and Moreno Diaz de la Espina, 2014). These proteins share characteristics with animal lamins, including the long, centrally-located coiled-coil domain (CCD).

There are four NMPCs known as CROWDED NUCLEI (CRWN) in Arabidopsis (Wang et al., 2013); these were previously known as Little Nuclei (LINC) proteins but were renamed to avoid confusion with LINC complexes (Dittmer et al., 2007; Sakamoto and Takagi, 2013; Wang et al., 2013). CRWN1 and CRWN4 have been found to be localised to the nuclear periphery whilst CRWN2 was localised in the nucleoplasm, and CRWN3 was observed in both regions (Fig. 1.1; Dittmer et al., 2007; Sakamoto and Takagi, 2013). In animals, lamins that are in some way disrupted result in mis-shapen nuclei; CRWN1 and CRWN4 mutants display near-spherical nuclei that are decreased in size but this is not observed in CRWN2 and CRWN3 mutants (Sakamoto and Takagi, 2013). This provides evidence that CRWN proteins have lamina like functions. Additionally, CRWN1 has been found to interact with the nucleoplasmic domains of *At*SUN1 and *At*SUN2 in apFRET experiments (Fig. 1.1; Graumann, 2014). CRWN1 was found to become less mobile when these interactions took place, suggesting that it plays a functional role when recruited to the NE (Graumann, 2014). Additionally, CRWN1 has been shown to both be required for chromatin positioning at the nuclear periphery, and to interact directly with chromatin domains at this site (Hu et al., 2019). Together, these results indicate that at least some CRWN proteins are a part of multiprotein complexes at the NE, and that they are functionally equivalent to animal lamina proteins. Another candidate of the plant lamina family is KAKU4, a plant-specific protein that was identified in Arabidopsis (Fig. 1.1; Goto et al., 2014). Similarly to CRWN1 mutants, KAKU4 mutants also produce small, spherical nuclei (Goto et al., 2014). KAKU has a predicted nuclear localisation signal (NLS) and though it does not possess a TM domain, over-expression of KAKU4 resulted in extra membrane growth at the NE. This overgrowth was exaggerated further when co-expressed with CRWN1 (Goto et al., 2014). Overall, both CRWNs and KAKU4 provide evidence that plants have developed proteins to regulate nuclear shape and size in the absence of lamin homologs. Another component of the plant nucleoskeleton are the Nuclear Envelope Associated Proteins (*At*NEAPs), which are comprised of three *At*NEAP proteins (*At*NEAPs

1-3) and a pseudogene, *At*NEAP4 (Pawar et al., 2016). *At*NEAPs are composed of a nuclear localisation signal (NLS), coiled coil domains (CCDs), and a predicted C-terminal TMD (Pawar et al., 2016). Their over-expression has been found to result in the relocation of CRWN1 to nucleoplasm; they have also been found to interact with plant SUN domain proteins *At*SUN1 and *At*SUN2, indicating that they contribute to the formation of bridging complexes at the NE (Pawar et al., 2016).

Plant lamina-like proteins have also been observed to regulate gene expression, similarly to the observations made of metazoan lamina proteins. For example *Os*NMCP1, a NMCP protein of *Oryza sativa* (*O. sativa)*, was reported to regulate drought resistance and root growth by interacting with a subunit of a chromatin remodelling complex, *Os*SWI3C (Yang et al., 2020). It was proposed that this interaction released *Os*SWI3C from the protein complex it associated with to alter chromatin accessibility in the genes controlling drought resistance and root growth (Yang et al., 2020). Additionally, CRWN1 was shown to interact with NAC WITH TRANSMEMBRANE MOTIF1-LIKE9 (NTL9), a NAC (NAM, ATAF1,2 and CUC2) TF with a role in plant immunity. This interaction was found to facilitate binding of the latter to the promoter of PATHOGENESIS-RELATED1 (PR1), resulting in its inhibition (Guo et al., 2017). Not only this but *At*NEAP1 was shown to interact with bZIP18 (Pawar et al., 2016), a TF that has recently been shown re-localise to the nucleus to regulate gene expression when subjected to heat stress (Wiese et al., 2021)

1.1.4 Further Insight on NE Protein Composition

It appears that the structure and function of the NE is conserved throughout Eukaryota, but that overall protein composition is not; this is evident from reports on the plant lamin-like proteins discussed above. Another example is the absence of the lamin B receptor (LBR) and lamin–emerin–man1 (LEM1) domain proteins, which are both key components of the metazoan NE (Brandizzi et al., 2004; Gruenbaum et al., 2005; Worman et al., 1988). LBR is required to form INM-chromatin interactions during interphase and mitosis and has been reported to bind to Lamin B and chromatin

via its N-terminus (Soullam and Worman, 1993; Ye and Worman, 1996; Ye et al., 1997). As well as this, LEM1 domain proteins are required for the NE-tethering of chromatin (Gruenbaum et al., 2005).

Some NE components do appear to be conserved, however. A recent study of the Arabidopsis nuclear membrane proteome identified over 200 potential plant NE transmembrane (PNET) proteins, highlighting the complexity of the plant NE (Tang et al., 2020). One candidate of interest was PNET1, a plant nucleoporin protein that was found to be a homologue of human TMEM209, which itself was reported to be an ortholog of POM34 in *S.cerevisiae* (Field et al., 2014; Tang et al., 2020).

It remains unclear as to why the plant NE proteome is so distinct in comparison to that of metazoans. It could be suggested that due to their sessile nature, the requirements of plant species resulted in a functional divergence of NE components early in their evolution. It has been shown that some SUN proteins were present in unicellular algae, whilst other NE components such as CRWN proteins were present in lycophytes before the ancient Zeta whole genome duplication event (WGD; Poulet et al., 2016). Further diversification of NE components followed in later WGD events and partial duplication events, coinciding with the origin of higher plant taxa (Poulet et al., 2016). It is therefore possible that these WGD events promoted the development of plant-specific features, such as flowering organs, that required the interactions of pre-existing and novel plant NE components to survive.

1.1.5 Functions of the NE

The NE is required to carry out a diverse set of functions and even though it is less well characterised in comparison to metazoans, the plant NE is by no means an exception. These include, but are not limited to, interacting with nucleo- and cytoskeletal components, cell signalling and responses to abiotic and biotic stimuli. Other functions of the NE, such as the targeting of proteins to the NE and its role in mitosis and meiosis, are discussed later in this chapter.

The ONM has been reported to act as a microtubule-organizing centre (MTOC) in plants (Shimumura et al., 2004). Outside of this kingdom however, γ-tubulin and five γ-tubulin complex proteins (GCPs) form the γ-tubulin ring complex (γ-TuRC), which in turn forms the central component of MTOCs and the spindle pole body (SPB; Murphy et al., 2001; Fava et al., 1999). Both structures are tethered to the ONM via KASH-mediated interactions (Friederichs et al., 2012; Elhanany-Tamir et al., 2012). Two homologs of yeast and Drosophila GCP2 and GCP3, *At*GCP2 and *At*GCP3, were identified in Arabidopsis and reported to be part of a soluble γ-tubulin complex at the NE (Seltzer et al., 2007). So far plant KASH proteins have not been demonstrated to interact with these components, but KASH-mediated tethering of cytoskeletal elements is being actively investigated and may provide further insight regarding this in the future.

On the other hand, interactions between INM proteins and nucleoskeletal components such as lamins are required for the regulation of nuclear shape and size in metazoans (Gueth-Hallonet et al. 1998; Coffinier et al., 2011; Jevtić et al., 2015; Kim et al., 2017). Plant lamin-like proteins have also been shown to potentially be involved in this; it was reported that CRWN protein knock-downs resulted in more spherical nuclei, as opposed to the typical elongated shape of plant nuclei (Dittmer et al., 2007).

As well as this, the plant NE has also been linked to the Ca^{2+} signalling pathway. The first NE component to be identified in this pathway was a Ca^{2+} pumping ATPase in tomato that was a plant homolog of the mammalian sarcoplasmic reticulum/endoplasmic reticulum (SERCA) pump, Lycopersicon Ca^{2+} ATPase (LCA; Wimmers et al., 1992; Ferrol and Bennett, 1996; Downie et al., 1998). Subsequent work has shown that NE components linked to the plant Ca^{2+} signalling pathway are involved in establishing mycorrhizal infection and nodulation (Peiter et al., 2007; Riely et al., 2007; Chabaud et al., 2011). Rhizobial-legume symbiosis is first established through the production of Nod factors from rhizobial bacteria in response to flavonoids excreted by legume roots (Redmond et al., 1986; Relić et al., 1994), prompting the induction of nucleus-associated Ca^{2+} spikes (Ehrhardt et al., 1996; Peiter et al., 2007). These signals subsequently activate genes involved with nodulation (Peiter et al., 2007; Riely et al., 2007; Chabaud et al., 2011). One such protein linked to this process is

Doesn't make infection 1 (DMI1), a cation channel of the legume *Medicago truncatula (M. truncatula*) which facilitates nodulation (Riely et al., 2007). *Mt*DMI1 has been reported to be required for generating and modulating Ca^{2+} spikes (Riely et al., 2007; Chabaud et al., 2011), which ultimately facilitate bacterial infection, although it is unclear whether it serves as the perinuclear ion channel responsible for Ca^{2+} spiking (Matzke et al., 2009). These results do indicate however that the NE plays a role in cell signalling as well as responses to environmental stimuli.

Due to associating with cytoskeletal components, nuclei are able migrate in response to environmental stimuli. It was demonstrated that Arabidopsis nuclei move in response to blue light; nuclei exposed to blue light were positioned along the anticlinal walls of cells, whilst nuclei kept in dark conditions were centrally located at the bottom of cells (Iwabuchi et al., 2007). It was further shown that light-mediated nuclear positioning is mediated by the blue light receptor phototropin2 via re-organisation of the actin cytoskeleton (Iwabuchi et al., 2010). It has been proposed that light-mediated nuclear positioning occurs to prevent DNA damage caused by UV exposure.

Additionally, viruses can exploit the nuclei of infected plant cells to facilitate the replication of mature virions, as observed in other Eukaryotic organisms (Dennison et al., 2007; Goodin et al., 2007). For example, the Sonchus yellow net virus (SYNV) is an RNA virus which requires a nuclear stage in its replication cycle. It is comprised of a ribonucleoprotein core encompassed by a membrane layer containing a viral glycoprotein that has been proposed to be attached to the core via a viral matrix protein. In cells infected with SYNV, NPCs facilitate the transport of the virus' ribonucleoprotein core into the nucleus (Jackson et al., 2005). This has been found to result in larger nuclei, and the development of intranuclear protrusions which were reported to be extensions of the NE; it is thought these protrusions are linked to the maturation of virions (Jackson et al., 2005; Goodin et al. 2007). Formation of the viral core and its replication has been reported to occur in the nucleus; the matrix protein is also located in the NE whilst the glycoprotein associates the nuclear side of the NE (Goodin et al. 2007). It has been suggested that the intranuclear protrusions allow virions to bud through the INM to acquire their membrane coats, where they can then begin the process of infecting new cells (Goodin et al. 2007).

1.2 ER structure and Function: A Brief Overview

The ER is the largest membrane-bound organelle in eukaryotic cells and is involved in a variety of cellular processes. As well as synthesising and folding one third of the cellular proteome, the ER is responsible for protein modification, phospholipid synthesis, and calcium (Ca2+) storage and release (Klusener et al., 1995; Wyatt et al., 2002; Burdakov et al., 2005; Anelli and Sitia, 2008; Fu et al., 2011; Henderson et al., 2014; Nagashima et al., 2018). It consists of interconnecting structural sub-domains, the largest of which flattens around the nucleus to form the NE. The part of the ER network that is closely situated to this organelle is known as perinuclear ER (PNER).

Additional to this is the peripheral ER, which is composed of either cisternae or tubules. Cisternae associate with ribosomes to synthesise and fold membrane and secretory proteins; this part of the ER network is termed rough ER (rER; Rolls et al., 2002; Shibata et al., 2006). ER tubules extend throughout the cytosol and are less associated with ribosomes, resulting in this part of the ER network being termed smooth ER (sER; Shibata et al., 2006). Together, cisternae and tubules form a polygonal network that connects the ONM to the ER via a shared luminal domain, making the two compartments contiguous with one another (Baumann and Walz, 2001; Voeltz et al., 2002).

1.2.1 The Relationship Between the NE and ER

In comparison to other organelles, the relationship between the ER and the NE is not as well characterised. As aforementioned, the lumen of the ER is contiguous with the PNS of the NE due to there being no physical barrier between them, therefore allowing free transport between the two (Voeltz et al., 2002). Despite their close proximity, the proteomes of the PNER and ONM are not identical; for example, KASH domain proteins exclusively localise to the ONM despite it being contiguous with the ER membrane (Roux et al., 2009; Zhang et al., 2009; Yu et al., 2011; Horn et al., 2013). In plants, it was observed that the distance between these two membranes ranged from 2-30nm, an even smaller range than that measured between the two nuclear membranes (Staehelin,

1997). It has been proposed that these tight spaces at ER-NE junctions reduce protein movement between the two organelles (Bahmanyar and Schlieker, 2020). It was further speculated that this may be regulated by a particular protein, although no candidates have been identified at this intersection in non-dividing cells. The protein composition of ER-NE junctions remains undefined, but is a potential source of further information regarding protein transport and regulation, in addition to any further roles that this sub-cellular region is involved in.

In metazoans, it has been noted that membrane synthesis and ER-NE connections potentially play a role in NE assembly during cell division (Anderson and Hetzer, 2007; Anderson and Hetzer, 2008; Golden et al., 2009). For example, there is evidence to suggest that ER network shaping proteins are required for assembly of the nuclear membranes, and that their facilitation of tubule to sheet transition is a rate-limiting factor in nuclear assembly (Anderson and Hetzer, 2008). Also, it has recently been shown that the PNER regulates nuclear growth and size during early development in *Paracentrotus lividus*, a sea urchin (Mukherjee et al., 2020). It was suggested that the PNER, facilitated by dynein, acts as a limited membrane pool in order to regulate this (Mukherjee et al., 2020).

Although there is still a significant amount of work required for further understanding, these findings do infer that the relationship between these two organelles is a complex one worth investigating.

1.3. LINC Complexes

1.3.1 LINC Complexes in Opisthokonts

In Eukaryotes, the INM and ONM are connected by protein-bridging complexes comprised of two sets of interacting proteins; the ONM-localised KASH proteins and the INM-localised SUN domain proteins (Fig. 1.1; Hagan and Yanagida, 1995; Starr and Han, 2002; Zhou et al., 2012; Zhou and Meier, 2013). SUN domain proteins interact with nucleoskeletal components, such as chromatin and

lamina proteins (Fig. 1.1), whilst KASH domain proteins interact with cytoskeletal components such as motor proteins (Fig. 1.1). These SUN-KASH bridging complexes are referred to as LINC complexes (Crisp et al., 2006), and are mediated through the interaction of the SUN and KASH domains in the nuclear periplasm (Stewart-Hutchinson et al., 2008; Sosa et al., 2012). These interactions are essential for nuclear processes to be carried out such as chromosome decondensation (Chi et al., 2007), nuclear positioning and anchorage (Gundersen and Worman, 2013; Razafsky et al., 2014).

Crystal structures of human SUN2 and KASH domain proteins provided further information as to how LINC complexes are formed (Sosa et al., 2012; Zhou et al., 2012). It was found that three SUN domains proteins are required to form a homotrimer (Zhou et al., 2012). This trimeric SUN structure proceeds to bind to the C-terminal 29 residues of three KASH proteins to form a hexamer (Sosa et al., 2012; Zhou et al., 2012). Further testing using *in vitro* pull-down assays revealed that in HeLa cells, a disulfide bond is formed between SUN and KASH proteins (Sosa et al., 2012). It was further demonstrated that this disulfide bond is required to stabilise the SUN-KASH complex for maximal force transduction across the NE (Cain et al., 2018). According to the crystal structure, this disulfide bond is formed between a cysteine at −23 of the KASH peptide and a conserved cysteine (C563) in SUN2 (Sosa et al., 2012). Modifications of the KASH peptide, either by truncation, augmentation, or mutation of other certain conserved residues, resulted in the loss of the SUN-KASH interaction *in vitro* (Sosa et al., 2012). This was also demonstrated in *Caenorhabditis elegans* (*C. elegans*) embryonic hypodermal development, where the addition of a single alanine was found to disrupt nuclear migration (Cain et al., 2018). This indicates that conserved residues are required for LINC complex formation.

LINC complexes have been reported throughout Eukaryota. For example, LINC complexes involved in nuclear positioning and migration have been observed in *Drosophila melanogaster* (Drosophila), *C. elegans*, and mammals. The Drosophila SUN protein Klaroid is required for localising the KASH proteins Msp-300 and Klarischt (Kracklauer et al., 2007; Technau and Roth, 2008). Klaroid was shown to require these KASH proteins for nuclear migration during eye disc and muscle cell migration (Kracklauer et al., 2007). The *C. elegans* SUN protein UNC-84 is likewise required to

localise the worm KASH proteins Anc-1 and Unc-83 to the ONM (Starr et al., 2001; Starr and Hann, 2002). Via its N-terminal actin binding domain, Anc-1 has subsequently been shown to tether nuclei to the actin cytoskeleton in hypodermal cells (Starr and Hann, 2002). On the other hand Unc-83 is involved in nuclear migration and associates with kinesin and dynein, with the former observed to have a more predominant role (Meyerzon et al., 2009; Fridolfsson et al., 2010). Furthermore, LINC complexes in yeast have conserved roles, including the recruitment of the SPB to the NE. For instance, the *Saccharomyces cerevisiae* (*S. cerevisiae*) SUN protein Mps3 interacts with the KASH protein Mps2, which is linked with the SPB, subsequently leading to its embedment within the NE (Conrad et al., 2008; Koszul et al., 2008; Friederichs et al., 2012).

1.3.2. LINC Complexes in Plants

Plant SUN protein homologues have been shown to be highly conserved (Graumann et al., 2010; Murphy et al., 2010), with INM-localised SUN1 and SUN2 demonstrated to interact with ONM-localised plant KASH domain proteins to form LINC complexes. It is interesting to note that whilst plant KASH domain proteins are structurally preserved, they show no sequence conservation. Plant LINC complexes have been found to be required for numerous functions, including the targeting of RanGAP to the NE, maintaining nuclear shape, as well as regulating nuclear movement and anchoring (Oda and Fakuda, 2011; Zhou et al., 2012; Tamura et al., 2013; Zhou et al., 2015). They have also been observed to play a role in mitosis and meiosis (Graumann and Evans, 2011; Oda and Fakuda, 2011; Murphy et al., 2014; Varas et al., 2015).

Bioinformatic analysis of 20 representative plant species indicates that only SUN proteins were present in unicellular organisms and that other NE components such as plant lamin-like proteins and KASH proteins began to arise with the land plants (Poulet et al., 2016; Ciska et al., 2019). This has led to the suggestion that whilst SUN proteins preceded multicellularity, different KASH proteins arose in response to the need to survive in increasingly diverse environments. This suggests LINC complexes have evolved in parallel with increasing complexity, not just in plants but throughout

eukaryotes; this would also provide a reason why similar NE components involved in LINC complexes carry out a variety of different functions.

1.4 KASH Domain Proteins and their Role at the NE

1.4.1 KASH Proteins in Opisthokonts

KASH domain proteins are large, tail-anchored proteins that extend into the cytoplasm, whilst a C-terminal peptide of ~10-30 residues extends into the PNS. The KASH domain itself is characterised by a TMD as well as these exposed luminal residues (Starr and Han, 2002). KASH peptides are highly conserved throughout opisthokonts; aromatic residues are located at set positions throughout the KASH domain, as well as prolines close to the C-terminus (except for yeast; Sosa et al., 2012; Kim et al., 2015). However, the transluminal domains of KASH proteins differ in length. Shorter KASH proteins do not possess a conserved membrane proximal domain, which is hypothesised to possess the cysteine residue at -23 that is required to form the disulfide bond with SUN proteins (Sosa et al., 2012; Jahed et al., 2015; Cain et al., 2018). It has been hypothesised that when short KASH proteins interact with SUN proteins, the mechanical force the resulting complex can withstand is reduced due to lacking this membrane-proximal domain (Jahed et al., 2019). It also been shown that there is an EEDY motif that is conserved in the membrane-proximal domains of long KASH proteins, such as ANC1 in *C.elegans*, that can interact with the lipid membrane (Jahed et al., 2019). Further work on this demonstrated that the membrane proximal domains of long KASH proteins mediate nuclear anchorage. By replacing the long KASH domain of ANC1 with the short KASH domain of UNC-83 in *C.elegans*, only partial anchorage of nuclei was observed (Jahed et al., 2019). These results imply that KASH proteins of different lengths are required for different LINC-complex related functions.

As previously mentioned, the cytoplasmic domains of KASH proteins are required to bind to cytoskeletal components. For example, there are several different KASH proteins recorded in vertebrates, including nuclear envelope spectrin-repeat proteins (Nesprins) 1-4, which possess spectrin repeats located in the cytoplasmic domain (Apel et al., 2000; Zhang et al., 2001). Various

isoforms of Nesprins 1 and 2 have been reported; the N-terminal actin-binding domain of these proteins have been shown to interact with actin, whilst other, smaller isoforms interact with microtubule motors (Zhen et al., 2002; Padmakumar et al., 2004; Zhang et al., 2009; Yu et al., 2011). Additionally, Nesprins 3 and 4 have been observed to interact with plectin and kinesin-1, respectively (Wilhelmsen et al., 2005; Roux et al., 2009; Horn et al., 2013).

The LINC complex has also been shown to have a signalling function; for instance, it was recently observed in *C. elegans* that Anc-1 can interact with Regulator of Presynaptic Morphology 1 (Rpm-1), a signalling protein that plays a variety of roles in neuronal development. This specific interaction was shown to positively regulate a β-catenin protein isoform, Bar-1, a Wnt signaling component involved in axon termination and synapse formation (Tulgren et al., 2014). Such a finding shows that LINC complexes are involved in regulating signalling pathways and gene expression, presenting an opportunity to determine novel functions for these bridging complexes.

1.4.2 Plant KASH Proteins

As well as identifying *At*SUN1 and *At*SUN2 as plant-SUN homologs (Graumann et al., 2010; Oda and Fukuda, 2011), further work has shown that there are also plant analogues of Opisthokont KASH proteins. A group of three plant-specific proteins in Arabidopsis named WPP domain– interacting proteins (*At*WIPs) were identified in the ONM (Fig. 1.1; Xu et al., 2007). These are nuclear-pore associated proteins that are required to interact with the NE-associated Arabidopsis Ran GTPase-activating protein (*At*RanGAP; Fig. 1.1), which is required for RanGTPase to carry out multiple cellular processes, including spindle assembly and NE reformation during cell division (Zhou et al., 2012). In animal KASH domain proteins, the PNS tail terminates in a PPPX motif whereas in plants, *At*WIPs terminate with a highly conserved X-VPT motif (Fig. 1.1; Xu et al., 2007). Similarly to mammalian KASH-SUN interactions, it was observed that the PNS tail was required for interaction with *At*SUNs 1 & 2 (Fig. 1.1; Zhou et al., 2012). These interactions were additionally found to require the SUN domains of the *At*SUN proteins. Moreover, similarly to Opisthokonts, *At*SUNs are required to

anchor *At*WIPs at the NE (Zhou et al., 2012). These findings provide evidence that SUN-KASH bridging complexes do take place at the plant NE. As well as *At*WIPs, plant LINC complexes have been found to possess KASH components.

Another example is that of the WPP domain–interacting tail-anchored proteins (*At*WITs). These are a group of nuclear pore-associated coiled-coil proteins (*At*WIT1 and *At*WIT2) that are structurally similar to *At*WIPs. They have been observed to interact with *At*WIPs, as well as with a plant-specific myosin, Myosin XI-I, which binds actin filaments to the NE (Fig. 1.1; Tamura et al., 2013). These NE-actin links are required for nuclear movement along the actin cytoskeleton and maintaining nuclear morphology, potentially in response to environmental stimuli.

Another identified plant KASH protein is TIR-KASH protein (*At*TIK) which is structured similarly to mammalian nesprins, in that it shares homologous amino acid sequences between its C-terminal transmembrane domain and characteristic PPPS motif (Graumann et al., 2014). This NE-associated protein has been demonstrated to interact with *At*SUNs, for which its KASH domain is essential (Fig. 1.1).

An additional subset of plant KASH proteins are the SUN-interacting nuclear envelope proteins (SINE), of which there are five that are localised to the NE (Fig. 1.1; Zhou et al., 2014). Of these five, only SINE1 & SINE2 are conserved across land plants, whilst SINE3 is only found in dicots and SINE4 and SINE5 are found in specific families (Zhou et al., 2014). This indicates that some plant KASH proteins may be highly conserved due to fulfilling a general function, whilst other KASH proteins are found in certain species to potentially carry out a specific function. All five SINE proteins have been found to interact with *At*SUN1 & 2 (Fig. 1.1), for which it was determined that the SUN domain of the SUN protein and the C-terminal 4 aa motif ((DTVAMPLIFY)(VAPIL)PT) of each SINE protein was required (Zhou et al., 2014). This C-terminal motif varies greatly even within protein groups, such as the *At*WIPs, accounting for why they had previously been so difficult to identify. Additionally, SINE1 has been found to be essential for F-actin dependent nuclear anchoring in guard cells, whilst SINE2 has been shown to be involved in an immune response against an oomycete pathogen (Fig. 1.2; Zhou et al., 2014). SINE1 and SINE2 have also recently been shown to be required for maintaining

microtubule (MT) organisation in open guard cells (Biel et al., 2020). Additionally, they were shown to mediate MT re-organisation in order to co-ordinate Abscisic acid (ABA)-induced stomatal closure (Biel et al., 2020).

1.5. SUN Domain Proteins

Originally named for Sad1p in *Schizosaccharomyces pombe* (*S. pombe*) and Unc-84 in *C. elegans* (Malone et al., 1999), SUN domain proteins are classified into two sub-groups. The first are Cter-SUN proteins, which are type II transmembrane proteins named for the highly-conserved SUN domain that is located at their C-terminus (Hodzic et al., 2004; Crisp et al., 2006; Haque et al., 2006). The second are mid-SUN proteins, which are type III transmembrane proteins distinguished by their internally-located SUN domain (Fig. 1.2; Murphy et al., 2010; Sohaskey et al., 2010; Friederichs et al., 2012; Graumann et al., 2014; Jaiswal et al., 2014; Vasnier et al., 2014).

1.5.1 Overview of the Cter-SUNs

1.5.1.1 Non-plant Cter-SUNs

Cter-SUNs are comprised of several functional domains (Liu et al., 2007). Their N-terminus is located in the nucleoplasm whilst the C-terminus extends into the PNS; this region contains both a CCD as well as the SUN domain. The nucleoplasmic domains of Cter-SUNs are not as well characterised as the C-terminal domains, but they have been shown to interact with nucleoskeletal components such as lamina proteins. Via these interactions, Cter-SUNs have been demonstrated to connect the nuclear lamina to the cytoskeleton by interacting with KASH proteins (Haque et al., 2006). There are strongly predicted regions of intrinsic disorder and it has been hypothesised that these facilitate several functions, including mediating interactions with chromatin and buffering nucleoplasm-based

mechanical forces (Meinke and Schirmer, 2015). Additionally, Cter-SUN proteins of opisthokonts have been reported to associate with NPCs (Liu et al., 2007).

There are five Cter SUN proteins that have been identified in mammals: SUN1, SUN2, SUN3, SPAG4 and SUN5. SUNs 1 and 2 are widely expressed, but the remaining three are specifically expressed in the testis (Shao et al., 1999; Hozdic et al., 2004; Crisp et al., 2006; Haque et al., 2006; Tzur et al., 2006). SUN1 has been shown to interact with A-type lamin, as well as to be involved in tethering meiotic telomeres to the NE (Haque et al., 2006; Ding et al., 2007; Morimoto et al., 2012; Horn et al., 2013). Interestingly, these lamin binding domains were reported to not be required for the NE-localisation of SUN1 (Haque et al., 2006). It has also been shown that SUN proteins are required to interact with KASH proteins to anchor them to the ONM (Padmakumar et al., 2005; Ostlund et al., 2009). Additionally, SUN-KASH interactions are required to form LINC complexes. A specific LINC complex between SUN1 and KASH5 was observed to facilitate telomere movement and chromosome pairing during meiosis (Horn et al., 2013). A meiosis-specific splice variant of SUN1, Sun1η, was identified and found to not possess either the emerin or short nesprin-biding domains (Gob et al., 2010). Furthermore, it was observed that SUN3 interacts with Nesprin 1 during mammalian sperm head formation (Gob et al., 2010). These are just a few examples of how SUN proteins interact with LINC complex components to regulate cellular processes.

SUN proteins have additionally been observed to be involved in roles outside of the traditional LINC complex-related processes. Both SUNs 1 and 2 have been shown to be involved in DNA damage response (DDR), and were found to interact with DNA-dependent kinase (DNAPK), Ku70, and Ku80 (Lei et al., 2012). They were further shown to have a redundant role; individual knockouts did not produce clear phenotypic defects, but double knockouts resulted in DNA damage and impaired DDR activation, indicating genomic instability in affected fibroblast cells (Lei et al., 2012). Redundancy of SUNs 1 & 2 have also been observed in nuclear anchoring in mouse cells (Lei et al., 2009), indicating that the redundancy reported in the previously mentioned study might not be specific to that role. Considering this in addition to the more recent observations made of KASH proteins, it can be suggested that LINC complexes have an even more diversified role than previously thought.

1.5.1.2 Plant Cter-SUNs

Plant SUN proteins were first characterised in *Z. mays* (Murphy et al.,2010) and in Arabidopsis (Graumann et al., 2010), which upon further analysis were found to consist of two sub-groups in both species (Fig. 1.2). Cter-SUNs were the first SUN group reported in plants and were found to be similarly sized to their yeast counterparts, with both groups being smaller than mammalian SUN proteins (Graumann et al. 2010; Murphy et al., 2010) but all having the same domain architecture of a transmembrane domain, a CCD and a C-terminal SUN domain (Fig. 1.2). This shows that Cter-SUNs are highly conserved throughout nature. Recent bioinformatics research using 20 representative species across the plant kingdom has shown that Cter-SUNs are present in all included species except for *Chlamydomonas reinhardtii*, a unicellular chlorophyte (Poulet et al., 2016). This suggests that plant Cter-SUN proteins are essential for multicellular plants and provides further support to previous studies which conclude that SUN proteins are present in most eukaryotes (Graumann et al., 2010; Murphy et al., 2010; Shimada et al., 2010; Zhang et al., 2017).

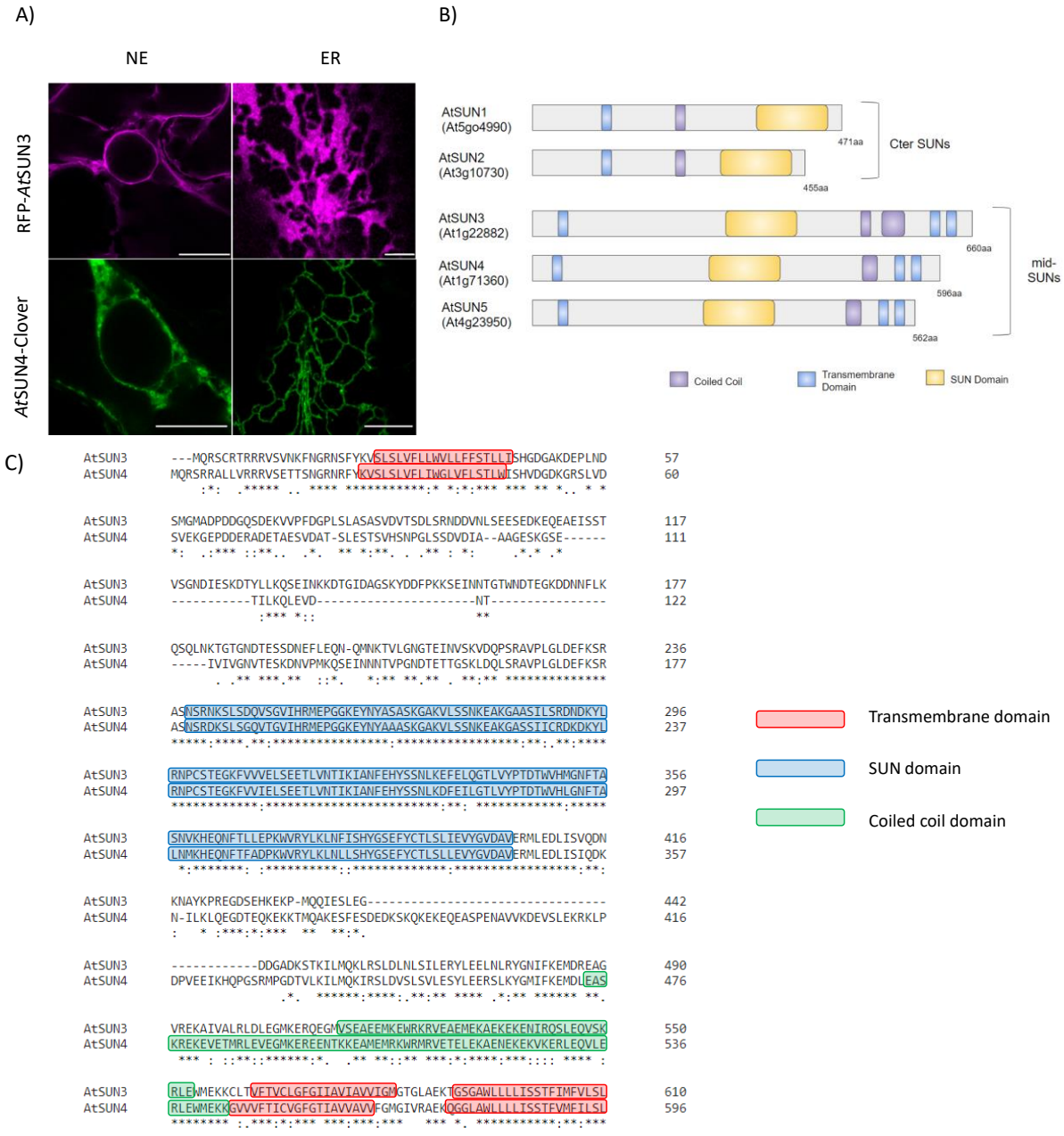

Figure 1.2. Known characteristics of mid-SUN proteins in *Arabidopsis thaliana*. A) Sub-cellular localisation of Arabidopsis mid-SUN proteins when transiently expressed in leaf epidermal cells of *Nicotiana benthamiana*. RFP-*At*SUN3 and *At*SUN4-Cl both localise to the NE and ER; Nucleus, scale bar 10µm; ER, scale bar 2µm. B) Domain architecture of SUN proteins, outlining how there are two different plant SUN sub-groups; the Cter-SUNs (*At*SUN1 and *At*SUN2) and the mid-SUNs (*At*SUN3, *At*SUN4 and *At*SUN5). Cter-SUN proteins possess the highly-conserved SUN domain at the C-terminus (positions 288-452aa in *At*SUN1 and 285-447aa in *At*SUN2) whilst mid-SUN proteins possess internal SUN domains (positions 238-402aa in *At*SUN3, 179-343aa in *At*SUN4, and 158-318aa in *At*SUN5). Similar homologues can be found in other eukaryotic organisms (Graumann et al., 2014). C) Sequence alignment of *At*SUN3 and *At*SUN4 show that the SUN domain (highlighted in blue) is highly conserved throughout the Arabidopsis mid-SUN protein sub-group. The transmembrane domains (highlighted in red) and coiled coil domains(highlighted in green) are less well conserved.

In plants, Cter-SUN proteins have been named SUN1 and SUN2 (Graumann et al., 2010; Murphy et al., 2010; Zhang et al., 2020). In Arabidopsis, Cter-SUNs have been shown to interact with the KASH domains of *At*WIP and SINE, resulting in the anchorage of *At*WIT in the latter interaction, demonstrating that LINC complexes form in plants (Zhou et al., 2012; Tamura et al., 2013; Graumann et al., 2014). Not only this but *At*SUN1 and *At*SUN2 were shown to be responsible for maintaining nuclear shape, as gene knockdowns resulted in more spherical nuclei (Oda and Fukuda, 2011; Zhou et al., 2012). The importance of maintaining the elongated shape in nuclei is currently unknown, but it has been proposed that it is required for reducing the effects of mechanical stress. Mis-shapen nuclei are also associated with disease and cell aging in humans (Dahl et al., 2008; Webster et al., 2009).

Varas et al., (2015) demonstrated that *At*SUN1 and *At*SUN2 associate with the NE throughout meiosis and have overlapping functions. A double mutant also resulted in delayed meiosis and provided evidence that *At*SUN1 and *At*SUN2 are required for telomere attachment to the NE (Varas et al., 2015). Meiotic roles for Cter-SUNs have also been observed in other plant species. In *Z.mays*, *Zm*SUN2 was shown to localise to the NE throughout meiosis; it was reported that *Zm*SUN2 assumed a belt-like structure that exhibited dynamic changes throughout meiosis (Murphy et al., 2014); at the zygotene stage, *Zm*SUN2 was shown to associated with a telomere cluster (Murphy et al., 2014). These findings subsequently indicated that *Zm*SUN2 has a functional role in meiosis, potentially in mediating telomere dynamics (Murphy et al., 2014). Additionally, the rice Cter-SUNs, *Os*SUN1 and *Os*SUN2, were demonstrated to have essential roles in meiosis that were also determined to be partially redundant (Zhang et al., 2020). It was further suggested that *Os*SUN2 was required after it was observed that meiosis was disrupted in the *Os*SUN2 single mutant.

It has been suggested that *At*SUN2 has a specific role during NE breakdown due to the fact it has low mobility during interphase and is retained in the mitotic membranes during nuclear envelope breakdown (NEBD) and NE reformation (Graumann and Evans, 2011). This latter process has been demonstrated to be spatially organised. The Arabidopsis Cter-SUNs accumulate at the surface of chromatin facing the spindle pole, progress along the spindle periphery, and eventually localise to

chromatin facing the cell plate (Graumann and Evans, 2011; Oda and Fukuda, 2011). During mitosis, both Cter-SUNs were observed to relocate to the mitotic membranes, providing evidence for the ER-retention model in plants (Graumann and Evans, 2011). This model hypothesises that the NE is absorbed into the ER during mitosis and is re-established from this reservoir during NE reformation (Anderson et al., 2009; Hetzer, 2010). The observation that *At*SUN1 and *At*SUN2 remain closely located to chromatin throughout cell division suggest that interactions between SUN proteins and chromatin are required for mitotic events to be carried out (Graumann et al., 2010; Graumann and Evans, 2011).

1.5.2 Overview of the mid-SUNs

1.5.2.1 Non-Plant mid-SUNs

There has been significantly less focus on mid-SUN proteins outside of plants, but published work shows that they are well conserved throughout eukaryotes (Murphy et al., 2010; Graumann et al., 2014; Vasnier et al., 2014). However, only a few mid-SUN domain proteins have been characterised outside of the plant kingdom. In mice a gene encoding a SUN-domain protein known as Osteopotentia (Opt) was found to be a regulator of postnatal skeletal development, after individuals deficient in this gene experienced debilitated bone function and spontaneous fractures (Sohaskey et al., 2010). In *Dictyostelium discoideum* (*D. discoideum*) a mid-SUN protein named SunB was identified and found to be essential for prestalk / prespore differentiation during development, as well as regulating cytokinesis (Shimada et al., 2010). More recent studies on the yeast mid-SUN domain-like protein Slp1 have demonstrated that it forms a protein complex with the ER-membrane proteins Emp65, which interacts with partially folded proteins to protect them from degradation (Zhang et al., 2017). Interestingly, this protein was first identified in a screen as a potential unfolded protein response (UPR) component (Jonikas et al., 2009). Slp1 has also been shown to be required for yeast Cter-SUN localisation to the NE (Friederichs et al., 2012). The mid-SUN protein of *Sordaria macrosporia* (*S. macrosporia*) is also known as Slp1 which has been proposed to be required for

karyogamy to occur during meiosis (Vasnier et al., 2014). It was found that meiosis was still able to proceed in cell lines lacking Slp1, but that recombination occurred between sister chromatids instead of homologous chromosomes (Vasnier et al., 2014). Although these separate findings do not provide further information as to the specific functional of the plant mid-SUN proteins, they do however highlight that this group of SUN proteins is essential for vital cell processes to be carried out.

1.5.2.2 Plant mid-SUNs

Plant mid-SUN proteins have also been demonstrated to interact with plant KASH proteins (Graumann et al., 2014; Gumber et al., 2019); they have also been suggested to have an additional function at the NE. As well as having a centrally-located SUN domain, mid-SUNs are bigger, larger and possess more CCDs and TMDs which are also found in different locations to that of the Cter-SUNs (Fig. 1.2). It should also be noted that plant Cter-SUNs have a bi-partite N-terminal NLS that targets them to the INM (Graumann et al., 2010), but no such signal has been detected in mid-SUNs. Work remains to be done concerning how these domains contribute to the function of the mid-SUNs, but these structural differences imply that a difference in their function may occur as a result. The similarity in the structure and size of mid-SUNs in different plant species indicates that they are highly conserved throughout the plant kingdom, suggesting that their role is essential for plant survival (Murphy et al., 2010; Graumann et al., 2014). Bioinformatic analysis of mid-SUN proteins in the plant kingdom produced results in agreement with this, where the 20 representative species used were all found to possess at least one mid-SUN protein (Poulet et al., 2016).

Three mid-SUN proteins, *Zm*SUN3-5, were identified in *Z. mays*; different tissues of this organism were analysed for levels of *Zm*SUN protein expression (Murphy et al., 2010). It was found that all *Zm*SUN proteins are expressed ubiquitously throughout the plant apart from *Zm*SUN5 (Murphy et al., 2010). This protein was expressed at low levels throughout all tissues except for pollen, suggesting a meiotic function (Murphy et al., 2010). This was also found to be the case when analysing the

expression levels of the Arabidopsis mid-SUN proteins, *At*SUN3-5 (Graumann et al., 2014). In *Gossypium barbadense* (*G. barbadense*) however, *Gb*SUN3 was found to be moderately expressed in all tissues but to have higher expression in petals and stamen (Yuan et al., 2021). Similarly to the observations made in *Z. mays* and Arabidopsis, *Gb*SUN5 was primarily expressed in mature pollen (Yuan et al., 2021).

*Zm*SUN3 has been proposed to play a role in meiosis after it was reported that a splice variant of this gene was detected in the mRNA from desynaptic (dy; Murphy et al., 2012), a mutant shown to disrupt meiosis (Bass et al., 2003). Additionally, a mid-SUN protein was identified in *Cicer arietinum (C. arietinum)*, the chickpea, and erroneously named *Ca*SUN1 (Jaiswal et al., 2014). This protein was found to localise to the NE and ER when expressed *in vivo* and was identified in a screen investigating potential components of the dehydration response pathway. Furthermore, it was suggested that *Ca*SUN1's involvement in this response is regulated via the UPR pathway (Jaiswal et al., 2014).

Single mutants of Arabidopsis mid-SUNs, *Atsun3-1*, *Atsun4-1*, and *Atsun5-1*, do not show obvious defects in growth or fertility; only *Atsun3-1* was shown to affect nuclear morphology when analysed (Graumann et al., 2014). Various combinations of double mutants were reported to be viable, but only the *Atsun4-1 Atsun5-1* double mutant was shown to affect nuclear size (Graumann et al., 2014). Mid-SUN triple mutants were found to be lethal, resulting in seeds being aborted in their siliques (Graumann et al., 2014). These results indicate that even though there is redundancy amongst mid-SUN proteins, that they are essential for plant survival.

Using confocal microscopy techniques, *At*SUN3 and *At*SUN4 expressed in *Nicotiana benthamiana* (*N. benthamiana*) were found to be localised to both the NE and the ER (Graumann et al., 2014), similarly to *Ca*SUN1 (Jaiswal et al., 2014). The localisation of *At*SUN5 could not be confirmed as it was not expressed sufficiently, which may be a result of being specifically expressed in meiotic tissues and suggests that its function is tissue-specific, similarly to *Zm*SUN5 and *Gb*SUN5 (Murphy et al., 2010; Graumann et al., 2014). Analysis of the mobile fractions of mid-SUN proteins that were transiently expressed in *N. benthamiana* leaf epidermal cells showed that *At*SUN4 was more mobile

in the ER, whilst *At*SUN3 was more mobile in the NE and more mobile overall (Graumann et al., 2014). It is interesting therefore that it is *At*SUN3 that has been found to most strongly interact with the ER-bound TF membrane anchored Myb (*At*maMyb; Tatout, personal communications; Andov, 2014). The mid-SUNs have also been found to interact with *At*WIPs and *At*TIK (Graumann et al., 2014), thus indicating that they potentially contribute to plant LINC complex formation.

1.5.2.3 mid-SUN Protein Interactions with *At*maMyb

Prior to the work described in this thesis, the ER-membrane anchored TF *At*maMyb (Slabaugh et al., 2011) was identified as a potential interaction partner of *At*SUN3 in a MY2H screen (Andov 2014). Subsequent work showed that when using *At*maMyb as bait, it was able to interact with all five SUN proteins using the MY2H system but was found to most strongly interact with *At*SUN3 (Tatout, personal communications). Conversely, the interaction between *At*maMyb and *At*SUN4 was observed to be weak (Tatout, personal communications). Prior to this work, none of these interactions had been confirmed *in planta*.

1.6 *At*maMyb and the R2R3-MYB Gene Family

*At*maMyb is a member of the R2R3-MYB subgroup of the homeodomain-like MYB superfamily which largely consists of TFs in animal cells. Similarly to SUN proteins, Myb proteins have a number of known homologues in plant species (Du et al., 2015; Chen et al., 2017). This interaction with proteins such as *At*maMyb and plant KASH proteins suggests that the mid-SUNs may be involved in the formation of multi-protein complexes at the plant NE. These in turn may contribute to putative LINC complex functions involved in gene expression.

The R2R3-MYB gene family are a large, plant-specific subfamily of the broader MYB gene family in eukaryotes. MYB genes are mostly TFs and are characterised by a conserved MYB domain that binds DNA (Dubos et al., 2010). The MYB domain consists of up to several imperfect 52 amino acid long repeats, each forming an alpha helix with the third being the recognised site for DNA binding (Dubos et al., 2010). MYB proteins in plants fall under three sub-categories depending upon the number of Myb domains that they possess; those that fall under the R2R3-MYB gene family, the largest of the three, possess two Myb repeats (Dubos et al., 2010). There are approximately 125 predicted R2R3-MYB genes in Arabidopsis (Stracke et al., 2001), the functional information for many of them being limited. However, the research that has been done would indicate that members of this family are involved in cell development and differentiation (Ramsay and Glover, 2005; Borg et al., 2011; Song et al., 2011), as well as responses to environmental stimuli (Lin-Wang et al., 2010).

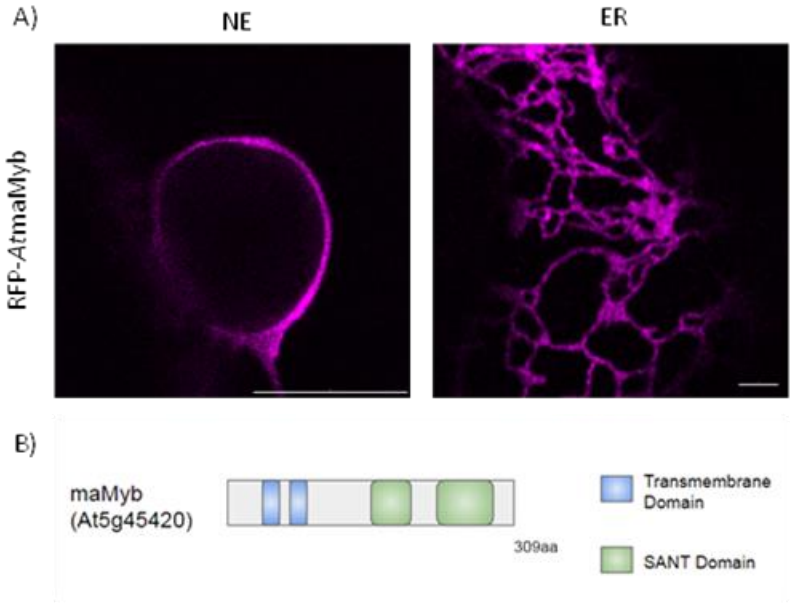

Figure 1.3. *At*maMyb protein structure and localisation. A) Confocal microscopy shows that RFP-*At*maMyb is distributed throughout the ER and NE, indicating that *At*maMyb is an ER-associated membrane protein (Nucleus – 10µm; ER - 2 µm). B) Analysis of *At*maMYB's domain structure revealed the presence of two transmembrane domains (positions 35-55aa and 63-83aa, respectively), in addition to two SANT domains (positions 156-209aa and 244-298aa, respectively) which are known to be involved in DNA binding, in particular the process of binding chromatin.

Bioinformatics predictions suggest that *At*maMyb is the only member of the R2R3-MYB group that is membrane bound (Kim et al., 2010), but investigation into a transcriptional regulation mechanism regarding the proteolytic processing of membrane-bound transcription factors (MTFs) has shown that there over 100 estimated MTF candidates present in the Arabidopsis genome (Bateman et al., 2009). Only a small number of these have been characterised (to varying extents), including *At*maMyb (Slabaugh et al., 2011). Of these characterised MTFs, each have been found to be involved in different aspects of plant development and responses to environmental stress, including cell division (Kim et al., 2006), hormone signalling (Park et al., 2011), and as aforementioned root hair elongation (Slabaugh et al., 2011).

Despite their broad variety of roles, plant MTFs appear to share mechanisms conserved throughout eukaryotes to induce responses to environmental and intracellular stimuli. There are two main regulated mechanisms of proteolytic processing; regulated intramembrane proteolysis (RIP) and regulated ubiquitin/proteasome-dependent processing (RUP; Liu et al., 2018). The former relates to a process whereby cytosolic elements of MTFs are cleaved from the rest of the protein and released for transportation to the nucleus where they can then go on to regulate transcription. This is observed in TFs bound to the plasma membrane where they remain dormant until targeted by signal induction to undergo RIP (Liu et al., 2018). On the other hand, RUP is a process used by ER-membrane tethered proteins where proteins are ubiquitinated and subsequently initiate the proteasome-dependent degradation process. If any part of the protein is present within the ER lumen and/or spans a membrane then they undergo degradation, and any active segments are directly transported to the nucleus (Liu et al., 2018).

According to the ubiquitination site prediction tool Ubpred, there are several potential ubiquitination sites present in *At*maMyb, with the site of most confidence (149aa) coinciding with the amino acids preceding the first Myb domain (Fig. 1.3; 156aa). This provides an interesting insight as to how *At*maMyb may be cleaved and able to achieve its purpose of binding with DNA.

There is little work describing how *At*maMyb is cleaved to become active in the cell, or how it functions as a TF. Slabaugh (2011) found that in accordance to the activation of other plant MTFs,

*At*maMyb is also proteolytically cleaved *in vivo*. This was proven by immunoprecipitating *At*maMyb-yellow fluorescent protein (YFP) through green fluorescent proteins (GFP)-Trap-A beads, and then conducting a western blot analysis using anti-GFP serum. The results of this produced two bands at the expected molecular weight of the truncated form of *At*maMyb, rather than just one (Slabaugh, 2011). Mass spectrometry analysis confirmed that *At*maMyb was present in both the full-length and truncated bands (Slabaugh, 2011). These results indicate that *At*maMyb acts as a MTF, but there has been no more work done to say if cleavage occurs as a result of specific or non-specific proteolytic processing.

Furthermore, BLAST analysis was conducted to identify a helix disrupting motif in the second TMD of *At*maMyb, an amino acid sequence (proline-phenylalanine-alanine-proline (PFAP)) conserved in all *At*maMyb homologs (Slabaugh, 2011). Such motifs are present in TMDs to allow for proteolytic processing to take place and it was hypothesised that they are required for the activation of *At*maMyb (Slabaugh, 2011).

Through swapping the TMDs of AtmaMyb with two TMDs of RETICULON-LIKE PROTEIN B13 (RTNLB13) and transforming them into fluorescent fusion proteins (full-length *At*maMyb-YFP and *At*maMybRTNLB13 24-70- GFP), stable lines of Arabidopsis transformants were generated. Extracted proteins from these were then used in a western blot analysis using an antibody against *At*maMyb, showing that of the two fusion proteins that only *At*maMyb-YFP could be detected (Slabaugh, 2011). These results indicate that the TMD region of *At*maMyb is required for proteolytic processing, potentially due to possessing a helix disrupting motif.

Alternative splicing has also been found to induce MTF activation (Deng et al., 2011; Kornblihtt et al., 2013). A number of MTFs have been found to undergo alternative splicing and produce a number of splice variants that still possess the nuclear TF domain but not TMDs (Huang et al., 2013; Moreno et al., 2013). These findings would suggest that there are multiple steps involved in MTF activation to ensure a proper response to stimuli. It could be suggested that at least one of the multiple bands detected in the western blot used to analyse the initial *At*maMyb truncations is in fact an

intermediate product from a cascade needed for activation. Part of the work described in this thesis was carried out to further characterise the interaction of mid SUNs with *At*maMyb (see Chapter 3).

1.7 Aims

The overall aims of this study were to characterise the Arabidopsis mid-SUN proteins *At*SUN3 and *At*SUN4 using a combination of molecular and confocal techniques. This included investigation of the putative *in vivo* interaction of *At*maMyb with *At*SUN3, and further investigating the membrane localisation of *At*SUN3 and *At*SUN4.

The main aims of the study were:

1. **Confirming protein-protein interactions at the plant NE:** putative interactions between full-length SUN proteins and *At*maMyb were tested using acceptor photobleaching Förster resonance energy transfer (apFRET). *At*SUN3 domain deletions, including deletion of the coiled coil domain, were used to investigate the key domains required to form homomers and heteromers. Förster resonance energy transfer measured by fluorescence lifetime microscopy (FRET-FLIM) was also used to investigate *At*SUN3 and *At*SUN4 homo- and heterodimerisation *in planta*.

2. **Assessing the sub-cellular localisation of *At*SUN3 and *At*SUN4:** A ratio method was used to establish the extent to which transiently expressed mid SUN proteins were localised to ER and NE. The fluorescence intensity of red fluorescent protein (RFP)-*At*SUN3 and *At*SUN4-RFP fusion proteins were measured at the both the ER and NE, and then used to calculate a final ratio of their enrichment in both organelles. These were then compared to protein-enrichment ratios calculated for the ER membrane protein GFP-RTN1 and the INM protein *At*SUN2-YFP.

3. **Using high-resolution confocal imaging to determine NE localisation:** A confocal imaging technique incorporating the use of the Zeiss Airyscan detector was previously used by our laboratory to investigate the sub-cellular localisation of fluorescent fusion proteins at the NE. This technique underwent further development to assess whether *At*SUN3 and *At*SUN4 truly localise to the NE, or instead localise to the ER. The proximity of GFP-*At*SUN3, *At*SUN3-GFP and GFP-*At*SUN4 fusion proteins were compared to the ER/ONM marker CXN-mCherry when transiently co-expressed *in planta*. Method development focused on selecting the most accurate measurement of distance between co-expressed proteins, in addition to determining which NE-labelling proteins were the most suitable control markers.

Overall, this work provides novel insights into the location and interactions of Arabidopsis mid-SUN proteins, and their activity contribution to the overall dynamics of the plant NE.

Chapter Two | Materials and Methods

2.1 Molecular Work

2.1.1. PCRs Used to Construct Fluorescent Fusion Products

To study the functional role of the mid-SUNs at the plant NE, it must be understood how each domain contributes to their interactions and localisation. Therefore, full-length genes were either truncated or different domains of importance were deleted, such as the coiled coil region (see Fig. 2.1 and Table 2.1). Additionally, full-length genes were used to characterise the mid-SUNs and for this were required to undergo Gateway cloning. YFP-*At*SUN3 and *At*SUN4-cyan fluorescent protein (CFP) containing vectors were used as template to generate full length and domain deletion clones (see Table 2.1; Mermet, 2018).

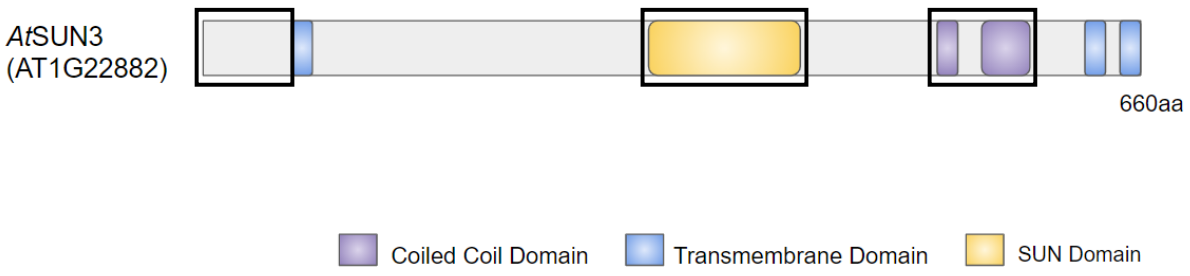

Figure 2.1. Graphic representation of the different truncations and domain deletions that were produced from full-length *At*SUN3. Domains encircled by black boxes indicate domains that were deleted using overlapping extension PCR. *At*SUN3 domain deletions were generated by project student Sarah Mermet.

Table 2.1. List of domain deletion mutants of Arabidopsis mid-SUN proteins generated using PCR

Name of Construct	aa deleted
*At*SUN3 del. N-terminus	1 - 20
*At*SUN3 del. SUN	237 - 402
*At*SUN3 del. coiled coil	506 - 610

Using the Gateway cloning system, PCR-generated *At*SUN3 deletion mutant sequences produced by Sarah Mermet (Mermet, 2018; see Fig. 2.1 and Table 2.1) were introduced to pDONR221 (see Appendix 3.1 and Table 2.2).

Full-length genes were amplified and gateway cloning sequences added (see section 2.1.3.1 and Appendix 2) using a gradient Polymerase Chain Reaction (PCR) method (see Fig. 2.2). All PCR reactions were carried out with proof-read Q5® High-Fidelity DNA Polymerase. A total volume of 50µl reactions were used, consisting of 35µl nuclease-free water, 10µl Quick-load Reaction Buffer (New England Biolabs, UK), 1µl deoxyribonucleotide triphosphates (dNTPs; 10Mm), 1µl of both forward and reverse primers (provided by Eurofins genomics; 10µM), 1µl of enzyme and 1µl of template. The thermocycler programme (Bio-rad) used to amplify PCR products is outlined below (see Fig. 2.2); annealing temperatures and extension times varied depending on the primers used (see Appendix 2) and constructs amplified.

For confirmation of plasmids following their transformation into competent *Escherichia coli* (*E.coli*; see section 2.1.4.1), candidates were tested by conducting a colony-gradient PCR. To do this, selected colonies were picked from selective agar media and resuspended in 10µl of nuclease-free water, providing the genetic material required for a PCR reaction. 25µl reactions were used, consisting of 17.5µl nuclease-free water, 5µl Quick-load Reaction Buffer (New England Biolabs, UK), 0.5µl dNTPs (10mM), 0.5µl of both forward and reverse primers (10µM), 0.5µl of enzyme and 1µl of template DNA. Transformed plasmids were confirmed using OneTaq® DNA polymerase. A variant of the PCR

programme outlined above was used (see Fig. 2.2); annealing temperatures and extension times varied depending on the primers used (see Appendix 2) and constructs amplified.

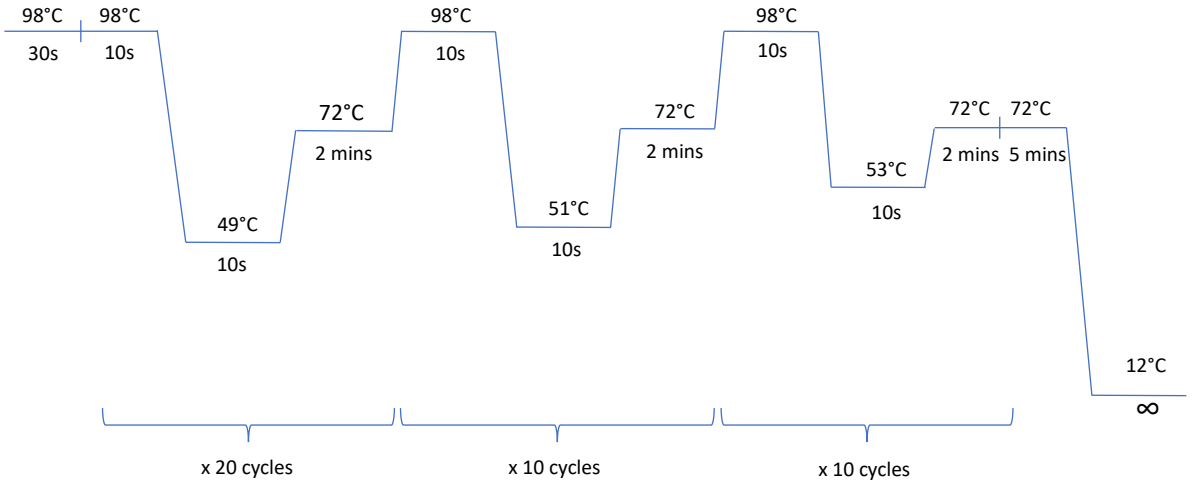

Figure 2.2. A graphic representation of a typical gradient PCR used to amplify a PCR product (using OneTaq® DNA polymerase). Annealing temperatures and extension times varied according to primers and/or polymerase used.

Results were confirmed using agarose gel electrophoresis (see section 2.1.2). Full-length genes, domain deletion mutants, and PCR products fused to Gateway cloning sequences were purified from PCR reactions prior to subsequent use (see sections 2.1.6 and 2.1.7). The remaining 9µl of the transformed *E.coli* plasmid suspension was transferred to liquid Lysogeny broth medium (LB: 10 g/L Bacto-trypton, 5 g/L yeast extract, 10 g/L NaCl in distilled water at pH 7.5 ± 1%). The appropriate antibiotics were added before cultures were incubated overnight at 37°C in an orbital shaker-incubator (approx. 200rpm).

2.1.2 Agarose Gel Electrophoresis

The results of PCR reactions were confirmed by conducting agarose gel electrophoresis. Agarose gels were prepared by weighing out agarose powder (1.0 % (W/V) agarose gel), which was added to an

appropriate amount of 1X Tris-acetate-EDTA (TAE) buffer (40 mM Tris, 20 mM acetic acid and 1 mM EDTA)). The solution was heated in a microwave to solubilise the agarose powder in the 1xTAE buffer; after having partially cooled, 2µl of SYBR Safe DNA Gel Stain (Invitrogen-ThermoFisher Scientific) was added to the 100ml solution.

DNA samples were loaded into gel wells alongside 1 kb DNA ladder (New England Biolabs, UK) for size comparison and reference. Gels were ran at 80V for 30-40 minutes using 1X TAE running buffer. Gels were imaged with a transilluminator and images were saved digitally. Confirmed PCR products were either purified (see section 2.1.7), or desired bands were cut out of the gel and then purified (see section 2.1.6) in the event there were multiple bands present in the gel.

2.1.3 Cloning and Expression Plasmids

2.1.3.1 Gateway Cloning

A standard gateway protocol provided by Invitrogen (https://www.thermofisher.com/uk/en/home/life-science/cloning/gateway-cloning.html) was followed for each stage of cloning genes into expression plasmids. The genetic material used for both the full-length and domain deletion mutant mid-SUN expression clones produced from this system was extracted (see section 2.1.6) from YFP-*At*SUN3 and *At*SUN4-CFP (see Table 2.2). This template DNA was then amplified using PCR (see section 2.1.1.1 and Fig. 2.2) and confirmed using agarose gel electrophoresis (see section 2.1.2).

DNA constructs generated by PCR underwent a BP reaction whereby they were cloned into the pDONR221 Gateway entry vector using 1µl of BP Clonase II Enzyme Mix, 1µl of pDONR221 vector DNA (approx. 200-300ng/µl) and 3µl (approx. 100-200ng/µl) of cleaned-up PCR product. Samples undergoing the BP reaction were incubated at 25°C overnight in a thermocycler. Reactions were terminated via the addition 0.5µl of proteinase-K and left to incubate at 37°C for 10 mins in a

thermocycler. Once this was done, the final BP product was either immediately transformed into competent *E.coli* (see section 2.1.4.1), or stored at -20°C until required.

Extracted entry clone DNA (see sections 2.1.6 and 2.1.7) was used in an LR reaction to then be cloned into desired expression vectors (see Appendix 3). The LR reactions consisted of 1µl LR Clonase II Enzyme Mix, 1µl of expression vector DNA (approx. 200-300ng/µl) and 3µl (approx. 100-200ng/µl) of entry clone DNA. Samples undergoing the LR reaction were incubated at 25°C overnight in a thermocycler. Reactions were terminated via the addition of 0.5µl of proteinase-K and left to incubate at 37°C for 10 mins in a thermocycler. Once this was done, the final LR product was either immediately transformed into competent *Agrobacteria tumefaciens* (Agrobacteria; see section 2.1.4.2) or stored at -20°C until required.

2.1.3.1 Expression Plasmids Used

Below is a list of expression plasmids used, along relevant information regarding their production:

Table 2.2. List of expression vectors and fluorescent constructs used in this thesis

Protein Name	Gene Number	Vector Used	Fusion Product	Contributor
$_{5}$-calnexin fusion	Last 236 amino acids of AT5G61790	pVKH18En6	GFP-CXN	Sarah Irons
$_{5}$-calnexin fusion	Last 236 amino acids of AT5G61790	pVKH18En6	CXN-mCherry	Norman Groves
***At*SUN2**	AT5G04990	pCambia 1300	*At*SUN2-YFP	Katja Graumann
***At*SUN2**	AT5G04990	pK7CWG2	*At*SUN2-CFP	Katja Graumann
***At*SUN3**	AT1G22882	pK7RWG2S	RFP-*At*SUN3	Bisa Andov
***At*SUN3**	AT1G22882	PB7WGF2	GFP-*At*SUN3	Bisa Andov
***At*SUN3**	AT1G22882	pB7FWG2	*At*SUN3-GFP	Bisa Andov
***At*SUN3**	AT1G22882	pCambia 1300	YFP-*At*SUN3	Katja Graumann
***At*SUN3**	AT1G22882	pCambia 1300	*At*SUN3-YFP	Katja Graumann
***At*SUN3**	AT1G22882	pB7WGC2	CFP-*At*SUN3ΔN-terminus	Sarah Mermet
***At*SUN3**	AT1G22882	pB7WGC2	CFP-*At*SUN3ΔSUN	Sarah Mermet
***At*SUN3**	AT1G22882	pB7WGC2	CFP-*At*SUN3Δcoiled coil	Sarah Mermet
***At*SUN3**	AT1G22882	pK7CWG2	*At*SUN3Δcoiled coil-CFP	Sarah Mermet
***At*SUN4**	AT1G71360	pK7WGR2	*At*SUN4-RFP	Bisa Andov
***At*SUN4**	AT1G71360	PB7WGF2	GFP-*At*SUN4	Bisa Andov
***At*SUN4**	AT1G71360	pK7CWG2	CFP-*At*SUN4	Katja Graumann
***At*maMyb**	AT5G45420	pCambia 1300	YFP-*At*maMyb	Katja Graumann
***At*maMyb**	AT5G45420	pCambia 1300	*At*maMyb-YFP	Katja Graumann
RTN1	AT4G23630	PB7WGF2	GFP-*At*RTN1	Imogen Sparkes

2.1.4.0 Preparation and Transformation of Competent Bacterial Cells

2.1.4.1 Transformation of Competent *E.coli* Cells

The final product of either a terminated BP or LR reaction were transformed into half of the recommended volume (25µl) of NEB 5-alpha Competent *E.coli* (High efficiency) cells. Competent *E.coli* cells were thawed on ice upon removal from -80°C storage; 2µl of BP or LR reaction (approx. 100-200ng/µl) were added to a 25µl aliquot under sterile conditions using a laminar flowhood. Individual tubes were flicked several times before left to incubate on ice for a further 30 minutes. At this point, samples underwent a 30 second heatshock in a waterbath set to 42°C. They were then left to recover on ice for 5 minutes. Cells were then transferred to 1ml of room-temperature Super Optimal broth (SOC) medium (Sigma-Aldrich) and incubated at 37°C in an orbital shaker-incubator (approx. 200rpm) for 1 hour.

Once the 1 hour incubation period was complete, transformed cells were spread onto LB agar plates (10g/L Bacto-Tryptone, 5g/ NaCl, 5g/L Yeast Extract, 10g/L Agar in distilled water at pH 7.5 ± 1%) under sterile conditions using a laminar flowhood. These were made under the same conditions to act as selection media of transformed cells, with selection antibiotics added at an appropriate concentration. 50µg/mL^{-1} of either spectinomycin or kanamycin (Sigma-Aldrich), or 10µg/mL^{-1} gentamicin (Sigma-Aldrich) was used. Use of specific antibiotics were dependent on the plasmid used (see Appendices 1 and 3).

Once dried, plates were left to incubate at 37°C overnight. Colonies that grew on the selection media were then used in colony PCRs to confirm the transformation had taken place (see section 2.1.1).

2.1.4.2 Generation of Competent Agrobacteria Cells

Competent Agrobacteria (strain GV3101) were grown at an approximate volume of 200ml in liquid LB media with 25 µg mL^{-1} rifampicin at 28°C. Unless otherwise stated, all work was carried out

under sterile conditions using a laminar flowhood. Upon reaching OD_{600}, the culture underwent centrifugation at 3500rpm for 30 mins at 4°C. The resultant pellet was then resuspended in cold 1M $CaCl_2$ before undergoing another round of centrifugation, this time for 10 mins at 5000rpm at 4°C. The pellet was resuspended once more in 15mls of cold 1M $CaCl_2$. 200µl Aliquots made from this bacterial suspension using pre-chilled Eppendorf tubes, and were flash frozen in liquid nitrogen before being stored at -80°C.

2.1.4.3 Transformation of Competent Agrobacteria Cells

Competent Agrobacteria cells were thawed on ice prior to transformation. Then approximately 100-300ng of expression plasmid DNA was added to each aliquot of cells before being left to incubate on ice for 5 mins. The cells were then either transferred to liquid nitrogen for 5 mins, or incubated at -80°C for 15 mins, and then rapidly thawed for 5 mins at 37°C for heat shock. The cells were then left to recover in 1ml liquid LB medium at 28°C in an orbital shaker-incubator (approx. 200rpm) for 2.5 hours. After this period, cells were spread onto agar plates made using the appropriate selection antibiotic(s) whilst working in a laminar flowhood. These were left to incubate at 28°C for 48 hours, after which transformed colonies were transferred to liquid LB medium for growth at 28°C in an orbital shaker-incubator (approx. 200rpm).

At this point, Agrobacteria cultures could be used to transiently transform plants (see section 2.3.1); alternatively, glycerol stocks could be made for long-term storage. 1.5ml of liquid culture was centrifuged for 3mins at 8000rpm. The pellet was resuspended in 1ml of liquid culture, followed by the addition of 700µl of sterile 70% glycerol; aliquots were frozen and stored at -80°C.

2.1.5 Plasmid DNA Extraction

When overnight cultures were sufficiently grown, *E.coli* cultures underwent plasmid DNA extraction using the Monarch Plasmid Miniprep Kit (New England Biolabs) according to manufacturer's

instructions. The DNA concentration was then measured using the NanoDrop™ ND-1000 UV-Vis Spectrophotometer (Thermoscientific). If found to be of a sufficient quantity, extracted entry clones were sent to be confirmed by sequencing using manufacturer-provided M13 primers (uni(-21), rev(-29); Eurofins Genomics).

2.1.6 DNA Gel Extraction

Upon confirming bands in agarose gels were of the correct size (see section 2.1.1), they were cut away from the main gel using a razor. Desired PCR products were extracted from the gel using the Monarch ® DNA Gel Extraction Kit (New England Biolabs, UK) according to manufacturer's instructions. DNA quantity of the final product was measured using the NanoDrop™ ND-1000 UV-Vis Spectrophotometer (Thermoscientific).

2.1.7 DNA Purification from PCR Reactions

Upon confirming bands in agarose gels were of the correct size (see section 2.1.1), PCR products were purified from the PCR mix using the Monarch® PCR & DNA Cleanup kit (New England Biolabs, UK) according to manufacturer's instructions. DNA quantity of the final product was measured using the NanoDrop™ ND-1000 UV-Vis Spectrophotometer (Thermoscientific).

2.2 Plant material

2.2.1 Wild Type Plant Material Production and Maintenance

All experiments involving the use of plant material were conducted using wild-type *N. benthamiana*. All plants were grown under greenhouse conditions (16 hours of light, 8 hours of darkness at a temperature of 21-22°C). Synchronised germination of seedlings sourced from ongoing lab stocks was induced from placing them onto 1/2 MS plates (2.4g/L Murashige and Skoog medium, 0.8% phytoagar in deionised water, pH 5.6-5.8), before sealing plates shut with micropore tape. These were then covered to sufficiently block out any light and incubated at 4°C for three days. After this period, plates were transferred to a growth cabinet where conditions where identical to those of the greenhouse. Seeds were left to germinate for 7-10 days in the growth chamber programmed to mimic greenhouse conditions before they were transferred to soil in the greenhouse. Transiently transformed plants were also kept in the growth chambers between infiltration and confocal imaging (see sections 2.3.1 and 2.4).

2.3 Plant Transformation

2.3.1 Transient Fluorescent Protein Expression in *N. benthamiana* Leaf Epidermal Cells

Transient Agrobacteria-mediated transformation was carried out on *N. benthamiana* specimens that had been grown in the greenhouse for 6-7 weeks, using the protocol developed by Sparkes et al.,(2006). 1ml of transformed Agrobacteria (see section 2.1.4.2) in liquid culture were centrifuged at 8000rpm at room temperature for 3 mins. Discarding the supernatant, the pellet was washed once with an infiltration buffer (5 mg ml^{-1} glucose, 50mM MES, 2mM $Na_3PO_{4.12}H_2O$ and 0.1 mM

acetosyringone) before being resuspended with 1ml of the same buffer. The optical density (OD) of this suspension was measured with the NanoDrop™ ND-1000 UV-Vis Spectrophotometer (Thermoscientific) using OD_{600}. Each bacterial suspension was then diluted with the infiltration buffer to an optical density of OD_{600} 0.05-0.15 (depending on the construct being infiltrated). Each fluorescent protein construct was transiently expressed in wildtype specimens (Sparkes et al., 2006). The underside of adult leaves was perforated with a needle before being infiltrated with a buffer containing Agrobacteria cells of each required construct using a 1ml syringe. The region of the leaf where the infiltrate had spread was marked out by a pen, so that these regions could be identified when conducting confocal experiments later.

2.4 Microscopy

2.4.1 Plant Material Preparations

To image plant material, small segments (typically up to 0.5cm^2) were cut away from the main part of the leaf. These were mounted in deionised water onto slides and the underside imaged using confocal microscopy. During imaging, transformed plants were placed underneath a light source whilst incubating in a temperature-controlled room of 21°C. Individual samples were imaged for no more than 25 minutes at a time to avoid cell phototoxicity, and to mediate the effects of excision from the plant.

2.4.2 Confocal Microscopy

A Zeiss LSM 880 confocal microscope was used for all experiments. All images were acquired using either a x63 1.46 NA oil immersion objective or x100 1.46 NA oil immersion objective at a zoom factor of either 2 or 2.5, respectively. Image acquisition and processing were carried out using ZEN imaging software (Zeiss). Images were saved as '.czi' files and raw data was stored on both an

external hard drive and on a file storage service. Details of region of interest (ROI) parameters and line profiles used in image analysis (see section 2.5) were recorded in Excel files and stored in the same systems.

Imaging settings used for visualising the fluorescent proteins used in this work are shown below:

Table 2.3. Excitation and detected emission wavelengths of fluorophores used in this work

Name of Fluorophore	Excitation spectra (nm)	Emission spectra (nm)
Green/Yellow Fluorescent Protein (GFP/YFP)	488	493-598
monomeric Red Fluorescent Protein (mRFP)	561	595-652
mCherry	561	595-652
Cyan Fluorescent Protein (CFP)	405	454-507

2.4.3 Use of Airyscan Detector

Whereas confocal microscopy operates using a single pinhole and point-detector, the Airyscan detector (Zeiss) is comprised of 32 individual gallium arsenide phosphide photomultiplier tube (GaAsP-PMT) channels (Huff, 2015). These 32 channels are arranged in a hexagonal pattern, each acting as a small pinhole and individual detector point focused around the conjugal image plane. Each channel collects its own pinhole-plane image based on its positional information, producing images of higher resolution and signal-to-noise ratio (SNR). Specifically, images acquired using the

Airyscan detector have 1.7x increased resolution in all three spatial dimensions (140 nm in x and y, and 400 nm in z; (Huff, 2015)). This in turn increases SNR 4-8x without compromising factors such as speed, as would be the case in standard CLSM (Huff, 2015).

2.4.4 NLI Ratio Image Acquisition

Z-stacks of nuclei were collected from live cells in the lower epidermal leaf tissue. Observations were carried out through use of CLSM (Zeiss LSM 880), and the addition of an Airyscan detector (Zeiss, Germany) was used to produce the images collected for analysis. All images were acquired using a x100 oil objective at zoom factor of 2. GFP/YFP samples were excited using 488nm laser lines, whilst RFP samples were excited with 561nm laser lines; signals were collected with emission wavelengths of 523nm and 579nm respectively (see Table 2.3). Laser power did not exceed 2% whilst imaging to avoid photobleaching. Z-stacks were taken of each cell used to collect sample data; each stack was organised in such a way that the entire cell was imaged with 1µm separation between slices. This was done to improve the likelihood of producing an image of a nucleus at its medial point for use in image analysis (see sections 2.6.1 and 2.6.2).

2.4.5 apFRET Image Acquisition

The combination of fluorophores used in these apFRET experiments were CFP and YFP, with CFP being the donor fluorophore and YFP the acceptor fluorophore, in accordance with emission spectra. All apFRET experiments were carried out by adapting the methods described by Graumann et al., (2010). A circular ROI of 7µm diameter was established at a region of the NE that was not in close proximity to artefacts that could influence FI measurements. These ROIs were bleached with 5 iterations of the 514nm laser at 100%. A total of 10 images were captured per sample imaged at the scan speed of 3.75 scans per second, 10 pre-bleach and 10-post bleach; these were then analysed, as outlined in section 2.5.3.

2.4.6 FRET-FLIM image acquisition

Epidermal samples of *N. benthamiana* leaves infiltrated as described in section 2.3.1 were cut away from the plant prior to imaging; images were collected by Charlotte Pain and Stefan Wojcik. A Nikon EC2 confocal microscope was used to confirm the expression levels of GFP and mRFP levels in plant samples with excitation at 488 and 543nm, respectively. Autofluorescence emission from chlorophyll was minimised with the use of a 633-nm interference filter. A two-photon microscope at the Central Laser Facility of the Rutherford Appleton Laboratory was used to capture FRET-FLIM data according to Schoberer and Botchway (2014).

Multiphoton FLIM was conducted by using a Nikon EC2 confocal scanning system combined with a two-photon microscope constructed around a Nikon TE2000-U inverted microscope (Botchway et al., 2015). A mode-locked titanium sapphire laser (Mira; Coherent Lasers) was used to produce a laser light of 920nm, which produced 200 fs pulses at 76 MHz whilst pumped with a solid-state continuous wave 532nm laser (Verdi V18; Coherent Laser). Specimens were illuminated on the microscope stage by using a water-immersion objective (Nikon VC; 360, numerical aperture of 1.2) to focus the laser beam to a diffraction limited spot. The scanning system was by-passed when collecting fluorescence emission, which was done without descanning (no pinhole was used); it was then passed through a BG39 (Comar) filter, blocking out near-infrared laser light. A fast microchannel plate photomultiplier tube (Hamamatsu R3809U) was used as an external detector, and synchronised with generated line, frame, and pixel clock signals. Raw FLIM data was produced by linking these via a time-correlated single-photon counting PC module SPC830.

2.4.7. Airyscan Localisation Microscopy Image Acquisition

Acquisition of this data is fully described in Chapter 5 (see section 5.2.1.) due to additionally including method development.

2.5 Image Analysis

2.5.1 Selection of Images Used for Calculating NLIs

Individual slices from Z-stacks collected as described (see section 2.4.4) were manually selected (see Fig. 2.3). Images where resolution or expression were sub-optimal were discounted from selection, allowing for a dataset of representative images for each construct to be compiled. The image processing program ImageJ (https://imagej.nih.gov/ij/) was used to draw line profiles along a consistent number of points in the NE and ER for each individual sample. FI of these two compartments was measured and plotted to produce intensity profiles.

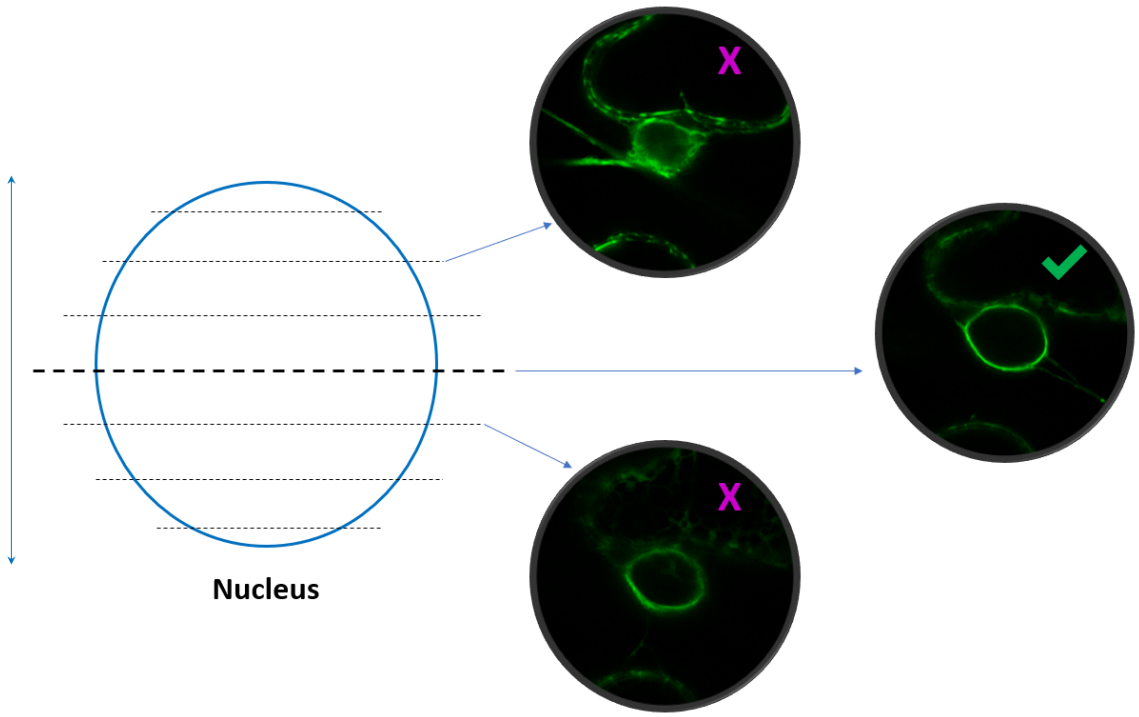

Figure 2.3. Selection process of images used for measuring fluorescence intensity to calculate NLI ratios. Z-stacks are taken of nuclei that are candidate samples for NLI ratio calculations. These images are then manually reviewed to select the layer where nuclei of good resolution and expression are at their optimum (indicated by a green tick). Layers where these criteria are not met are rejected from being used to calculate NLI ratios (indicated by a magenta cross).

The ratio of intensity at the NE and in the ER provides an indication of enrichment at each membrane with a value closer to one indicating that protein is NE-enriched, whereas values closer to zero indicate a protein is ER-enriched. Such indicatory values are determined by experimental controls. NLI ratios were calculated according to the following formula:

$$NLI = \frac{(NE_1 + NE_2)}{(ER_1 + ER_2)} \quad \text{(i)}$$

NE_x/ER_x refers to the ranking of peaks produced by the intensity profiles, which are ranked from highest to lowest fluorescence intensity. Therefore it is the only two highest fluorescence intensity values for each sub-compartment that are used to calculate the NLI ratio.

2.5.2 Statistical Analysis of NLI data

NLI ratios were calculated for each sample in Excel; an overall NLI ratio was generated by calculating the average of each cohort. R (R Core Team, 2013) was used to generate boxplots from this data to show sample distribution and to identify outliers that needed to be removed. Graphical representation of the final results were generated in Excel, with error bars representing standard error of the mean (S.E.M). Statistical tests were conducted using R with the addition of the onewaytests package (Dag *et al.*, 2019). R scripts were used to automatically test for statistically significant differences within the data (Kruskal–Wallis test and Dunn's test).

2.5.3 Statistical Analysis of apFRET Data

The original data was normalised to a percentage of average pre-bleach FI using the formula stated below:

$$E_F = 100 \times ((I_{pre} - I_{post}) / I_{pre}) \quad \text{(ii)}$$

In this formula I_{pre} is defined as the average intensity of fluorescence pre-bleach, and I_{post} the timepoint of the first post-bleach measurement, which in these experiments was the 6th scan out of 10.

These calculated values were used to calculate the overall FRET efficiency (E_F). This value represents the percentage of energy transfer between the two fluorophores used. A minimum of 30 individual samples were collected from a minimum of three biological replicates to generate the final dataset. E_F was expressed as the average of the final dataset, with the addition of the S.E.M. This E_F value was compared with a value calculated from pre-bleach measurements as an internal control. Paired t-tests were performed on the experimental and control datasets, with a p-value of <0.05 used to determine significance.

2.5.4 Analysis of FRET-FLIM Data

Raw data was analysed, and final values were provided by Verena Kriechbaumer. Data was collected by recording the excited-state lifetimes of an ROI at the nucleus. Using SPC Image analysis software version 5.1 (Becker and Hickl), the distribution of lifetime values within the ROI were calculated and presented as a curve. Only values that had a $\chi 2$ between 0.9 and 1.4 were used. The range of lifetimes per sample were produced from taking the median lifetime value, and the minimum and maximum values for one-quarter of the median lifetime values, from the curve. A minimum of five

nuclei from at least two independent biological samples per protein-protein combination were analysed.

Chapter Three | Testing protein-protein interactions *in vivo*

3.1 Introduction

Fluorescence Resonance Energy Transfer (FRET) is a quantitative, ratiometric technique that has been adapted for confocal microscopy to confirm protein-protein interactions in planta (Elmore et al., 2004; Liu et al., 2007; Zhang et al., 2018). FRET is defined as the transfer of energy from a donor fluorophore to an acceptor fluorophore so long as they are within close proximity to one another, and if the emission wavelength of the donor fluorophore overlaps with the excitation wavelength of the acceptor fluorophore (Karpova et al., 2003). One way that this technique has been adapted is through the development of acceptor-photobleaching Fluorescence Resonance Energy Transfer (apFRET; Karpova et al., 2003). apFRET operates by bleaching the acceptor fluorophore, thereby reducing or ending the transfer of energy which results in an increase in donor fluorescence providing they meet the criteria above (Karpova et al., 2003; Fig. 1). This has become a recognised technique in cell biology to determine protein-protein interactions (Weems et al., 2017; Rozés-Salvador et al., 2020), including those that take place at the plant NE. For example, apFRET was used to determine that *At*NEAPs are able to not only interact with themselves but also Cter-SUNs (Pawar et al., 2016). Similarly, the Arabidopsis mid-SUN proteins have also been demonstrated to not only interact with each other, but Cter-SUNs and the KASH domain of *At*TIK (Graumann et al., 2014). Interestingly the same work showed that whilst *At*SUN3 was able to interact with *At*WIP1, *At*SUN4 was not (Graumann et al., 2014).

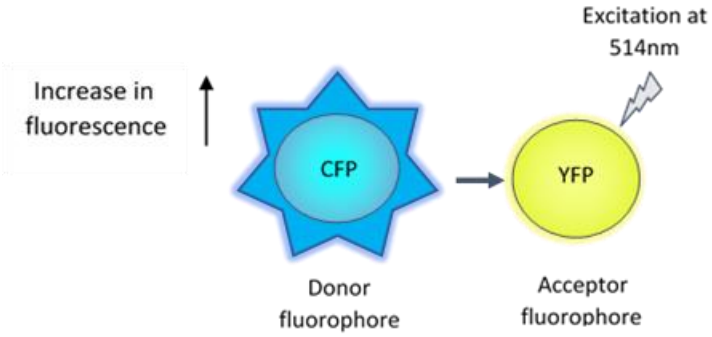

Figure 3.1. Graphic representation of how the confocal technique acceptor-photobleaching fluorescence resonance energy transfer (apFRET) operates, using a CFP-YFP combination. Differently to standard FRET, apFRET measures the change in fluorescence emission from the donor fluorophore (CFP) as a result of bleaching the acceptor fluorophore (YFP), and reducing/ending the transfer of energy between the two fluorophores.

An alternative approach to investigating cellular processes is through using fluorescence lifetime imaging microscopy (FLIM). Here, the fluorescence lifetime of a fluorophore is defined as the amount of time required for it to revert from its excited state to its ground state by emitting a photon. The fluorescence lifetime of a fluorophore is sensitive to its molecular environment independently of its concentration in the cell, meaning that this property can be used to provide details regarding a protein it is fused to (Chen et al., 2003; Becker, 2012).

FLIM can be used for several applications, including the functional imaging of ion concentrations, including in combination with FRET in live cells (Sanchez et al., 2010; Bücherl et al., 2014; Dikovskaya and Dinkova-Kostova, 2020). This latter technique, FRET-FLIM (Förster resonance energy transfer measured by fluorescence lifetime microscopy), can be used to determine protein conformational changes and protein-protein interactions (Miserey-Lenkei et al., 2007; Caron et al., 2012; Long et al., 2018; Dikovskaya and Dinkova-Kostova, 2020).

When FRET occurs between two fluorophores, quenching reduces the excited state of the donor fluorophore resulting in a decrease in its fluorescence lifetime (Fig. 2). Therefore FRET-FLIM measures changes in the fluorescence lifetime of a donor fluorophore in the presence of an acceptor fluorophore, where physical interactions between the two are indicated by FRET taking place (Fig. 2;

Schoberer and Botchway, 2014; Kriechbaumer et al., 2017). Every pixel within a FLIM image provides both spatial and fluorescence decay data. It has been observed that even a reduction of ~200ps in the donor fluorescence lifetime can be an indicator of protein-protein interactions (Stubbs et al., 2005).

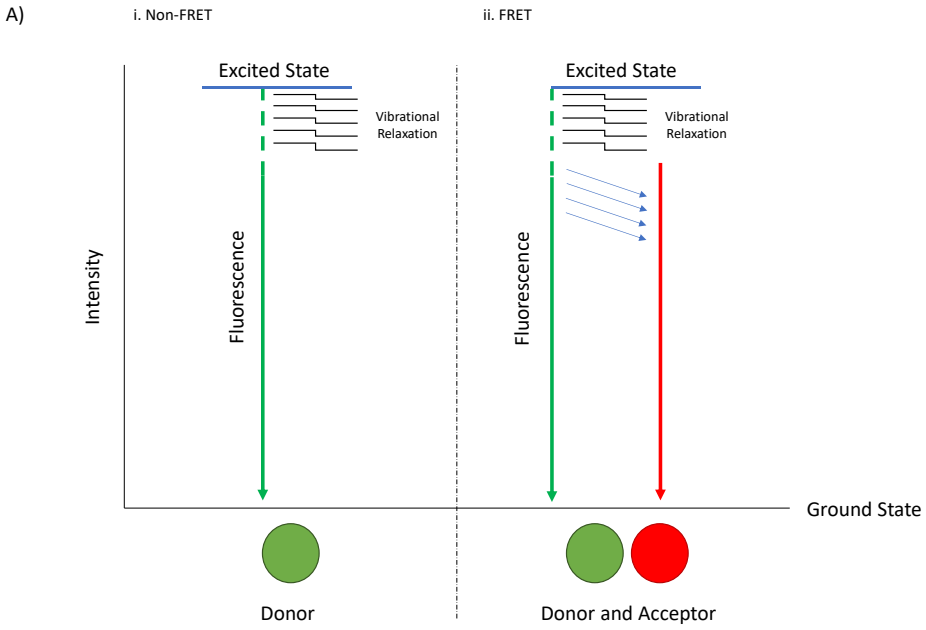

Figure 3.2. Graphic representation of the FRET-FLIM principle. FRET-FLIM measures the change in the fluorescence lifetime of a donor fluorophore (GFP) in the presence of an acceptor fluorophore (RFP). FRET interactions are defined as GFP-tagged proteins being measured to have shorter fluorescence lifetimes in the presence of RFP-tagged proteins when compared to that of a donor fluorophore only due to quenching. Downwards pointing arrows indicate excited fluorophores transitioning back to the ground state post-excitation. Blue arrows indicate the non-radiative transfer of energy of a donor fluorophore to an acceptor fluorophore due to being in very close proximity. Adapted from Simkova et al., (2012).

FRET-FLIM is frequently used to conduct protein-protein interaction studies (Cremazy et al., 2005; Doré et al., 2014; Venditti et al., 2019), particularly in plants (Osterrieder et al., 2009; Sparkes et al., 2010; Camborde et al., 2017; Kriechbaumer et al., 2017; Long et al., 2017; Long et al., 2018). For example, this technique has been used to show how TF's formed cell-type-specific protein complexes that underwent conformational changes to regulate target genes in Arabidopsis roots (Long et al., 2017). In another instance, FRET-FLIM has been used to show that several members of the plant

reticulon (RTN) family are able to interact with themselves and each other (Sparkes et al., 2010; Kriechbaumer et al., 2015; Kriechbaumer et al., 2018). Through understanding how they dimerise and oligomerise, in conjunction with other data, a further understanding has been gained of how RTNs affect ER modelling in planta (Sparkes et al., 2010; Breeze et al., 2016).

It has been shown using apFRET that Yellow Fluorescent Protein (YFP)-*At*SUN3 and Cyan Fluorescent Protein (CFP)-*At*SUN4 are able to interact, indicating that this is mediated by their N-termini (Graumann et al., 2014). No further work has been published regarding how they form homodimers and heterodimers with each other however. Such information is important as it would contribute to the broader understanding of how the protein network at the NE functions, and how proteins such as *At*maMyb are incorporated. It could also potentially confirm the predicted topology of the Arabidopsis mid-SUN proteins.

FRET-FLIM experiments were carried out to test interactions between *At*SUN3 and *At*SUN4. Subsequently, the work in this chapter focused on further investigating the homo- and heterodimeric interactions of *At*SUN3 and *At*SUN4. The methodology of these experiments is detailed in sections 2.4.6 and 2.5.4.

3.1.1 Protein-Protein Interactions Indicated by MY2H Screens

In the MY2H system, the reconstitution of ubiquitin due to the interaction of two proteins leads to the release of a membrane-bound TF that activates yeast reporter genes in the nucleus (Stagljar et al., 1998). This differs from the yeast two-hybrid (Y2H) system, which relies upon the reformation of the soluble GAL4 protein to activate transcription. The former technique is preferred when working with integral membrane proteins as it overcomes issues raised by the hydrophobic nature of such proteins, and/or the fact that many undergo post-translational modification. Despite its valuable uses, alternative methods must also be used to prove MY2H-confirmed interactions *in vivo*.

In previous MY2H screens, it was found that all the Arabidopsis SUN proteins were able to interact with *At*maMyb, an ER membrane-bound TF (Andov, 2014; Tatout, personal communications; see section 1.5.2.3). As well as establishing interactions between full-length proteins, it was also of interest to determine which domains were responsible for interactions observed. It was found that N-terminal truncations of *At*SUN3 did not interact with *At*maMyb in subsequent MY2H screens; N-terminal truncations of *At*maMyb were also shown to not interact with a full-length *At*SUN3 protein. Interactions were also determined to not take place between the SUN domain of *At*SUN3 alone and full-length *At*maMyb (Tatout, personal communications). While the SUN domain of *At*SUN3 alone was not able to interact with *At*maMyb, *At*SUN3Δcoiled coil was able to interact with *At*maMyb (Tatout, personal communications). These results indicate that neither the SUN domain nor the CCD are required for *At*SUN3-*At*maMyb interactions.

3.1.3 Aims

The apFRET experiments discussed below were carried out to test *At*maMyb-*At*SUN interactions *in planta* and see how they compare to the MY2H findings. FRET-FLIM experiments were additionally carried out to test interactions between *At*SUN3 and *At*SUN4. Subsequently, the work in this chapter focused on further investigating the homo- and heterodimeric interactions of *At*SUN3 and *At*SUN4. The methodology of these experiments is detailed in sections 2.4.5, 2.4.6, 2.5.3, and 2.5.4.

3.2.0 Results

3.2.1 Optimisation of constructs for Protein Expression in *N. benthamiana* Leaf Cells

Transient expression of fluorescent protein fusion constructs in *N. benthamiana* was achieved via agrobacterium-mediated transformation using a specific optical density (OD) of agrobacteria (see section 2.1.4.3), which can vary depending on the construct to be expressed. Expression assays were carried out whereby different constructs of interest were expressed either on their own, or in combination with known/potential protein interactors at different ODs. The expression of single and co-expressed constructs was then assessed to see which OD was optimal for use in apFRET experiments. Not only was FI used as an indicator of optimal expression but also the proportion of cells that were found to express the construct within the field of view were used as an indicator of optimal expression.

For example, *At*maMyb tagged at either terminus was found to be expressed in most cells regardless of the fluorophore being used and had a high FI. On the other hand, mid-SUN proteins were found to express well in fewer cells, with low expression commonly observed throughout a greater proportion of cells in a sample. Interestingly, it was observed that Cter-SUNs had a higher FI in a greater number of cells in comparison to their mid-SUN counterparts. It should be noted that it was the FI of each construct at the NE that was compared when making these observations. The FI of *At*maMyb and the mid-SUNs were observed to be high in the ER, particularly in comparison to the FI observed at the NE. For the expression assays, *At*maMyb, mid-SUNs and *At*SUN3Δcoiled coil expression were optimised for apFRET experiments. The optimal ODs determined by these expression assays were used for all subsequent experiments incorporating mid-SUNs or *At*maMyb. The ODs used in these experiments were: 0.1 for *At*maMyb, and 0.15 to improve the expression of the SUN proteins. The RNA silencing suppressor p19 was co-expressed with each protein combination tested.

3.2.2 Localisation of Full-Length Constructs in Transiently Transformed Plant Cells

Transiently expressed fluorescent protein fusions of both full-length mid-SUN proteins and *At*maMyb were localised in the ER and NE (Fig. 3.3). *At*maMyb and *At*SUN3 exhibited this localisation regardless of which terminus the fluorophore was fused to (Fig. 3.3), as well as which fluorophore was used. However, for *At*SUN4, only N-terminally tagged *At*SUN4 localised to the NE and ER while C-terminally tagged *At*SUN4 resulted in cytoplasmic localisation. This meant only N-terminally tagged *At*SUN4 was used for apFRET (Fig. 3.4).

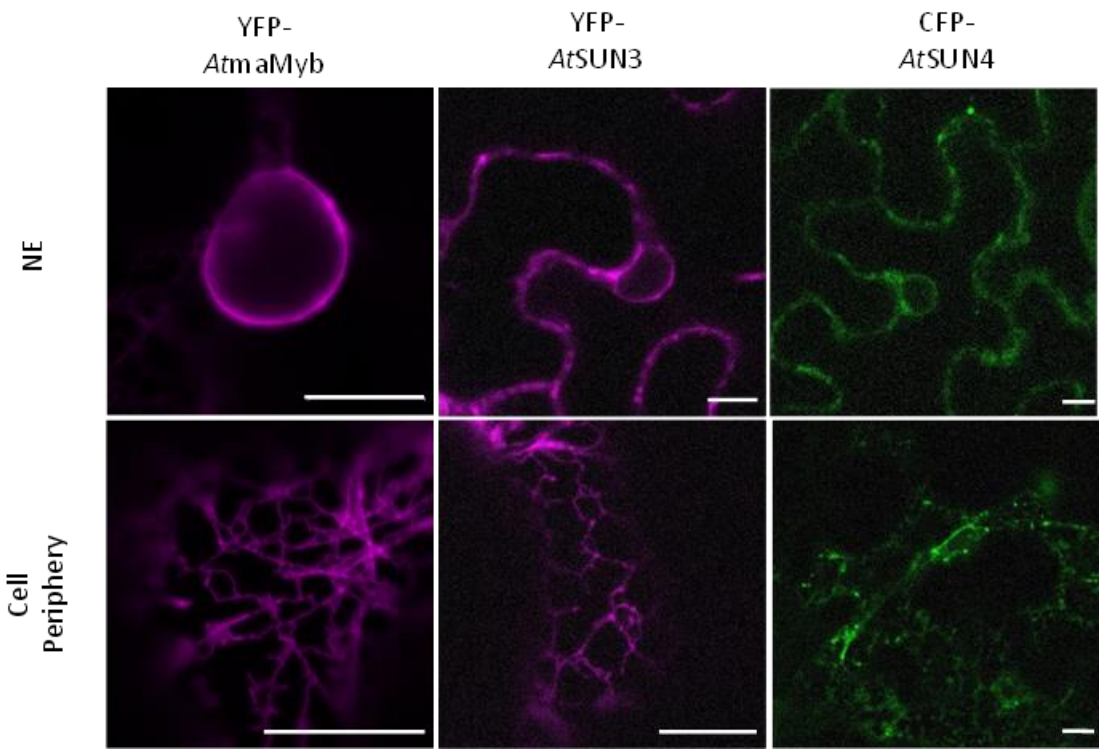

Figure 3.3. Sub-cellular localisation of CFP-*At*maMyb, YFP-*At*SUN3, and CFP-*At*SUN4 when transiently expressed in *Nicotiana benthamiana* with p19. The mid-SUN proteins and *At*maMyb all localise to both the NE and ER (scale bar 10μm).

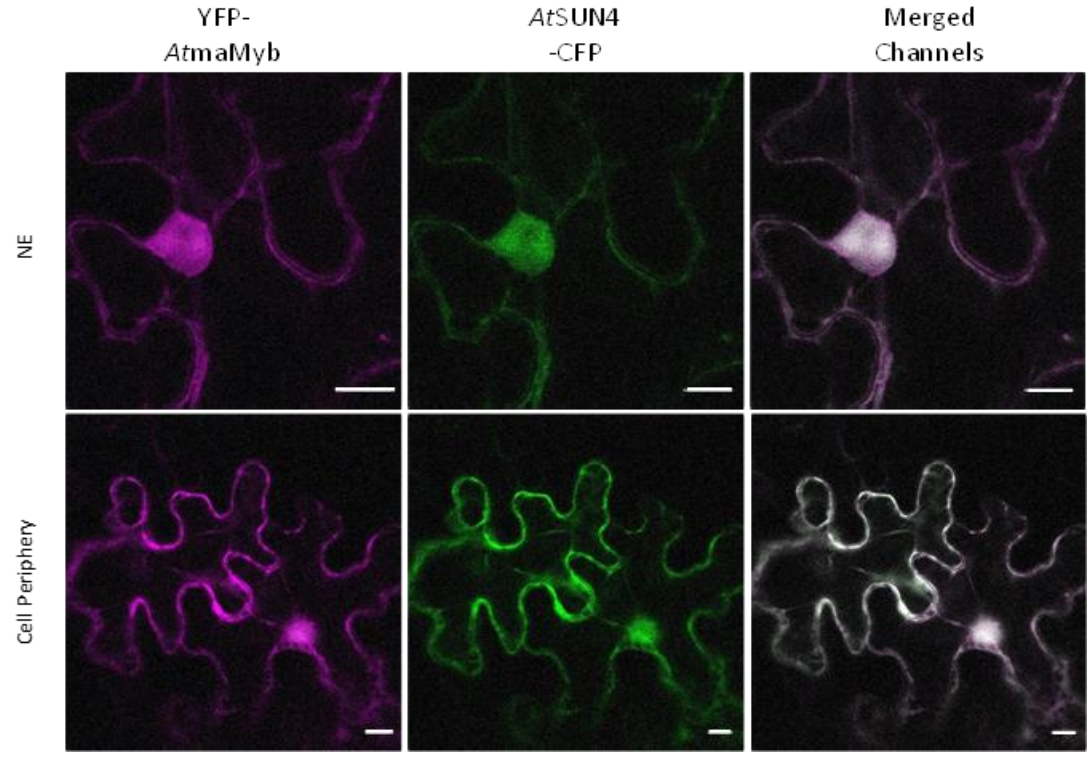

Figure 3.4. Sub-cellular localisation of YFP *At*maMyb and *At*SUN4-CFP when transiently co-expressed in *Nicotiana benthamiana* with p19. Co-expression of these two constructs results in nucleoplasmic localisation (scale bar 10μm).

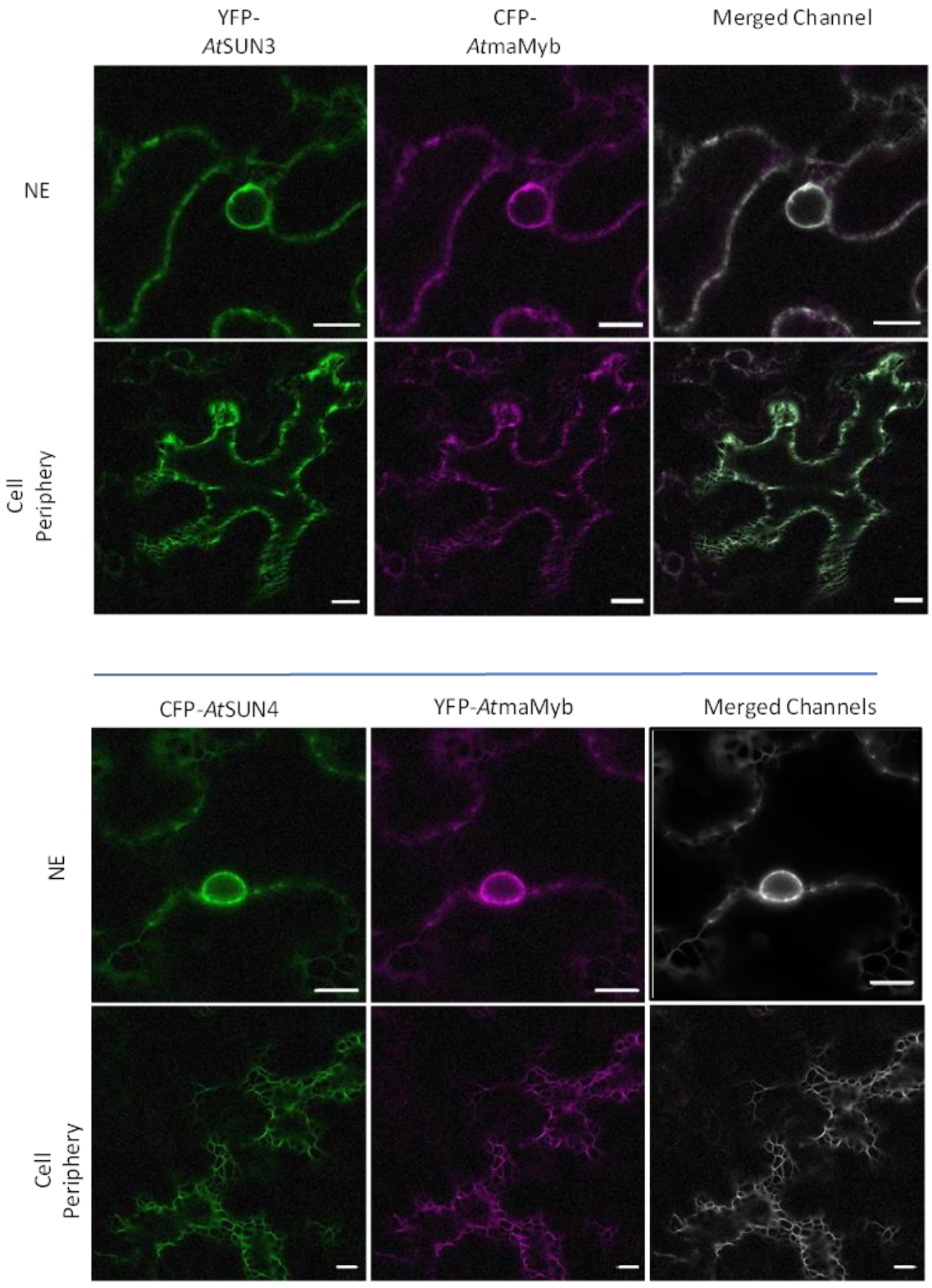

Figure 3.5. Sub-cellular localisation of CFP-*At*maMyb, YFP-*At*SUN3, and CFP-*At*SUN4 when transiently co-expressed in *Nicotiana benthamiana* with p19. The mid-SUN proteins and *At*maMyb localise to both the NE and ER (scale bar 10μm).

3.2.2.1 Determining Protein-Protein Interactions between Full-Length SUN Proteins and *At*maMyb

Protein-protein interactions were determined by calculating the FRET efficiency (E_F) between each pair of proteins tested, representing the percentage energy transfer between the two fluorophores measured (see section 2.5.3). Protein interactions were measured in an ROI at the NE (see section 2.4.5). YFP-tagged proteins were bleached in each experiment and it was the change in the FI of CFP-tagged proteins that was used to calculate E_F. Control E_F values were calculated from changes in CFP FI pre-bleach measurements and compared to experimental E_F values. Experiments initially were focused on testing interactions between *At*maMyb, and *At*SUN3 and *At*SUN4 (Fig. 3.5).

Positive protein-protein interactions were defined as having a positive experimental E_F that was significantly higher than the control E_F. Analysing E_F values, protein interactions were detected between CFP-*At*MaMyb and YFP-*At*SUN3 (E_F =0.64, control E_F =-0.84, p =0.01; Table 3.1, Figs. 3.6&3.7). Protein interactions were also detected between *At*MaMyb-CFP and YFP-*At*SUN3 (E_F =-1.99, control E_F =-0.92, p =0.005; Table 3.1, Figs. 3.6&3.7). No protein interactions were detected between CFP-*At*SUN4 and YFP-*At*MaMyb (E_F =0.64, control E_F =-0.84, p =0.68; Table 3.1, Figs. 3.6&3.7). Interactions were also not detected between YFP-*At*SUN1 and *At*MaMyb-CFP (E_F =-2.72, control E_F =-1.2, p =0.23; Table 3.1, Figs. 3.6&3.7), nor YFP-*At*SUN2 and *At*MaMyb-CFP (E_F =-0.03, control E_F =-1.2, p =0.29; Table 3.1, Figs. 3.6&3.7). This indicates that despite co-localisation at the NE, only *At*SUN3 can interact with *At*Mamyb *in planta* whilst *At*SUN4 and the Cter-SUNs cannot. It was observed that experimental data varied more than control data overall (see Table 3.1 and Fig. 3.7).

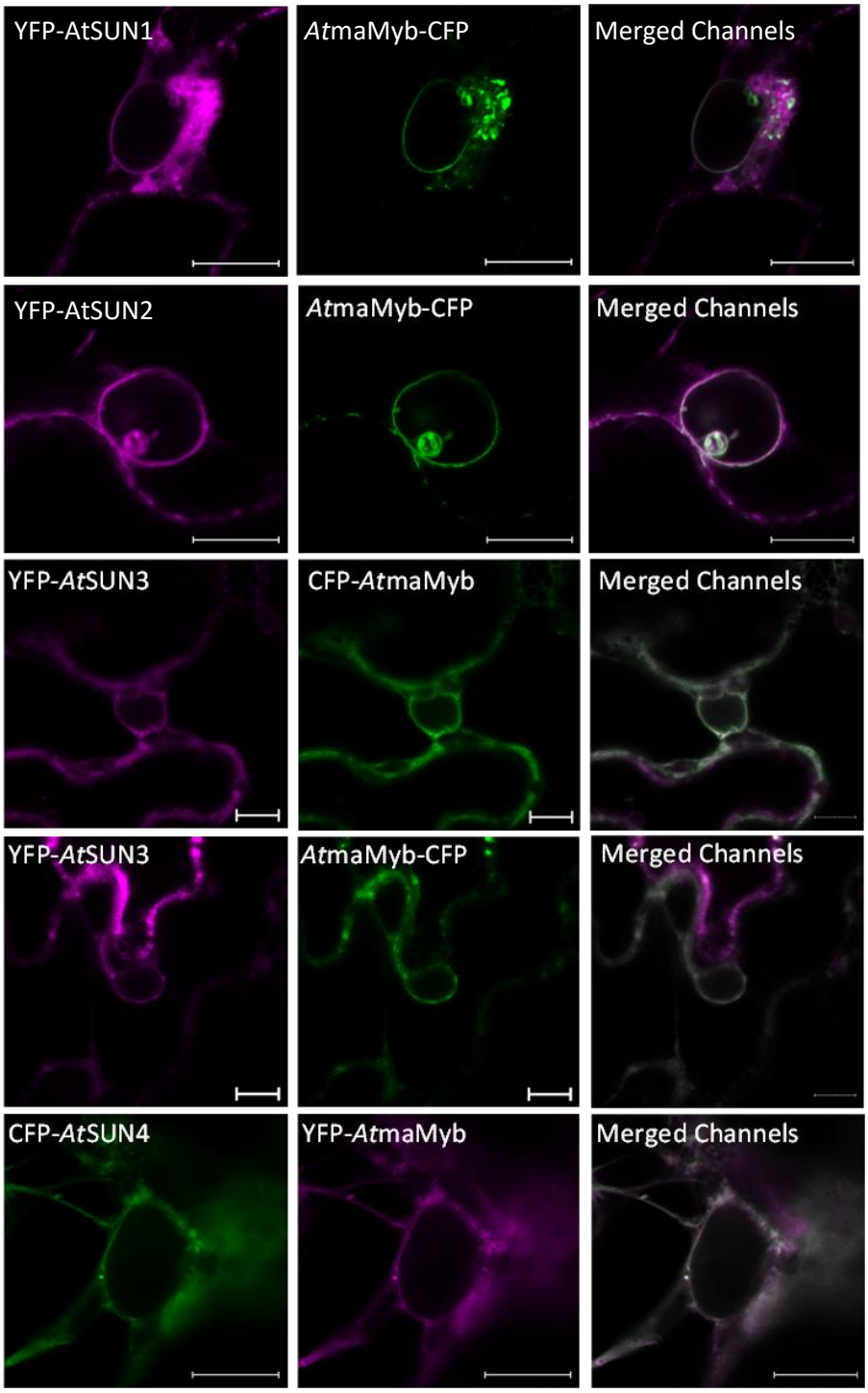

Figure 3.6. Confocal images of the Arabidopsis SUN proteins (both Cter-SUN and mid-SUN) co-expressed with *At*maMyb. Proteins were transiently co-expressed in *Nicotiana benthamiana* with p19. apFRET experiments were carried out at the nuclear envelope. (scale bar 10μm).

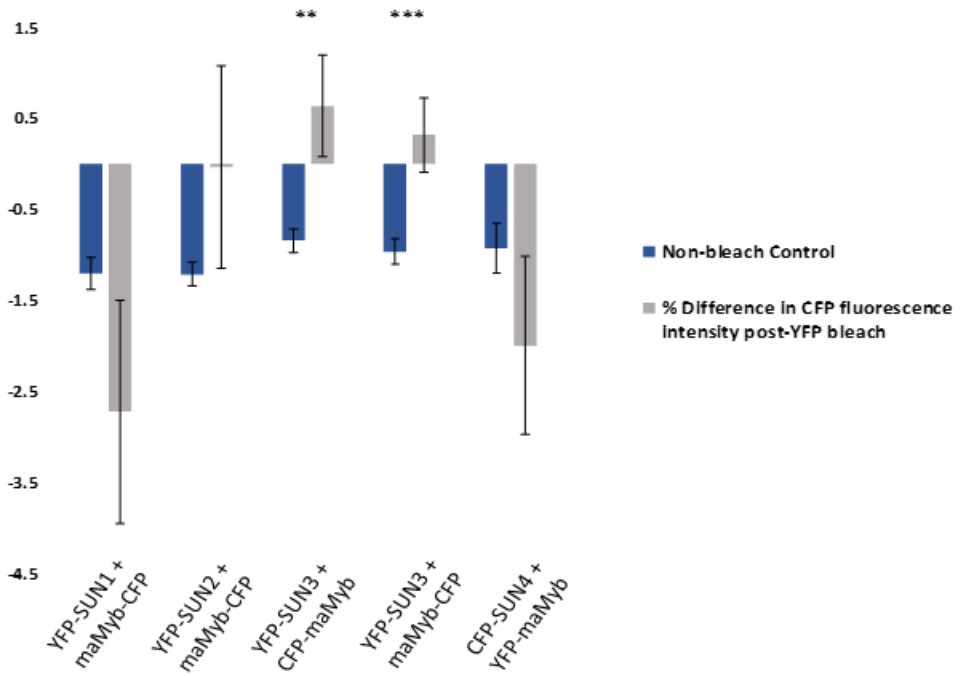

Figure 3.7. Interactions between the Arabidopsis SUN domain proteins and *At*maMyb, as measured by apFRET. FRET efficiency (E_F) was measured as changes in FI of CFP-tagged proteins after bleaching YFP-tagged proteins (blue). Protein-protein interactions were identified by significant increases in CFP fluorescence post-bleaching (n = 30+). Values shown are the percentage mean energy transfer ± standard error of the mean; control E_F values are calculated from pre-bleach measurements (grey).

Table 3.1. FRET efficiency (E_F) demonstrates interactions (or absence of interactions) between different components of the plant nuclear envelope. Positive protein-protein interactions are displayed in green.

Construct combinations	Experimental E_F ± S.E.M	Control E_F ± S.E.M	p-Value [t-test]
YFP-*At*SUN1 + *At*maMyb-CFP + p19	-2.72 ± 1.22	-1.2 ± 0.18	0.23
YFP-*At*SUN2 + *At*maMyb-CFP + p19	-0.03 ± 1.11	-1.21 ± 0.13	0.29
CFP-*At*maMyb + YFP-*At*SUN3 + p19	0.64 ± 0.56	-0.84 ± 0.13	0.01
*At*maMyb-CFP + YFP-*At*SUN3 + p19	0.32 ± 0.41	-0.96 ± 0.14	0.005
CFP-*At*SUN4 + YFP-*At*maMyb + p19	-1.99 ± 0.98	-0.92 ± 0.27	0.68

3.2.3 Localisation of *At*SUN3 Domain Deletions in Transiently Transformed Plant Cells

Single expression of CFP-*At*SUN3ΔN-terminus caused the protein to either localise to the NE or in the nucleoplasm (Fig. 3.8). CFP-*At*SUN3ΔSUN was not observed to localise to the nuclear periphery. Instead CFP-*At*SUN3ΔSUN was observed to localise in the nucleoplasm, indicating that removal of the SUN domain makes the protein soluble (Fig. 3.8). Only CFP-*At*SUN3Δcoiled coil and *At*SUN3Δcoiled coil-CFP were expressed in the NE and ER (Fig. 3.8). Due to their localisation CFP-*At*SUN3Δcoiled coil and *At*SUN3Δcoiled coil-CFP were used for apFRET experiments, whilst CFP-*At*SUN3ΔN-terminus and CFP-*At*SUN3ΔSUN were not. The optimal OD determined for expressing full-length mid-SUN proteins was also used to infiltrate plants with the *At*SUN3 domain deletions.

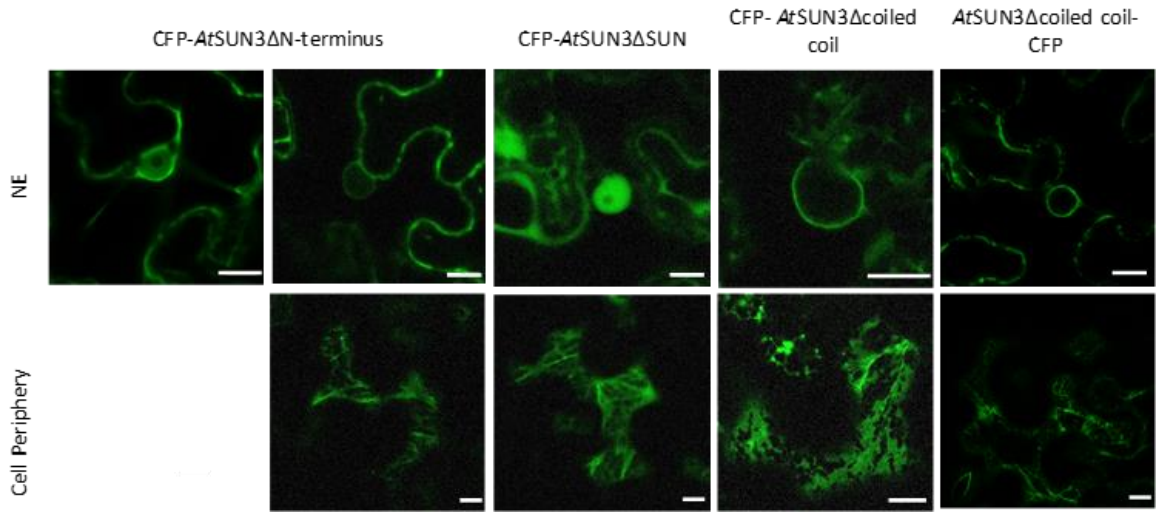

Figure 3.8. Sub-cellular localisation of *At*SUN3 domain deletion mutants transiently expressed in *Nicotiana benthamiana* with p19. *At*SUN3ΔN-terminus was found to be both cytosolic and NE localised. *At*SUN3ΔSUN showed cytosolic localisation, whilst *At*SUN3Δcoiled coil localised to both the NE and ER (scale bar 10μm).

3.2.3.1 Determining Protein-Protein Interactions between *At*SUN3Δcoiled coil and Full-Length Proteins

Upon determining that *At*SUN3 interacts with *At*maMyb, this interaction was investigated further by using the *At*SUN3 domain deletion mutants to identify which domains are required for an interaction to take place *in vivo*. apFRET experiments were carried out to investigate whether the coiled coil domain (CCD) of the *At*SUN3 protein is required to interact with *At*maMyb (see Figs. 3.9&3.10 and Table 3.2), as this was the only domain deletion mutant localised to the NE. It was found that an interaction between YFP-*At*maMyb and CFP-*At*SUN3Δcoiled coil did not take place (Experimental E_F = -2.1, control E_F = -0.21, p = 9.048E-03; see Figs. 3.9&3.10 and Table 3.2). This indicates that the CCD is required to mediate *At*SUN3-*At*MaMyb interactions.

Previous work has found that mid-SUN proteins are able to interact with themselves as well as other NE components (Graumann *et al.,* 2014; see section 1.5.2.2). To investigate whether the CCD is required for *At*SUN3 homomer formation, full-length *At*SUN3 and *At*SUN3Δcoiled coil were tested for interactions. It was found that YFP-*At*SUN3 can interact with *At*SUN3Δcoiled coil -CFP (Experimental E_F= 0.35, control E_F = -1.28, p = 7.50E-04; see Figs. 3.9&3.10 and Table 3.2). Interestingly however, YFP-*At*SUN3 did not interact with CFP-*At*SUN3Δcoiled coil (Experimental E_F = -0.65, control E_F= -0.17, p = 0.38; see Figs. 3.9&3.10 and Table 3.2). This would indicate that the terminal tag as well as the CCD can affect protein interactions.

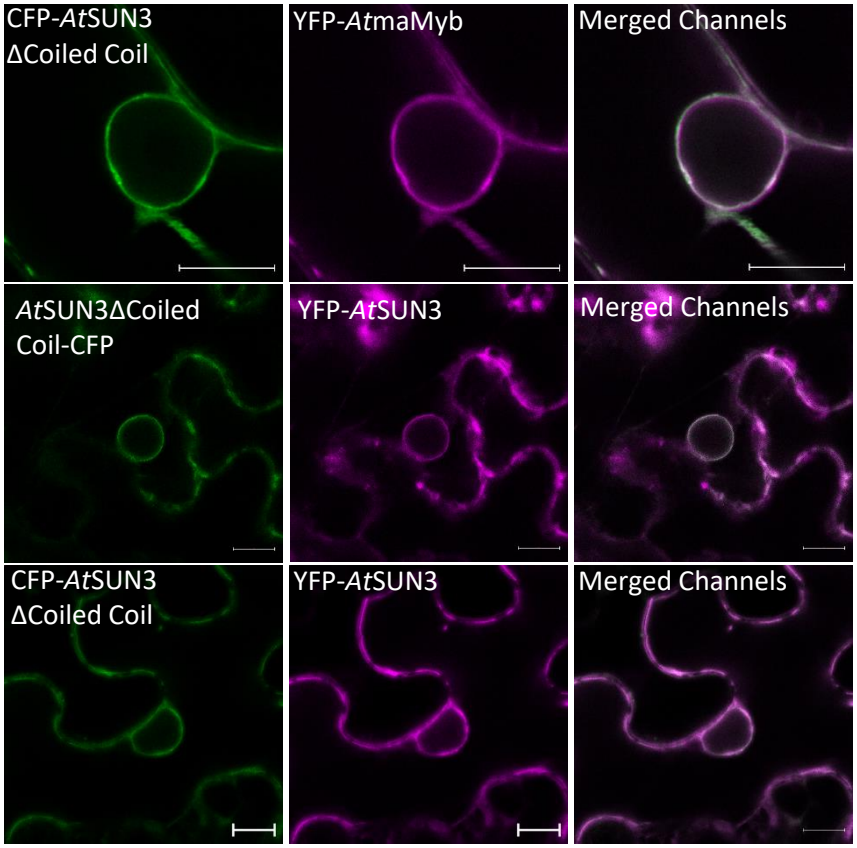

Figure 3.9. Confocal images of CFP-tagged *At*SUN3Δcoiled coil co-expressed with either full-length YFP-*At*SUN3, or YFP-*At*maMyb. Proteins were transiently co-expressed in *Nicotiana benthamiana* with p19. apFRET experiments were carried out at the nuclear envelope. (scale bar 10μm).

Table 3.2. FRET efficiency (E_F) demonstrates interactions (or absence of interactions) between different components of the plant nuclear envelope and *At*SUN3Δcoiled coil. Positive protein-protein interactions are displayed in green.

Construct combinations	Experimental E_F ± S.E.M	Control E_F ± S.E.M	p-Value (t-test)
CFP-*At*SUN3 Δ coiled coil + p19 + YFP-*At*maMyb	-2.1 ± 0.67	-0.21 ± 0.15	9.048E-03
YFP-*At*SUN3 + p19 + *At*SUN3Δcoiled coil- CFP	**0.35 ± 0.4**	**-1.28 ± 0.21**	**7.50E-04**
YFP-*At*SUN3 + p19 + CFP-*At*SUN3Δcoiled coil	-0.65 ± 0.51	-0.17 ± 0.19	0.38

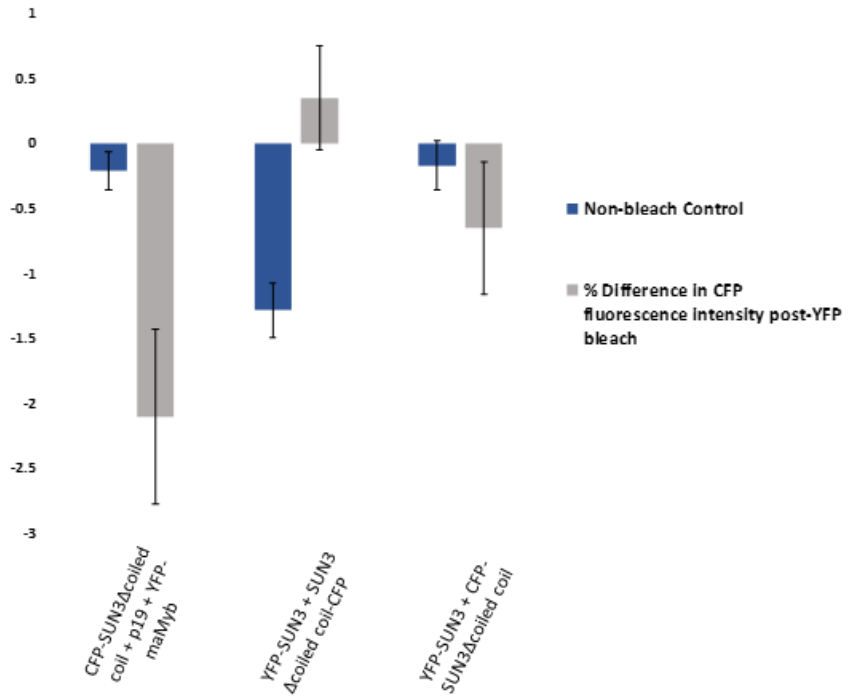

Figure 3.10. Interactions between *At*SUN3Δcoiled coil co-expressed with either full-length *At*SUN3 or *At*maMyb, as measured by apFRET. FRET efficiency (E_F) was measured as changes in FI of CFP-tagged proteins after bleaching YFP-tagged proteins (blue). Protein-protein interactions were identified by significant increases in CFP fluorescence post-bleaching (n = 30+). Values shown are the percentage mean energy transfer ± standard error of the mean; control E_F values are calculated from pre-bleach measurements (grey).

3.2.4 Investigating the Homo- and Heterodimeric Interactions of *At*SUN3 and *At*SUN4

Protein-protein interactions were determined by calculating fluorescence lifetimes for singularly expressed donor proteins and comparing them to those of donor proteins co-expressed with acceptor proteins (see sections 2.4.6 and 2.5.4). Green Fluorescent Protein (GFP)-fused proteins were considered as donors; the fluorescence lifetime of donor proteins were used as negative controls when expressed alone. Proteins fused to monomeric-RFP (mRFP) were used as acceptor proteins. Experiments were focused on testing which termini mediated homomeric and heteromeric interactions between *At*SUN3 and *At*SUN4 (Fig. 3.11).

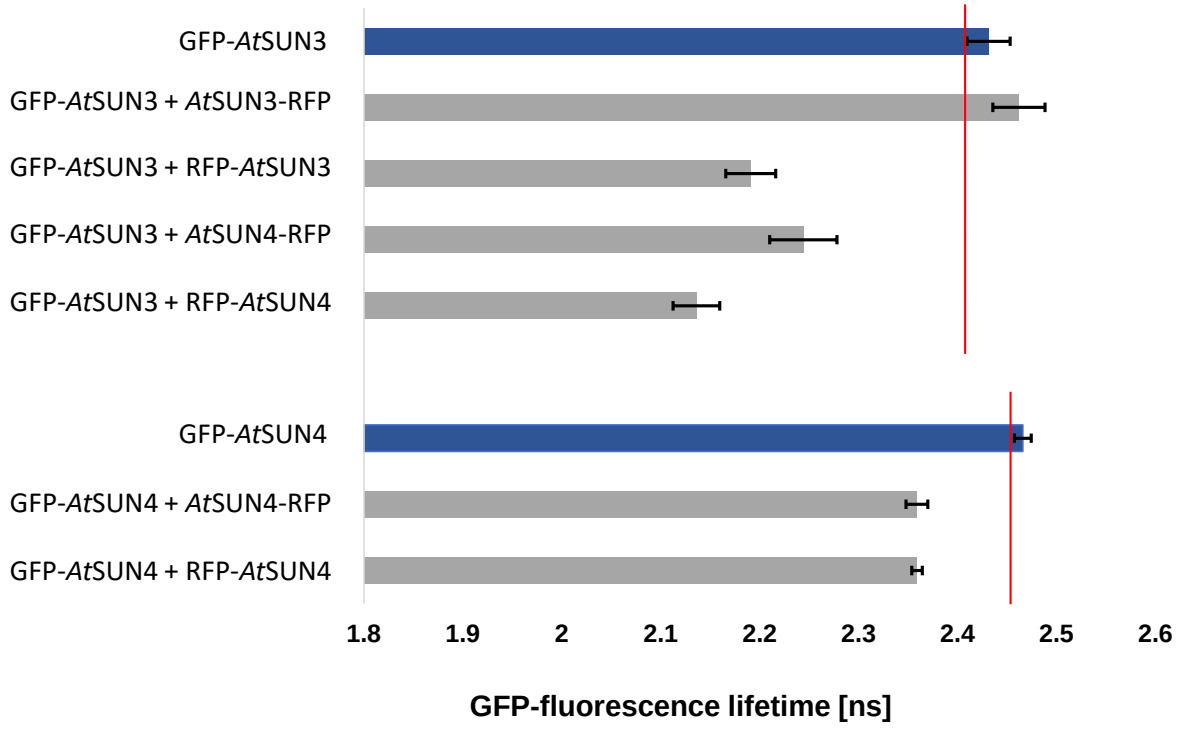

Figure 3.11. *At*SUN3 and *At*SUN4 interactions as measured using FRET-FLIM. Bar chart displays the fluorescence lifetimes (ns) for the donors GFP-*At*SUN3 and GFP-*At*SUN4 alone (shown in blue), and in combination with *At*SUN3 and *At*SUN4 fused to mRFP at either terminus as an acceptor (shown in grey). Combinations that have a measured GFP-fluorescence lifetime (ns) that is significantly lower than that of GFP-*At*SUN3 and GFP-*At*SUN4 alone (marked by a red line) indicate protein-protein interactions. Values shown are average fluorescence lifetime ± standard error.

Protein-protein interactions were defined as a GFP-mRFP fusion protein combination having a lower average fluorescence lifetime than that of a singularly expressed donor protein. For example, protein-protein interactions were detected between GFP-*At*SUN3 and RFP-*At*SUN4 as the fluorescence lifetime value (2.14 ± 0.024ns; Fig. 3.11) was lower than GFP-*At*SUN3 alone (2.43 ± 0.022ns; Fig. 3.11); this protein combination was used as a positive control. Analysing fluorescence lifetime values, interactions were shown between GFP-*At*SUN3 and *At*SUN4-RFP (2.36 ± 0.011ns; Fig. 3.11). It was also found that GFP-*At*SUN3 homodimerised with RFP-*At*SUN3 (2.19 ± 0.025ns; Fig. 3.11), but no interactions were detected between GFP-*At*SUN3 and *At*SUN3-RFP (2.46 ± 0.026ns; Fig. 3.11).

Protein-protein interactions using GFP-*At*SUN4 and mRFP-fused *At*SUN4 were also tested. Alone, the former was shown to have a fluorescence lifetime of 2.47ns (± 0.009; Fig. 3.11). GFP-*At*SUN4 was

shown to interact with RFP-*At*SUN4 (2.36 ± 0.005ns; Fig. 3.11), as well as *At*SUN4-RFP (2.36 ± 0.011ns; Fig. 3.11).

3.3 Discussion

This chapter focused on the localisation and interactions of *At*Mamyb, full length mid-SUNs and domain deletions of *At*SUN3 when transiently expressed as fluorescent protein fusions (see Figs. 3.6&3.9). Most of the constructs localised to the NE and ER, as expected from previous data (et al., 2010; Slabaugh et al., 2011; Graumann et al., 2014; Mermet, 2018) with the notable exceptions of *At*SUN4-CFP, CFP-*At*SUN3ΔN-terminus and CFP-*At*SUN3ΔSUN (Fig. 3.8). Constructs co-localised at the NE were then tested for their ability to interact *in planta* using apFRET (Figs. 3.7&3.10 and Tables 3.1&3.2).

The findings from these experiments showed that of all the SUN proteins tested, only *At*SUN3 interacted with *At*maMyb (Table 3.1 and Fig. 3.7). *At*SUN4 did not interact with *At*maMyb despite it also being a mid-SUN protein (Table 3.1 and Fig. 3.7). *At*maMyb was also found to not interact with the Cter-SUNs (Table 3.1 and Fig. 3.7).

Further investigation into which of the domains facilitated the interaction between *At*SUN3 and *At*maMyb showed that the CCD of *At*SUN3 was required (Table 3.2 and Fig. 3.10). This was not the case when investigating which domain of *At*SUN3 was required to interact with itself. *At*SUN3 was able to interact with itself without a CCD depending on which terminus of *At*SUN3Δcoiled coil was fused to a fluorophore (Table 3.2 and Fig. 3.10). A C-terminally tagged *At*SUN3Δcoiled coil protein did interact with a full-length *At*SUN3 protein, but an N-terminally tagged *At*SUN3Δcoiled coil protein did not (Table 3.2 and Fig. 3.10).

This chapter also investigated how *At*SUN3 and *At*SUN4 dimerise *in planta* (Fig. 3.11). The findings from the FRET-FLIM experiments showed that protein-protein interactions can be detected when

testing *At*SUN3 proteins that are both N-terminally tagged (Fig. 3.11). Interactions could not be detected however when testing an N-terminally tagged *At*SUN3 protein against another *At*SUN3 protein that was C-terminally tagged (Fig. 3.11). An N-terminally tagged *At*SUN3 protein was shown to interact with *At*SUN4 regardless of whether the latter was tagged at its N- or C-terminus (Fig. 3.11). Similarly, homomeric interactions were detected between N-terminally tagged *At*SUN4 and other *At*SUN4 proteins regardless of which terminus of the latter was tagged with a fluorescent protein (Fig. 3.11).

Table 3.3. mid-SUN-*At*maMyb interactions were tested using two different methods. Protein-protein interactions confirmed using both apFRET and MY2H screens are highlighted in green.

	Construct combinations	**Confirmed in MY2H**	**Confirmed in apFRET**
mid-SUN-*At*maMyb Interactions	***At*SUN3 + *At*maMyb**	**Yes**	**Yes**
	*At*SUN3Δcoiled coil + *At*maMyb	Yes	No
	*At*SUN4 + *At*maMyb	Yes (weak interaction)	No
***At*SUN3-*At*SUN3 Interactions**	*At*SUN3Δcoiled coil + *At*SUN3	Yes	Dependent on terminal fusion of fluorophore – YFP-*At*SUN3 + *At*SUN3Δcoiled coil–CFP positively interact, but not when using YFP-*At*SUN3 + CFP-*At*SUN3Δcoiled coil

3.3.1 Mis-localisation of *At*SUN3 Domain Deletion Mutants

As stated in section 3.2.3, deletion of the N-terminus and SUN domain caused fusion proteins to solubilise and be localised to the nucleoplasm and cytoplasm (Fig. 3.8). Protein misfolding is likely the reason that this occurs when CFP-*At*SUN3ΔSUN is expressed. By removing an internal domain within the protein, it is likely that this would affect overall protein structure. Deletion of the SUN

domain in Arabidopsis Cter-SUNs also results in a loss of NE labelling; these mutants instead aggregate in the cytoplasm (Graumann et al., 2010). In turn, these results differ to those found by Hodzic et al. (2004) where it was determined that the SUN domain of mammalian SUN2 did not affect its localisation.

In the case of CFP-*At*SUN3ΔN-terminus, the nucleoplasmic localisation observed suggests that the protein is unable to insert itself into the membrane properly. This differs to the localisation observed of N-terminal truncations of the Cter-SUNs. Unlike CFP-*At*SUN3ΔN-terminus, mRFP-*At*SUN1ΔN-terminus and YFP-*At*SUN2ΔN-terminus were still NE-localised when observed using confocal microscopy. Observations using EM however showed that they mainly localised to the ONM and ER (Graumann et al., 2010).

3.3.2 Structural Differences between mid-SUN Proteins May Result in Different Interaction Partners

Sequence alignment of *At*SUN3 and *At*SUN4 show that there is a sequence similarity of 61.6% (Uniprot). This can partially be attributed to the difference in size; *At*SUN3 has ~65aa more than *At*SUN4 (Uniprot; see Fig. 1.2). Analysis of sequence alignments between the two proteins show that there is decreased sequence similarity in the N-terminal region of the proteins, where the first TMD of each is located (Uniprot; see Fig. 1.2). There is also decreased sequence similarity in the region between the SUN domain and the C-terminus, a region that encompasses the CCD (Uniprot; see Fig. 1.2). It can be inferred from this that *At*SUN3 differs in its tertiary structure to *At*SUN4, and that it is these differences in structure that allow it to interact with *At*maMyb. The differences between the CCDs in particular may explain why *At*SUN4 cannot interact with *At*maMyb.

3.3.2.1 How the CCD of *At*SUN3 Contributes Towards Homomeric Interactions

The CCD is a likely candidate to mediate mid-SUN-protein interactions. This tertiary structure is comprised of at least 2 α-helices wrapped around one another to form a supercoil (Mason and Arndt, 2004). CCDs are regarded to mediate oligomerization (McAlinden et al., 2003), or act as molecular spacers that separate functional domains or structurally support macromolecular complexes (Wang et al., 2012; Truebestein and Leonard, 2016). However, they have also been observed to undergo conformational changes that can regulate a proteins function (Al-Bassam *et al.,* 2003; Kon *et al.,* 2009; Liu et al., 2013).

The CCDs of Cter-SUN proteins have been found to regulate protein activity and mediate LINC complex formations, as is the case with human SUN2 (Nie *et al.,* 2016). This work found that the two CCDs (CC1 and CC2) of SUN2 regulate the activity of the SUN domain; CC2 acts as a monomer that interacts with the SUN domain and keeps it in an inactive state (Nie *et al.,* 2016). On the other hand, CC1 forms a trimeric coiled coil that both activates and trimerizes the SUN domain of three SUN proteins (Nie *et al.,* 2016). It has been proposed that this dynamic regulation of the SUN domain by the two CCDs mediates its interaction with human KASH proteins, as well as its involvement in cellular processes such as nuclear envelope breakdown (NEBD; Nie *et al.,* 2016).

Research into the Arabidopsis Cter-SUNs found that the CCD of *At*SUN1 was required to form homomers, as determined by apFRET (Graumann *et al.,* 2010). FRAP experiments carried out on YFP-*At*SUN1Δcoiled coil and CFP-*At*SUN2Δcoiled coil showed increased mobility in these proteins compared to their full-length counterparts, indicating that the CCD of Cter-SUNs are involved in binding (Graumann *et al.,* 2010). The CCD of Arabidopsis Cter-SUNs has also been found to be required for interacting with mid-SUNs (Graumann *et al.,* 2014). A reduced interaction was detected between *At*SUN3 and *At*SUN1Δcoiled coil and/or *At*SUN2Δcoiled coil using MY2H assays. The interaction was not detected at all when testing *At*SUN4 with *At*SUN1Δcoiled coil and/or *At*SUN2Δcoiled coil (Graumann *et al.,* 2014). These experiments suggest that the CCD of mid-SUN

proteins play a similar role in mediating homomeric and heteromeric interactions. It was also found that *At*SUN1 and *At*SUN2 deletion mutants, where both the N-terminus and the SUN domain were removed, were still able to interact with *At*SUN3 and *At*SUN4 through their CCD (Graumann et al., 2014).

It is interesting to note that *At*SUN3Δcoiled coil-CFP was able to interact with full-length YFP-*At*SUN3, whilst CFP-*At*SUN3Δcoiled coil was not (Table 3.2 and Fig. 3.10). This was unexpected as the termini of *At*SUN3 are separated by a membrane, meaning an interaction between the N- and C-termini would be undetectable by apFRET. Apart from this one result, all apFRET experiments conducted using CFP-*At*SUN3Δcoiled coil has shown no interaction with its candidate partner (Table 3.2 and Fig. 3.10). Work carried out in a related project also showed that there was no detectable interaction between YFP-*At*SUN3 and CFP- *At*SUN3Δcoiled coil (E_F = -2.90 ± 0.83, p = 0.03424; Mermet, 2018). It is possible that the result from apFRET experiments testing interactions between YFP-*At*SUN3 and *At*SUN3Δcoiled coil-CFP is a false-positive, but no interactions between full-length *At*SUN3 and CFP-*At*SUN3Δcoiled coil have been detected in separate studies (Mermet, 2018). This indicates that this experimental result is repeatable. It is also possible that *At*SUN3 does not require its CCD to form homomers, but that these interactions are not detected when using CFP-*At*SUN3Δcoiled coil due to an obstruction of the N-terminus. Further testing of interactions between *At*SUN3-YFP and fluorescent fusion proteins of *At*SUN3Δcoiled coil tagged at either terminus would also provide further insight. If the CCD is required for homomeric interactions to take place, its removal may result in *At*SUN3's tertiary structure being altered so that it is no longer able to facilitate these interactions.

Additional experiments of interest would be to test interactions between *At*SUN3Δcoiled coil and full-length Cter-*At*SUNs. Whilst it has been demonstrated that the CCD of *At*SUN2 is not required to interact with *At*SUN3 using apFRET (Graumann *et al.,* 2014), it would provide useful insight as to whether the CCD of *At*SUN3 is required to interact with Cter-*At*SUNs. It would be especially intriguing if it did not, as it would raise further questions as to which domain mediates interactions between the two sets of *At*SUN proteins.

As well as this, apFRET experiments testing interactions between *At*SUN4 domain deletions and full-length *At*SUN proteins would also provide insight to as to how *At*SUN4 interacts with other proteins. It would be of interest to compare the results from these experiments with those focusing on how *At*SUN3 interacts with other proteins. Not only this but further investigation needs to focus on how *At*SUN3 and *At*SUN4 form heteromers with each other, as previously detected by both apFRET and MY2H screens (Graumann *et al.,* 2014).

3.3.2.2 Importance of *At*SUN3's CCD for Interacting with *At*maMyb

Given that mid-SUN orientation is unclear, there remains a potential for *At*SUN3's CCD to localise to a different sub-cellular compartment than the cytosolic termini of *At*maMyb (Slabaugh *et al.,* 2011). The detected interactions between mid-SUNs and Cter-SUNs, as well as with KASH proteins (Graumann *et al.,* 2014), suggest this to be the case. If this is so, then it is unlikely that the CCD of *At*SUN3 and *At*maMyb directly interact with one another. This would mean that a positive interaction between the two proteins should have been detected using apFRET regardless of whether *At*SUN3 possessed a CCD or not. However, the effect of deleting this domain might have resulted in misfolding to the point where the tertiary structure of *At*SUN3 no longer supported the interaction. Additionally, the evidence that the conformational state of CCDs in SUN proteins also regulate function suggests the *At*SUN3-*At*maMyb interaction cannot be properly facilitated without this domain (Nie et al., 2016). It is worth noting that when using the MY2H system that *At*SUN3Δcoiled coil and *At*maMyb can interact with each other, as can *At*SUN3ΔSUN and *At*maMyb (Tatout, personal communications). This further indicates that neither of these domains are required for the *At*SUN3-*At*maMyb interaction. The only *At*SUN3 deletion mutants found to not interact with *At*maMyb were *At*SUN3-core (which consisted of *At*SUN3's SUN domain alone), and *At*SUN3ΔN-terminus (Tatout, personal communications). *At*SUN3-core would not be able to interact with *At*maMyb as there are no other protein domains that would help to target it to the membrane. The latter truncation included the removal of *At*SUN3's first TMD (Tatout, personal

communications), which would result in interactions not being detected due to *At*SUN3 not being properly inserted into the membrane.

As well as investigating which of the other domains of *At*SUN3 are required to interact with *At*maMyb, further investigation can be carried out to identify which domains/regions of *At*maMyb mediate this interaction. MY2H assays have already shown that that *At*maMyb's N-terminus is required (Tatout, personal communications). It should be noted that this truncation included the removal of both of *At*maMyb's TMDs (Tatout, personal communications), meaning that interactions would not be detected due to *At*maMyb not being properly inserted into the ER membrane. Of all the *At*maMyb domain deletions tested however, only this deletion mutant was found to not interact with *At*SUN3 (Tatout, personal communications). This indicates that it is not the SANT domains of *At*maMyb (see section 1.6 and Fig. 1.3), nor any residues in the C-terminus of the protein that mediates its interaction with *At*SUN3. Further investigation can be carried out using apFRET to determine which of *At*maMyb's domains or regions interact with *At*SUN3, including the use of *At*maMyb deletion mutants that still maintain both TMDs.

3.3.3 Differences between Results Generated from apFRET and MY2H Screens

The use of MY2H screens has previously been used to test for interactions between NE proteins that have also been confirmed using apFRET. For example, interactions between *At*NEAP2 and the Arabidopsis Cter-SUNs were confirmed using both techniques (Pawar *et al.,* 2016). The use of MY2H screens verified the mid-SUN interactions detected using apFRET, which showed that *At*SUN3 and *At*SUN4 can interact with themselves and the Cter-SUNs (Graumann et al., 2014).

The results of the MY2H screens testing for interactions between *At*SUN proteins and *At*maMyb, as well as interactions between *At*SUN3Δcoiled coil and *At*maMyb, differ from those of the apFRET experiments (see Table 3.3). The MY2H screens detected interactions between *At*SUN proteins (1-5)

and *At*maMyb, whereas the apFRET results show that only *At*SUN3 and *At*maMyb interact (Tatout, personal communications; Tables 3.2&3.3). The MY2H results also identified that *At*SUN3Δcoiled coil and *At*maMyb interact (Tatout, personal communications; see Table 3.3) but this interaction was not detected when using apFRET (see Table 3.2). It was instead shown that the MY2H system could not detect interactions between *At*SUN3ΔN-terminus and *At*maMyb (Tatout, personal communications). As mentioned previously, this N-terminal truncation included the removal of the first TMD of *At*SUN3 (Tatout, personal communications). This interaction could not be tested using apFRET due to the mis-localisation of CFP-*At*SUN3ΔN-terminus when transiently expressed *in planta* (see Fig. 3.8).

There were also differences between the MY2H and apFRET results regarding interactions between *At*SUN3Δcoiled coil and full-length *At*SUN3 (see Table 3.3). The MY2H results showed that an interaction between *At*SUN3Δcoiled coil and a full-length *At*SUN3 protein was detected, which was the case when using apFRET to test *At*SUN3Δcoiled coil-CFP and YFP-SUN3 (Tatout, personal communications; Tables 3.2&3.3). MY2H tests could also not detect interactions between *At*SUN3ΔN-terminus and a full-length *At*SUN3 protein (Tatout, personal communications).

MY2H experiments testing interactions between *At*SUN4 and *At*maMyb have found that any interactions detected are weak (Tatout, personal communications), so it may be that this interaction is too weak to be detected using apFRET. It is also possible that *At*SUN4 can indirectly interact with *At*maMyb as a result of heteromerising with *At*SUN3, which is why it was not detected using apFRET. No MY2H screens have been carried out using *At*SUN4 as bait. Using this method, it would be interesting to see if *At*SUN4 could interact with any of the proteins found to interact with *At*SUN3 (Andov, 2014; Tatout, personal communications). It would be particularly interesting to see if an interaction with *At*maMyb could be identified.

Though the results from each technique differ, it is possible that this has occurred due to the limitations of both methods. Whilst the MY2H assay was specifically developed to act as a sensor of protein-protein interactions of intrinsic membrane proteins, one of its main limitations is that this

screen is carried out in *S. cerevisiae*. This raises the potential that protein interactions detected in this system may be true of what occurs in the yeast system, but not *in planta*.

In addition, there are restrictions of apFRET experiments that may also result in interactions not being identified; deleting integral domains of a protein will affect its tertiary structure and will likely cause misfolding. For an interaction to be confirmed using apFRET, potential interaction partners must be localised within 10μm without obstructions, such as a membrane. It may be that even though *At*SUN3Δcoiled coil and a potential interaction partner (e.g. *At*maMyb) are within a close enough distance of each other, the tertiary structure of *At*SUN3Δcoiled coil has been changed to the point that energy transfer can no longer take place. Changes in folding and tertiary structure may likewise be responsible for any false negative/positive results produced in the MY2H screens.

As well as this, there are published examples of differences between apFRET and MY2H data. One such example is that despite being able to detect interactions between *At*NEAP2 and the Cter-SUNs using the MY2H system, interactions were not detected when using *At*NEAP1 as bait. Both *At*NEAPs were found to interact with the Cter-SUNs using apFRET however (Pawar *et al.,* 2016).

3.3.4 Putative Function of *At*SUN3-*At*maMyb Interactions

The detection of an interaction between *At*SUN3 and an ER membrane protein such as *At*maMyb in both MY2H assays and apFRET points to a functional role outside of the LINC complex. This will require further investigation to prove this to be correct. It can however be speculated as to what this function may be. As previously stated (see section 1.6), *At*maMyb is a membrane bound TF; it is currently unknown how the catalytic part of this TF is cleaved and transported to the nucleus, or what DNA it binds to when it arrives there and what it regulates.

The apFRET and MY2H results indicate that *At*SUN3 interacts with the non-active TF, inferring that *At*SUN3 is not directly involved in the transport of the active TF. It is possible however that by interacting with each other, *At*SUN3 could bring the transcriptional domains of *At*maMyb into the

proximity of NPCs, where the active TF could then be transported into the nucleus upon cleavage. Alternatively, this interaction may be part of a larger multi-protein complex that contributes to the activation and transportation of *At*maMyb as part of a response to external stimuli. Further work needs to be carried out into the *At*SUN3-*At*maMyb complex, and in turn provide further understanding of *At*SUN3's overall functional role.

3.3.5 Investigation of mid-SUN Dimerisation *in planta*

These results further advance upon what had been reported by Graumann et al. (2014) using apFRET. In this work, it was shown using the MY2H system that *At*SUN3 and *At*SUN4 were able to homodimerise, as well as heterodimerise with each other (Graumann et al., 2014). It was also shown using apFRET that YFP- *At*SUN3 was able to interact with CFP-*At*SUN4 (Graumann et al., 2014). The results produced from the FRET-FLIM experiments confirm that mid-SUN proteins homo- and heterodimerise *in planta* (Fig. 3.11). In this manner, mid-SUN proteins can be likened to Cter-SUN proteins.

Regarding this protein sub-group, N-terminal fusions of *At*SUN1 and *At*SUN2 were shown to interact with themselves and each other using apFRET, proving that Cter-SUNs homodimerise and heterodimerise with each other *in planta* (Graumann et al., 2010). Similar observations were also made in mammalian SUN proteins (Zhou et al., 2012). These results also provide evidence that the N-terminus of Cter-SUN proteins are located on the same side of the INM as one another, due to the nature of FRET. Protein-protein interactions were detected when testing *At*SUN3 proteins that were N-terminally tagged, but not when testing interactions between an N-terminally tagged *At*SUN3 protein and a C-terminally tagged *At*SUN3 protein (Fig. 3.11). These results indicate that the two termini are located on different sides of the membrane to one another. However, homomeric interactions of *At*SUN4 were detected regardless of which protein terminus was tagged (Fig. 3.11). Both *At*SUN3 and *At*SUN4 are predicted to have three TMDs (Fig. 1.2; Uniprot), meaning that protein-protein interactions should only be able to be detected if both candidates are tagged at the

same terminus. Therefore, it could be suggested that *At*SUN4 has three TMDs rather than two, but this cannot be proven without further testing. It could also be considered that the protein-protein interaction detected between GFP-*At*SUN4 and *At*SUN4-RFP is a false positive (Fig. 3.11), and that it should not be used as an indication of *At*SUN4's topology in the membrane. Further testing using the same constructs in the apFRET system could demonstrate whether these results are repeatable whilst conducting topology studies in the meantime.

It is worth noting that the dimerisation of mid-SUN proteins has not yet been investigated outside of the plant kingdom, meaning these results may provide insight into this for mid-SUN proteins overall. It would be interesting to identify whether these interactions are also conserved throughout Eukaryota. Additionally, work could be done to see if these interactions are also conserved throughout plants, since there are no records of such work outside of Arabidopsis. For example, similar experiments could be conducted on *Zm*SUN3 and *Zm*SUN4 to observe whether they could also homo- and heterodimerise.

It would be of interest to investigate using either FRET-FLIM or apFRET (or preferably using both methods) which domains of either mid-SUN protein facilitate interactions with Cter-SUN proteins. As well as providing insight into the interaction network of the Arabidopsis SUN family, these results could provide further information into mid-SUN protein orientation in the membrane. FRET-FLIM could also determine interactions between *At*SUN3Δcoiled coil and full-length *At*SUN3, as well as *At*maMyb, and confirm the findings from either the MY2H or apFRET data regarding this.

3.3.6 Mid-SUN Proteins as Part of Protein Complexes

These results indicate that, similarly to Cter-SUNs, mid-SUN proteins can form multimeric protein complexes for cellular processes to be carried out. This is supported by the results of MY2H assays which showed that *At*SUN3 and *At*SUN4 can interact with Cter-SUNs as well as plant KASH proteins; the former interactions were also proven using apFRET (Graumann et al., 2014). By being able to

interact with components of the LINC complex *in vitro* and *in planta*, it is possible that mid-SUN proteins contribute to this complex in some manner.

It has previously been suggested that *At*SUN3 and *At*SUN4 may be involved in different protein complexes based on differences in their mobility as determined by FRAP experiments (Graumann et al., 2014). *At*SUN3 was shown to be more mobile in the NE than the ER, whereas *At*SUN4 mobility was similar in both sub-cellular compartments (Graumann et al., 2014). This is supported by the findings that *At*SUN3 was found to interact with *At*maMyb, but that *At*SUN4 was not (Fig. 3.7). If there truly is a difference in the topology of *At*SUN3 and *At*SUN4, as suggested by these findings (Fig. 3.7), then this may account for why these differences were observed.

Further investigation into these interactions shall be required to determine the composition of these protein complexes, as well as the circumstances under which they take place.

3.4 Conclusions

Overall, the *in vivo At*SUN3-*At*maMyb reported in this work supports previous evidence of their interaction in MY2H. The fact that none of the other *At*SUN proteins can interact with *At*maMyb suggests that this is potentially a *At*SUN3-specific function. Investigating *At*SUN3-*At*maMyb complexes further may also provide further insight into mid-SUN function, particularly one outside of the LINC complex. Any differences observed between the MY2H and apFRET experiments involving mid-SUN mutants are likely to be due to a combination of experimental limitations for both techniques, as well as differences in how the mutants were constructed. It was also demonstrated that *At*SUN3 and *At*SUN4 can homodimerise *in planta* supporting previous evidence of these interactions detected using the MY2H system. The interactions detected using FRET-FLIM also indicate that the number of TMDs may differ for each mid-SUN protein that was tested. Ultimately this work shall contribute to understanding how mid-SUN proteins fit into the dynamic protein network of the NE and encompassing ER.

Chapter Four | Investigating the Enrichment of the Arabidopsis mid-SUN Proteins at the Nuclear Periphery

4.1 Introduction

As previously stated, *At*SUN3 and *At*SUN4 were observed to localise to both the NE and ER and were reported to be enriched at both organelles (Graumann et al., 2014). Because of this, as well as the detected interactions between mid-SUN proteins and LINC complex components (Graumann et al., 2014), it was suggested that the mid-SUN proteins localise to the NE as Cter-SUNs do. The work carried out during this project has indicated that this may not be the case. Through the confirmed interactions of *At*SUN3 with the ER membrane-localised protein *At*maMyb, and comparisons with mid-SUN domain proteins in other kingdoms (Sohaskey et al., 2010; Friederichs et al., 2012; Vasnier et al., 2014), the exact location of the Arabidopsis mid-SUNs at the nuclear periphery are now being called into question.

Primarily, the expression of fluorescent fusion proteins allows for their subcellular localisation to be observed using CLSM (Colcombet et al., 2013; Brown et al., 2017; Fu et al., 2021). Through observing which organelle fluoresces, it can be proposed that the protein of interest is localised there. If protein localisation cannot be resolved by eye when fluorescent fusion proteins are observed using CLSM, as is the case with NE proteins (Zhou et al., 2012; Groves et al., 2019), further investigation can be undertaken to determine this.

Quantitative data can be acquired through measuring the FI of a protein, which is defined as the amount of light produced by a fluorophore upon excitation. Measuring FI underpins numerous imaging techniques that can be used to provide information that can further characterise a protein of interest. These include (but are not limited to) apFRET which is used to determine protein-protein interactions (as discussed in the previous chapter), and Fluorescence Recovery After Photobleaching (FRAP) which can inform on protein trafficking and binding (Graumann et al., 2014; Pawar et al., 2016; Weems et al., 2017).

One such means of using FI to inform upon a protein of interest's localisation to the NE is by calculating NE-ER FI ratios. The intensity of a fluorescent fusion protein is measured at both organelles and used to calculate a final value, which is then compared to that of control proteins in order to assess which organelle the protein is enriched in (Onischenko et al., 2007; Meinema et al., 2011; Zhou et al., 2012; Graumann et al., 2014; Groves et al., 2019). Due to the ER membrane being contiguous with the ONM, calculating protein enrichment as a ratio is more informative than simply comparing raw values.

This technique has been shown to be suitable for use in resolving protein localisation at the NE. For example, the NE-ER FI ratios calculated for the reporter protein h2NLS-L-TM in *S. cerevisiae* that indicated its enrichment at the INM were validated by ultrastructural analyses (Meinema et al., 2011). In this work, it was shown that the NLS signal of this protein is required for its import to the INM through NPCs. NE-ER FI ratios have also been used to demonstrate how particular Nups are recruited to NPCs in rat models (Onischenko et al., 2007). Due to being reported to resolve the localisation of NE components in multiple kingdoms, calculating NE-ER FI ratios can therefore be considered a suitable method to use in the investigation of protein localisation at the nuclear periphery.

Similar ratios have been used in previous publications to report on the enrichment of candidate NE proteins at the nuclear periphery in plant cells (Zhou et al., 2012; Graumann et al., 2014; Groves et al., 2019). In these studies, NE-ER FI ratios are referred to as NE Localisation Indices

(NLIs) and shall be referred to as such in this thesis. For instance, NLI calculations was one of multiple methods used to assess the targeting of the ER membrane proteins Pamp-Induced Coiled-Coil (PICC)-Like (PICL) to the NE after they were fused with a NLS (Groves et al., 2019). In another publication, this method was used to show that the Arabidopsis Cter-SUNs localise *At*WIP1 and *At*RanGAP1 to the NE by comparing their enrichment at the NE in wildtype and mutant lines (Zhou et al., 2012).

The work in this chapter aims to further assess the enrichment of *At*SUN3 and *At*SUN4 at the NE when heterologously expressed as fluorescent protein fusions *in planta*. Image acquisition and analysis are described in sections 2.4.2, 2.5.1 and 2.5.2. These results generated from this analysis will contribute to the investigation concerning mid-SUN localisation in plant cells (see Chapter 5).

4.1.1. Aims

The FI experiments described below were carried out to determine whether *At*SUN3 and *At*SUN4 are more enriched in the NE or peripheral ER. Subsequently the work in this chapter provided a preliminary insight into the localisation of the Arabidopsis mid-SUN proteins and how it potentially differed to that of Cter-SUN proteins.

4.2 Results

Before calculating the NLI of the Arabidopsis mid-SUN proteins, the methods outlined in section 2.4.2 were first used to conduct a series of control experiments. This was done to determine that adjustments made to the method yield accurate results, as well as to provide representative NLI ratios for INM- and ER-enriched proteins. Two established markers were used: *At*SUN2-YFP as a NE membrane marker, and GFP-RTN1 as an ER membrane marker. *At*SUN3 fused to an N-terminal RFP

and *At*SUN4 fused to a C-terminal RFP, RFP-*At*SUN3 and *At*SUN4-RFP, were used to provide a comparison to previous findings regarding mid-SUN enrichment. The use of approximately 30 nuclei for each control group allowed for analysis of protein enrichment at the NE and ER. The representative images of each construct were then used in the analysis of NLI ratios (Fig. 4.1).

The sub-cellular localisation of each construct was observed to differ, except for the mid-SUN fusion proteins which were localised in the same sub-cellular compartments (Fig. 4.1). GFP-RTN1 was found to localise in both the NE and ER. Interestingly, once this protein was observed at the plane where nuclei were closest to their medial point, it localised mostly to the NE and only some ER membrane at the periphery of the cell was observed (Fig. 4.1). Distinct tubules and cisternae were observed more in the highest and lowest planes of individual cells. By comparison, mid-SUNs varied in their amount of ER labelling with less observed at peripheral locations and more labelling of ER tubules and cisternae observed at the medial plane (Fig. 4.1). Localisation of *At*SUN2-YFP was observed almost exclusively at the NE, with little localisation observed in the ER (Fig. 4.1).

By calculating NLI ratios from intensity profiles intersecting the NE and ER of the same Z-stack layer in ImageJ, differences were able to be drawn between the NLI ratios of both control and mid-SUN fluorescent fusion proteins (See section 2.5.1; Figs. 2.3 and 4.2).

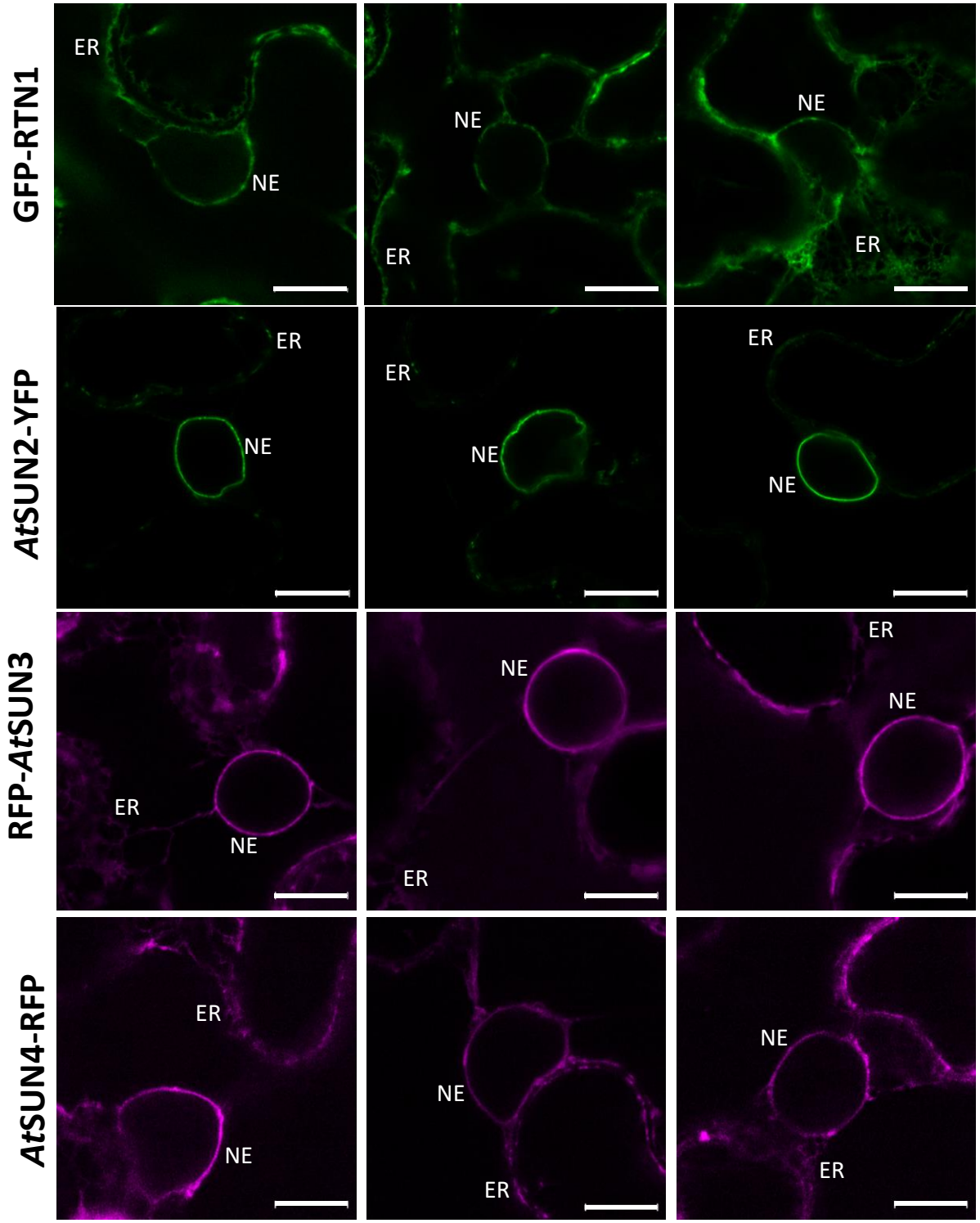

Figure 4.1. Representative images of fluorescent fusion constructs used for calculating NLI ratios, collected after transiently expressing constructs in the leaf epidermal cells of *N. benthamiana*. GFP-RTN1 and *At*SUN2-YFP were used as control markers for NE and ER ratios, respectively. RFP-fusion proteins of *At*SUN3 and *At*SUN4 proteins were used to expand upon previous studies of their sub-cellular enrichment. A minimum of 30 images were used to analyse each construct [Nucleus – 10µm; ER - 2 µm].

The largest NLI value was calculated for *At*SUN2-YFP (3.3 ± 0.28), whilst lower ratios were calculated for GFP-RTN1, RFP-*At*SUN3 and *At*SUN4-RFP (1.2 ± 0.09, 1.4 ± 0.09, and 1.2 ± 0.07, respectively). The same trend was also observed for variability within the datasets, as displayed by the error bars (Fig. 4.2). These results show that when using this method, high NLI values indicate that a protein is NE-enriched, whilst low NLI ratios indicated that a protein is ER-enriched (Fig. 4.2). Concurrently these results indicated that full-length mid-SUN proteins are more ER-enriched (Fig. 4.3), as opposed to the equal distribution across both compartments that was previously published (Graumann et al., 2014).

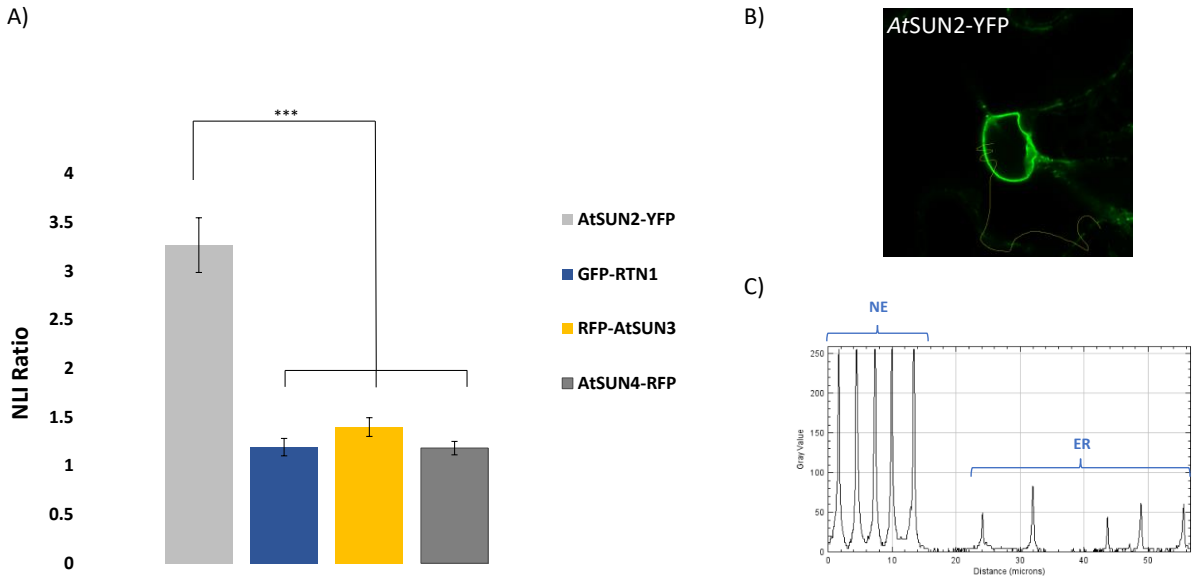

Figure 4.2. Image analysis used to produce NLI ratios of ER and NE proteins. A) NE/ER fluorescence intensity ratios as measured for NE marker *At*SUN2-YFP, ER marker GFP-RTN1, as well as for RFP-*At*SUN3 and *At*SUN4-RFP, when transiently co-expressed with p19 in *N. benthamiana* leaf epidermal cells (excepting GFP-RTN1). A minimum of 30 nuclei were analysed for each construct tested. There were statistically significant differences between group means as determined by Kruskal-Wallis H test, $\chi 2(3) = 48.95$, p=1.377e-10. B) Typical line profile drawn through both the NE and ER sub-compartments. C) Intensity profile generated from line profiles drawn.

The total cohort of NLI ratios calculated were shown to be statistically significant from one another (p=1.377e-10), The control ER marker GFP-RTN1 was shown to have a statistically significant NLI to the control NE marker *At*SUN2-YFP (p = 4.6e-09), indicating that it is ER-enriched and subsequently

that NE and ER-enrichment can be distinguished from one another. It was also found that the NLI ratios calculated for RFP-*At*SUN3 and *At*SUN4-RFP significantly differed to that calculated for *At*SUN2-YFP (p =5.8e-06 and 2.8e-08, respectively), but not when compared to GFP-RTN1 (p =1 for both).

4.3 Discussion

This work focused on determining whether the Arabidopsis mid-SUN proteins were more enriched at the NE or the ER. Data was acquired by measuring the FI of both organelles at the same Z-layer; proteins of known localisation and enrichment at the nuclear periphery were used as controls. The NLI ratios calculated from these datasets were used as comparisons when assessing the enrichment of RFP-*At*SUN3 and *At*SUN4-RFP at the nuclear periphery.

The results shown in this thesis differ to the data produced in Graumann *et al.* (2014). Instead of showing that mid-SUN proteins are enriched at both the NE and ER, the NLI ratios calculated for both mid-SUN proteins were not significantly different to that calculated for GFP-RTN1 (Fig. 4.2; p=1). On the other hand, the NLI ratio calculated for *At*SUN2-YFP was significantly different to those calculated for RFP-*At*SUN3 and *At*SUN4-RFP (Fig. 4.2; p =5.8e-06 and 2.8e-08, respectively). Additionally, the NLI ratios calculated for each mid-SUN protein were also found to not significantly differ from one another (Fig. 4.2; p=1 for both), indicating that they are enriched at the same part of the nuclear periphery.

These results therefore indicate that whilst observed by eye to localise to both the NE and the ER when transiently expressed *in planta* (Fig. 1.2 & 4.1; Graumann *et al.* 2014), that mid-SUN domain proteins are more enriched in the ER (Fig. 4.2; p=1.377e-10). This differs in comparison to their Cter-SUN counterparts, which localise almost exclusively to the NE when transiently expressed *in vivo* (Fig. 4.1). The NLI ratio calculated for *At*SUN2-YFP was significantly different to that calculated

for GFP-RTN1 (Fig 4.2; p = 4.6e-09), indicating that they are indeed NE-enriched (Fig. 4.2; Graumann *et al.* 2014).

At the very least, these results indicate that *At*SUN3 and *At*SUN4 are not enriched at the NE as Cter-SUNs are (Fig. 4.2; p =5.8e-06 and 2.8e-08, respectively). The Arabidopsis Cter-SUN proteins have been shown to localise to the INM (Graumann et al., 2010), and have previously been used as an NE control for published NLI ratio analyses (Graumann et al., 2014); RTN1 however has been shown to localise to the ER membrane (Sparkes et al., 2010). Therefore, the fact that the NLI ratios calculated for both mid-SUNs are not significantly different to that calculated for GFP-RTN1 (Fig 4.2; p=1 for both) indicate that they are ER-enriched. Since the ONM and the ER membrane are contiguous with one another however, it is also possible that the mid-SUNs are located to the ONM rather than the ER membrane.

These results support the protein-protein interaction detected between *At*SUN3 and *At*maMyb (Fig. 3.7 and Table 3.10). Due to the latter being localised to the ER membrane (Slabaugh et al., 2011), these results indicate that this interaction can indeed take place (Fig. 4.1). Additionally, these results also correlate with the reported localisation of mid-SUN proteins outside of Arabidopsis; for example, mid-SUN proteins have been reported to localise to the ER in chickpeas, mice, fungi and yeast (see section 1.5.2; Sohaskey et al., 2010; Friederichs et al., 2012; Jaiswal et al., 2014; Vasnier et al., 2014). In consideration of this, these results raise further questions about the function of the mid-SUN proteins at the NE.

It would be of interest to carry out these experiments using the *At*SUN3Δcoiled coil deletion mutants used in the apFRET experiments described in the previous chapter (see Chapter 3). By investigating whether deletion of the CCD affects *At*SUN3's enrichment at the nuclear periphery, the results could provide further information regarding how the functional domains of mid-SUN contribute to their localisation.

Although these results provide further evidence to suggest that the mid-SUN proteins are not localised to the NE, further work is required in order to investigate this. The results of NLI ratio analyses are commonly used in conjunction with other experiments to assess protein localisation at

the NE. For example, the work carried out on the targeting of PICL proteins to the NE used NLI ratios in conjunction with another high-resolution confocal imaging technique to assess their localisation (see Chapter 5; Groves et al., 2019).

4.3.1 Comparison of Findings to Previously Published Data

Reasons as to why results differ between these experiments and those published by Graumann *et al.* (2014) can be potentially attributed to differences in the way the experiments were carried out. Whilst the underlying principal remained the same, a different methodology was used to acquire the images prior to analysis. In the work carried out in Graumann *et al.* (2014), cells that transiently expressed a construct of interest underwent a Latrunculin B treatment 30 minutes prior to imaging. Latrunculin B is a drug treatment that has been shown to disrupt F-actin formation, resulting in the induction of cisternae which either reduces ER movement or halts the organelle from moving altogether (Spector et al., 1989; Gupta and Heath, 1997). FI was measured at several points in the cisternae of ER and the uppermost layers of the NE that were cisternae-like in appearance (Graumann *et al.,* 2014), meaning that two separate images from the same cell were used to calculate an NLI ratio. From reviewing the Z-stacks acquired during this project, it has been observed that FI of an organelle differs depending on which plane is being observed. For example, the FI of GFP-RTN1 is higher in the upper and lower layers of the nucleus where more of the ER network can be observed compared to the middle layers, where the NE is best observed and lower proportions of the ER are visible. This indicates that light scattering differs throughout the cell, meaning that calculating NLI ratios from multiple planes are less comparable due to the disproportionate levels of fluorescence being used.

The method used in these experiments followed the protocol of Zhou *et al.* (2012) and Groves *et al.* (2019) where only a single image was used to measure FI, with the only addition to the protocol being that Z-stacks were used. This was done to ensure that the most suitable Z-layer from the stack was selected for image analysis. By measuring the intensity of the two different sub-compartments

from the same image, the two sets of FI values are more comparable and therefore are more likely to be accurate. Notably, lower NLI ratios in the Groves *et al.,* (2019) studies were also indicative of ER-enrichment; the NLI ratios of PICL proteins that had been fused to an NLS were found to be significantly higher compared to those that had not. This can be attributed to the fact that in this work and the Groves *et al.,* (2019) work that NLI ratios were calculated as NE/ER values, whereas in the work published by Graumann *et al.* (2014), NLI ratios were calculated as ER/NE values.

4.3.2 Conclusions

To conclude, these results show that Arabidopsis mid-SUNs are more ER-enriched rather than being distributed throughout both the ER and NE as previously described. It also highlights a difference in enrichment between this SUN protein sub-group and the more thoroughly characterised Cter-SUNs. These results alone cannot prove that *At*SUN3 and *At*SUN4 are localised to a specific sub-cellular compartment but can be used to provide evidence about this in conjunction with other experiments. These results do however show that this needs to be investigated, as the implications of their being localised to a region outside of the NE could be profound within the context of this field. Further work on the localisation of *At*SUN3 and *At*SUN4 is discussed in the next chapter.

Chapter Five | Resolving the sub-cellular localisation of the mid-SUN proteins using Airyscan Localisation Microscopy Analysis

5.1 Introduction

Microscopy is one of the principal tools of cell biology research and encompasses a range of different techniques that are all used to further understanding within the field (Narayan et al., 2014; West et al., 2016; Dufrene et al., 2017; Versari et al., 2017; Chang et al., 2021). One such way that microscopy can do this is by identifying the localisation of proteins within specific sub-compartments of the cell (Peddie et al., 2017; Ariotti et al., 2018; Tuijtel et al., 2019; Dvořák et al., 2020).

Differentiating between the NE- and PNER-localisation of a protein using imaging techniques however is technically challenging. EM is a common technique used to identify the sub-cellular localisation of NE/ER proteins. This particular technique is highly regarded due to its ability to generate high resolution images; sub-nanometer resolution can be achieved using both scanning electron microscopy (SEM) and transmission electron microscopy (TEM; Armstrong et al., 2007; Vladár et al., 2009). It is for this reason that EM is the only technique considered sufficient enough to resolve the sub-cellular localisation of a protein (Ellenberg et al., 1997; Kim et al., 2006; Zuleger et al., 2011; Wang et al., 2016; Oliver et al., 2020). For example, immunogold labelling of mRFP-*At*SUN1 and YFP-*At*SUN2 identified that they were INM-localised at the plant NE (Graumann et al., 2010).

Even using this method however, there are still considerations to be made; the distance between the INM and ONM is reported to be 50nm. Due to the nature of the methodology, the combination of the primary and secondary antibodies can result in gold particles being visualised 15-30nm away from

the site of the target protein (Hermann et al., 1996). Such occurrences can cause difficulties in distinguishing protein localisation, therefore reducing the spatial resolution that this method offers of localising proteins at the NE. More importantly for this project, antibodies were not available to *At*SUN3 or *At*SUN4, and the use of antibodies to the available FP-constructs would further reduce the resolution of the technique. However, a recently developed live-cell imaging technique that had been used to explore protein localisation at the NE was suggested to provide sufficient resolution to differentiate NE and PNER localisation (Groves et al., 2019).

5.1.1 Using Airyscan Confocal Microscopy to Resolve the Sub-Cellular Localisation of Proteins

CLSM is a standard technique used throughout the biological sciences (Stricker et al., 1992; Hutzler et al., 1998; Jalbert et al., 2003; Tan et al., 2005; Margues et al., 2015; Santana et al., 2020). CLSM can be used to produce optically sectioned images by blocking out-of-focus light (Cox and Sheppard, 2004). This is achieved through a combined use of a single pinhole and a unitary detector (Conchello and Lichtman, 2005). The size of the pinhole can vary, which consequentially affects optical section thickness, spatial resolution and signal-to-noise ratio (SNR; Conchello and Lichtman, 2005). The smaller the pinhole, the better the spatial resolution of an image. However there is a practical disadvantage to this, whereby the use of a very small pinhole would result in few of the emitted photons reaching the detector. As a result, the default pinhole size is set to 1 Airy Unit (AU) to provide the optimal balance between SNR and spatial resolution (Cox and Sheppard, 2004).

The Zeiss Airyscan detector is comprised of a 32-channel GaAsP photomultiplier tube (PMT) array, with each individual detector set to 0.2-AU (Fig. 5.1; Huff, 2015). This design enables confocal imaging to be carried out with both increased SNR and spatial resolution. By projecting 1.25-AU onto the detector using zoom optics, the collection efficiency of this larger pinhole size can be maintained whilst each detector uses 0.2-AU (Fig. 5.1; Huff, 2015). By allowing for more light to be collected than in standard CLSM, higher contrast images can be collected without increasing noise. Concurrently,

the inclusion of a deconvolution step results in increased image resolution. Through these means, the Airyscan detector enables high-quality imaging whilst still allowing for optical sectioning as with CLSM (Fig. 5.1; Huff et al., 2017; Korobchevskaya et al., 2017). Specifically, it can provide a lateral resolution to 120nm, and an axial resolution to 350nm (Huff et al., 2017).

Since its launch, CLSM coupled with the use of an Airyscan detector has not only been used to provide high-quality images, but also to produce data for image analysis. One example that is relevant to this research was how Airyscan was used to resolve the localisation of proteins targeted to the plant NE. In this work, the ER membrane proteins Pamp-Induced Coiled-Coil (PICC)-Like (PICL) were fused with a nuclear localisation signal (NLS) to observe if they would be targeted to the NE (Groves et al., 2019). As well as calculating NLI ratios of PICL proteins, both unmodified and modified, image analysis was conducted using images of the target proteins at the NE to identify if they were truly NE localised (Groves et al., 2019). This work even went so far as to determine which NM the candidate proteins were localised to (Groves et al., 2019). This was achieved by using several line profiles drawn across the NE to measure the FI of each candidate protein.

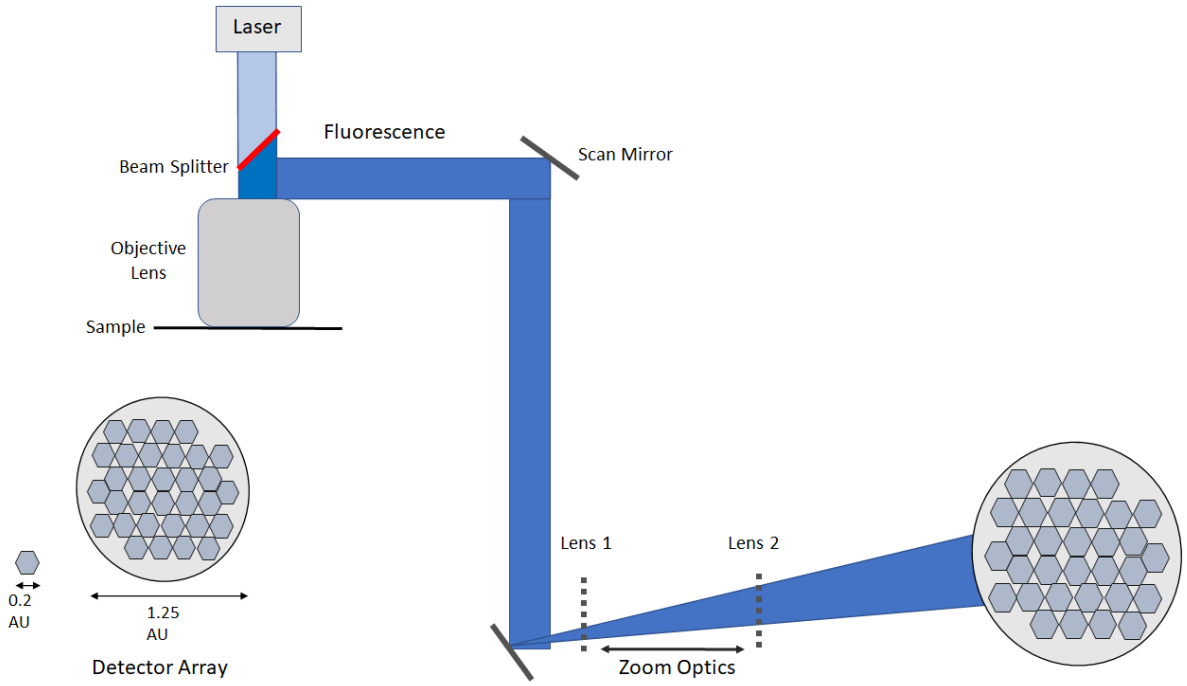

Figure 5.1. Graphic representation of the Zeiss Airyscan detector configuration when used in addition to a confocal microscope. The 32 -channel GaAsP photomultiplier tube array of the Airyscan detector is arranged in a hexagonal pattern; each individual channel is set to 0.2-AU. This is used in place of a singular pinhole and detector, and uses zoom optics to project 1.25-AU onto the detector. This produces images that have a greater resolution and an improved signal-to-noise ratio (adapted from Korobchevskaya et al., 2017).

Peak FI for each candidate was compared to that measured for the ER membrane protein CXN-mCherry, which was used as a marker of the ONM/ER continuum (Liu et al., 2017). By comparing line profiles of candidate proteins to a 'reference' protein, statistical comparison using Pearson's correlation co-efficient and one-way Analysis of variance (ANOVAs) tests were carried out to determine whether proteins were INM or ONM localised (Groves *et al.*, 2019). Using this method, it was identified that PICL can indeed be targeted to the INM if fused to an NLS (Groves *et al.*, 2019).

Although the spatial resolution of this method is significantly lower than that of immunogold labelling, the work described above demonstrates that Airyscan confocal microscopy is a viable alternative. Since the maximum resolution of Airyscan microscopy (120nm) is greater than the distance between the INM and ONM (~30-50nm), this means that localisation cannot be resolved visually when using this method. By recording multiple measurements of fluorescent proteins of

known localisation at the plant NE however, these can be used as a comparison when investigating proteins of unknown localisation.

Previously publication have been directed towards determining the localisation of *At*SUN3 and *At*SUN4, and investigating their interactions, as components of the LINC complex at the NE (specifically at the INM like Cter-SUNs). The results presented in previous chapters (see Chapters 3&4) suggest ER-membrane localisation. Rather than localising to both the NE and ER, the ER-enriched NLI ratio (see Chapter 4) of both mid-SUN proteins, as well as the positive interactions between *At*SUN3 and *At*maMyb (see Chapter 3) infer that the Arabidopsis mid-SUN proteins may not be NE-localised after all. Subsequently, Airyscan microscopy was used to determine the localisation of *At*SUN3 and *At*SUN4. The original method used in Groves et al., (2019) was further refined throughout the duration of this work and is described below.

In this chapter, fluorescent probes of known localisation at each nuclear membrane are used. For the purposes of this work, nuclear membranes include the INM, ONM and potentially the closely associated perinuclear ER (PNER). The ONM is considered an extension of the ER (Watson, 1955; Craig and Staehelin, 1988; Zhou et al., 2015); the ER probe Calnexin (CXN) has subsequently been shown to localise to ONM as well as to PNER (Irons et al., 2003; Liu et al., 2017; Groves et al., 2019).

5.1.2. Aims

The Airyscan localisation experiments described below were carried out to further investigate the localisation of the *At*SUN3 and *At*SUN4, the results of which were compared with the *ap*FRET data presented in Chapter 3 and FI enrichment data presented in Chapter 4. To do this, a published methodology was further refined and tested using proteins of known localisation at the NE prior to collecting novel data. The methodology of these experiments is outlined below rather than in Chapter 2 since this work also involved method development.

5.2 Methodology

5.2.1 Image Acquisition

Data was collected from live cells in the lower epidermal leaf tissue. Observations were carried out through use of CLSM (Zeiss LSM 880), and the addition of an Airyscan detector (Zeiss, Germany) was used to produce the images collected for analysis (Fig. 5.2). All images were acquired using a x100 oil objective at a zoom factor of 4.5. Samples were excited according to conditions outlined in Table 2.3 (see 2.4.2). Laser power did not exceed 2% whilst imaging to avoid photobleaching. Z-stacks were taken of each nucleus used to collect sample data; each Z-layer had a thickness of 1µm. This was done to select an image of a nucleus closest to its medial layer for further analysis.

5.2.2 Image Analysis

ImageJ was used to draw radial line profiles within an established ROI of 30° for each sample, using the Radial Profile Extended plugin (Philippe Carl, September 2019 update; Fig. 5.2). Radial line profiles measured the FI of each co-expressed protein from the estimated centre of the nucleus to the nuclear periphery. FI was measured at consistent points along each radial line profile, which were pre-determined by the Radial Profile Extended plugin. The FI values produced from each radial line profile within the ROI were averaged to produce a final integrated average of FI, which were formatted so that measurements of intensity were plotted as distances along the radius (microns; Fig. 5.2).

This was done for each fluorescent protein construct tested, producing respective sets of FI values measured using the same radial line profile. This was carried out at each layer of the Z-stack; the ROI was maintained in the same position throughout.

An R script was developed to process the raw data and identify the maximum FI value per Z-layer in each dataset (Fig. 5.2). This in turn calculated the maximum distance of the fluorescent protein

construct from the centre of the nucleus. This was conducted for both sets of FI values per protein combination used. The R-script also calculated the difference in distance between the maximum distances of each protein from the centre of the nucleus (Fig. 5.2). All the above numerical values were produced as a single table.

Additionally, graphical outputs were produced using the R script. Firstly, the maximum distance of each fluorescent protein construct from the centre of the nucleus, for each Z-layer, was plotted as a graph (see Appendix 4). Secondly, line profiles illustrating FI distribution of each protein along the radius in each layer of the Z-stack were produced (see Appendix 5).

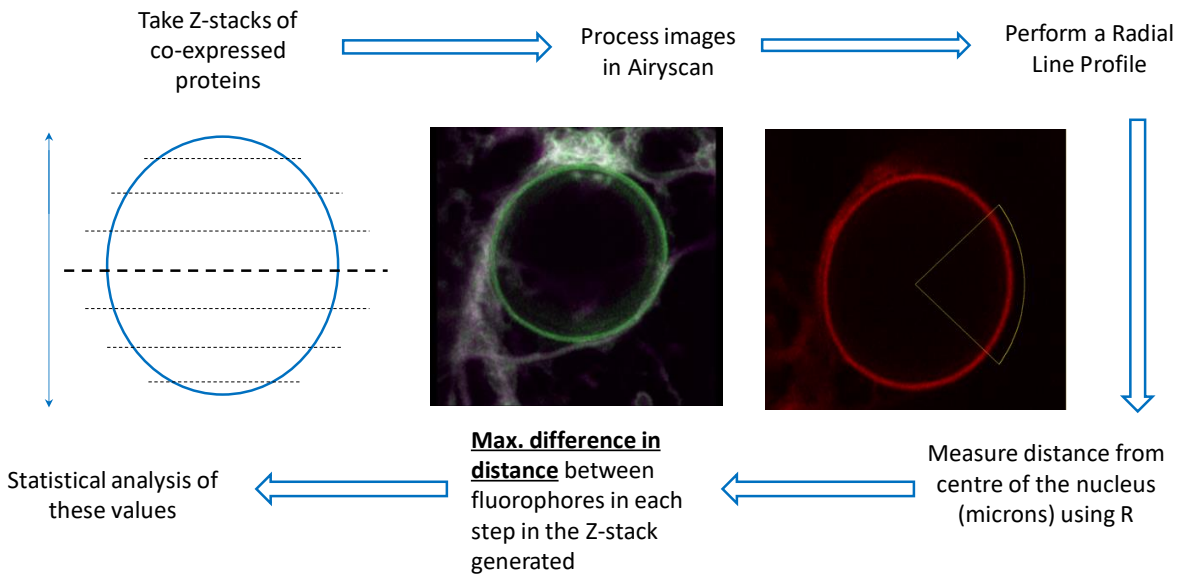

Figure 5.2. Workflow of the developed Airyscan-localisation method used to resolve protein localisation at the plant NE. ImageJ was used to measure fluorescence intensity (FI) of a fluorescent fusion protein along radial line profiles. Radii originated at the centre of the nucleus and extended to the nuclear periphery. An R script was then used to identify the maximum FI value along the radius for each protein, at each layer of the Z-stack. The difference between the maximum FI values for each protein was calculated for each layer of the Z-stack. A combination of original images, and data produced using R was used to determine which Z-step was used for statistical analysis. The difference in distance (microns) between fluorophores at the decided Z-step was used in the final statistical tests.

5.2.3 Statistical Analysis

The values produced from an R script (R Core Team, 2013) were used to calculate the estimated medial distance (EMD) of each sample (Figs. 5.2-5.7). Here, 'EMD' is defined as the Z-layer within each Z-stack where the nucleus is closest to its medial section. To calculate this, the FI profiles of both constructs at each Z-layer were used as an indicator of the optimal layer (Fig. 5.3). FI profiles showing distinct peaks in fluorescence for each construct were considered as candidates; these peaks corresponded to the point where the line profiles bisected the NE (Fig. 5.3). Samples were rejected if FI values were below 50, or if the measured peaks were too broad.

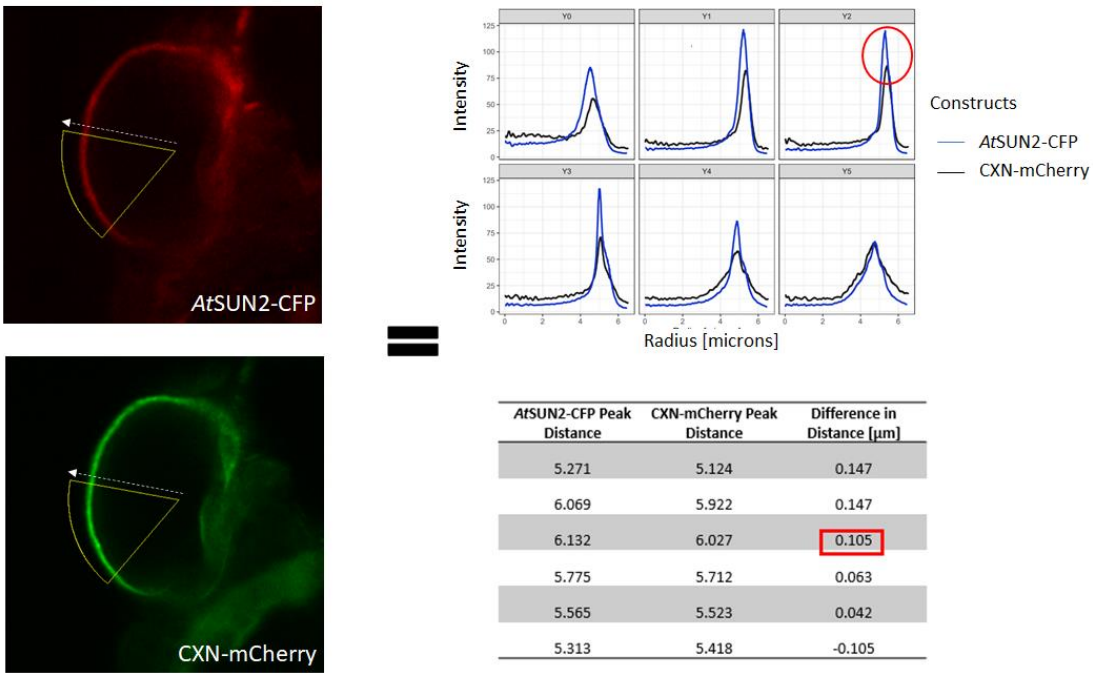

*At*SUN2-CFP Peak Distance	CXN-mCherry Peak Distance	Difference in Distance [µm]
5.271	5.124	0.147
6.069	5.922	0.147
6.132	6.027	0.105
5.775	5.712	0.063
5.565	5.523	0.042
5.313	5.418	-0.105

Figure 5.3. Graphic representation of how estimated medial distance (EMD) of different protein combinations are calculated from raw images. A representative image of *At*SUN2-CFP + CXN-mCherry and the data produced from subsequent analysis is shown as an example. Fluorescence intensity (FI) is measured along a line profile originating from the centre of the nucleus and terminating in the cytoplasm (indicated by a white dotted arrow). FI is measured within a consistent ROI for each construct throughout a Z-stack of each nucleus (indicated by a yellow outline). Intensity profiles showing distinct peaks of sufficient FI where line profiles bisect the NE are considered as a potential medial layer of the Z-stack. These FI profiles are compared to images from the original Z-stack to determine which is the medial layer (indicated by a red circle). The value in the table corresponding to this layer is the one that is taken forward for statistical analysis (indicated by a red outline).

When these candidate Z-layers had been identified, their respective profiles were then compared to the original image (Fig. 5.3). Comparison focused on identifying layers in the original image that clearly displayed NE expression; Z-layers that did not show this were rejected (Fig. 5.3). This was done to confirm that any values used for statistical analysis were representative of distances measured between fluorophores at the nucleus' medial layer. It was also a more unbiased means of selecting a layer from a Z-stack for analysis.

Once this Z-layer had been identified, the corresponding measurement was selected from the values generated from R as the calculated EMD (Fig. 5.3). For the control datasets the mean, median, and maximum measurements were also calculated from the values produced in R.

These values (EMD, mean, median and maximum) were then used to calculate the overall difference in distance between fluorophores measured at the NE (Fig. 5.8). A minimum of 20 individual samples were collected from a minimum of three biological replicates to produce the final dataset. R was used to produce histograms and boxplots from this data to show sample distribution, and to identify outliers that needed to be removed. Samples that were shown to not fit the normal distribution of data were removed from the final dataset before further analysis was carried out. This was done for each dataset used in these experiments. Graphical representation of the final results was produced in Excel, with error bars representing S.E.M. Statistical tests were conducted using R with the addition of the onewaytests and DescTools packages (Signorelli et al., 2020; Dag et al., 2019). R scripts were used to automatically test for statistically significant differences within the data (Kruskal-Wallis test and Dunn's test).

5.3 Results

5.3.1 Identifying Appropriate Control Protein Markers

Proteins of known localisation at the NE were co-expressed in different combinations. This was done to generate localisation profiles representing protein combinations that varied in membrane localisation and protein terminal fluorophore-fusions (Figs 5.4-5.7). Co-expressed proteins were observed at the NE to determine if each protein combination would serve as suitable control markers for Airyscan localisation analysis. Clear and consistent expression of both proteins at the NE were used as indicators of suitability.

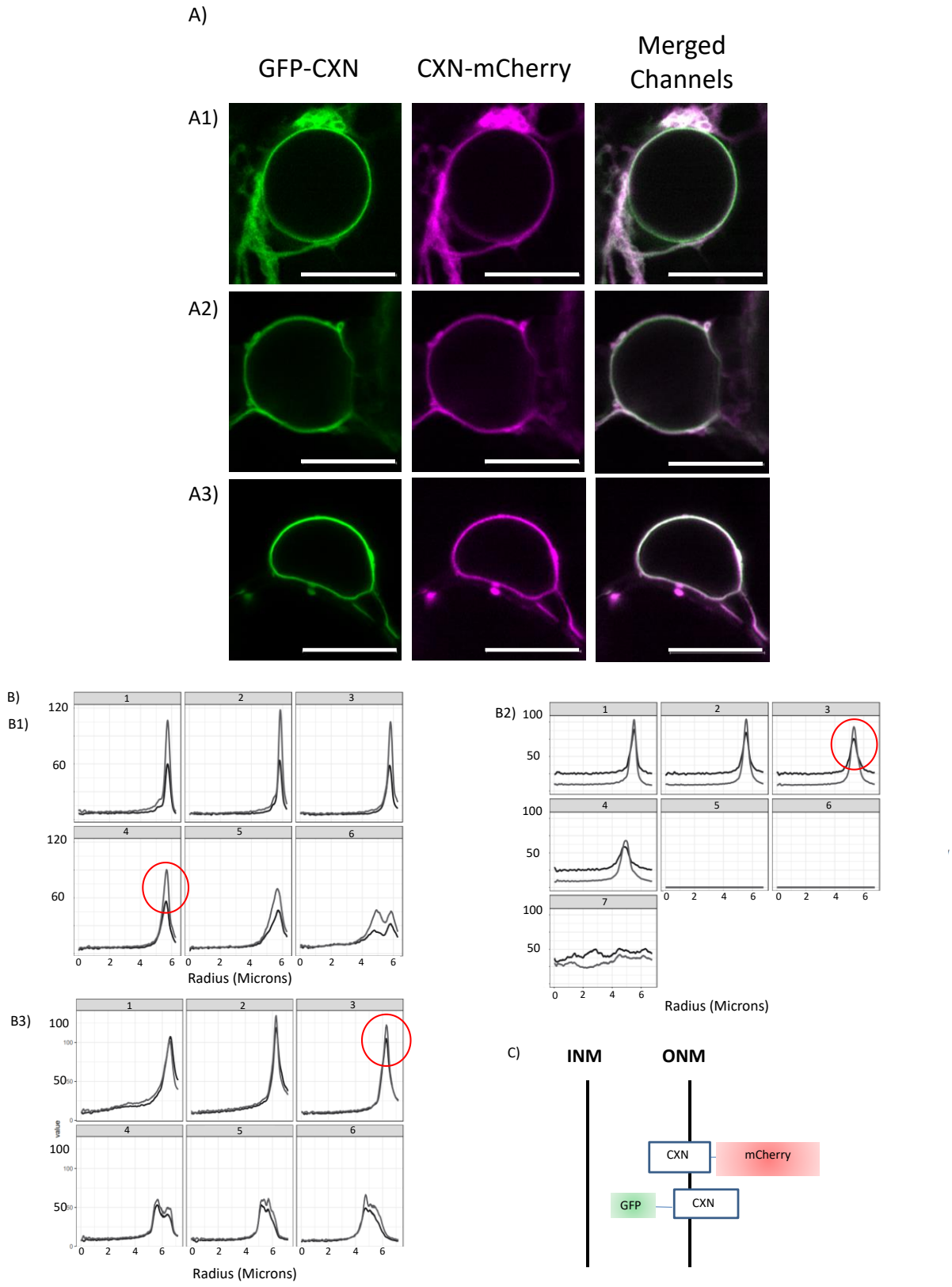

Figure 5.4. Selection of GFP-CXN + CXN-mCherry images and data used in Airyscan localisation analysis. A1-3) Representative images of GFP-CXN + CXN-mCherry used for localisation analyses. Nucleus – 10µm, images taken at x4.5 zoom. B1-3) Line profiles of GFP-CXN (shown in grey) + CXN-mCherry (shown in black) measuring peak fluorescence intensity along a radius, originating from the centre of the nucleus to the cytosol. Red circles indicate the z-layer used in statistical analyses. C) Graphic representation of where the constructs used in these experiments are situated at the plant NE.

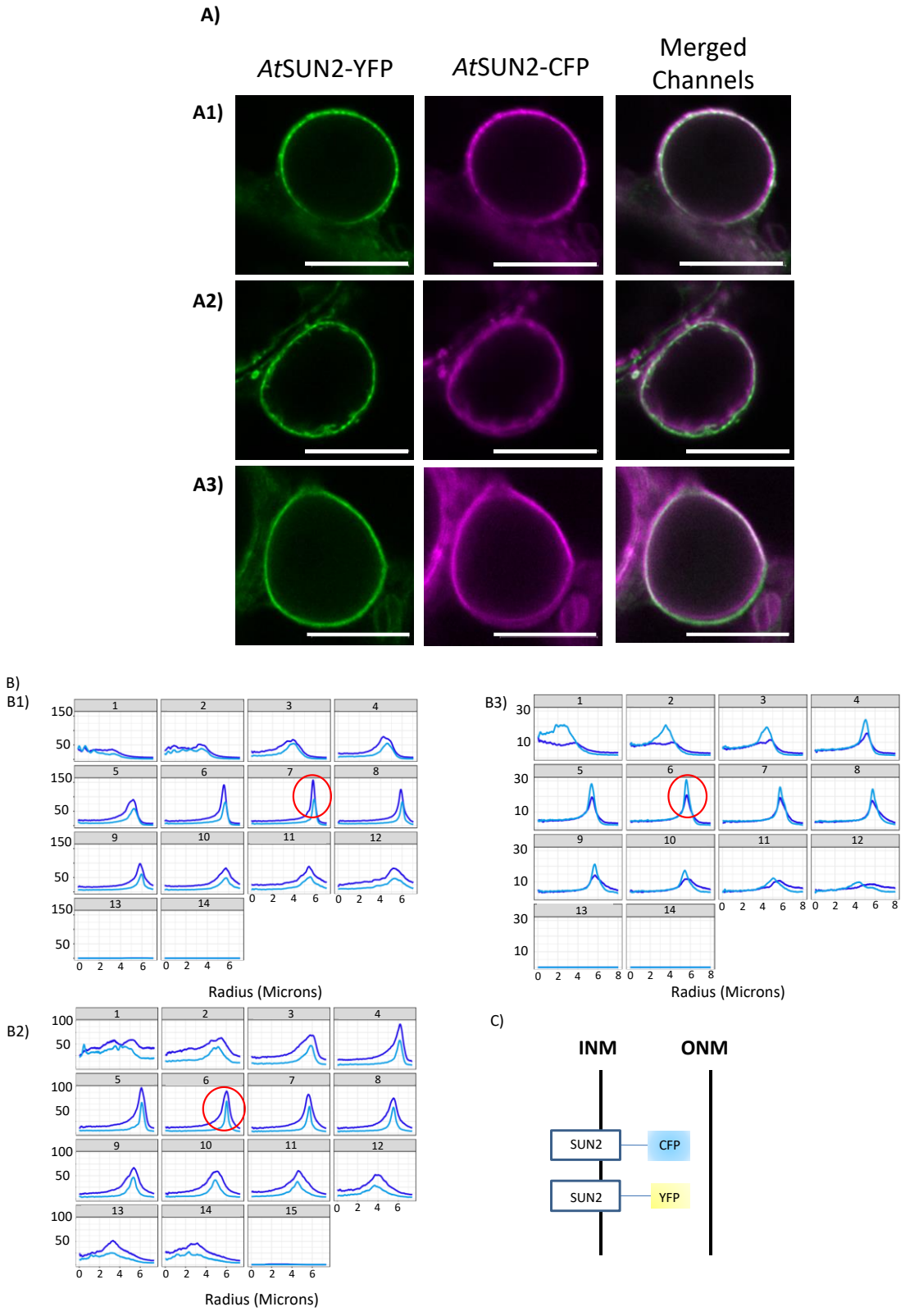

Figure 5.5. Selection of *At*SUN2-CFP + p19 + *At*SUN2-YFP images and data used in Airyscan localisation analysis. A1-3) Representative images of *At*SUN2-CFP + p19 + *At*SUN2-YFP used for localisation analyses. Nucleus – 10µm, images taken at x4.5 zoom. B1-3) Line profiles of *At*SUN2-CFP (shown in blue) + p19 + *At*SUN2-YFP (shown in cyan) measuring peak fluorescence intensity along a radius, originating from the centre of the nucleus to the cytosol. Red circles indicate the z-layer used in statistical analyses. C) Graphic representation of where the constructs used in these experiments are situated at the plant NE

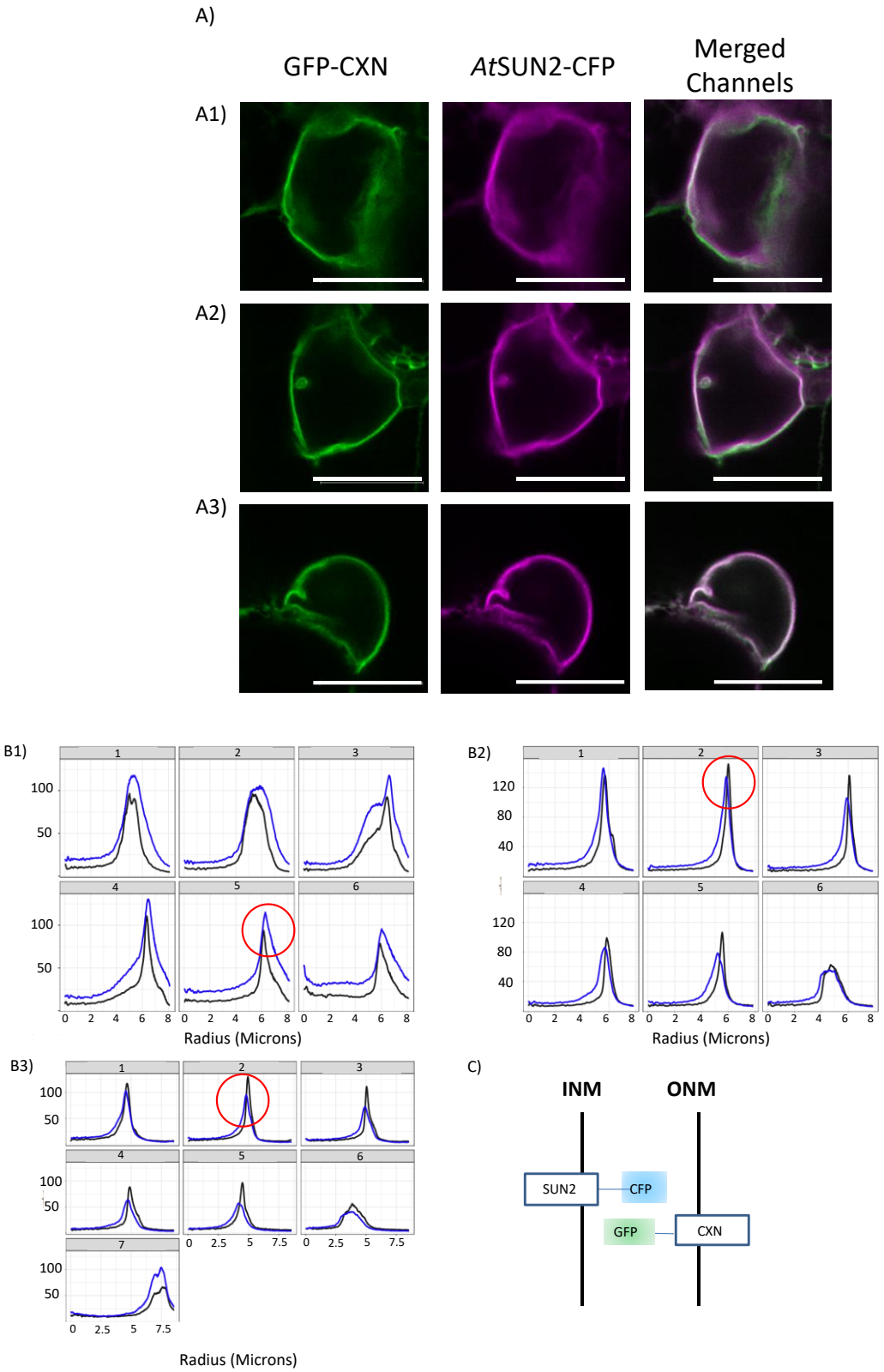

Figure 5.6. Selection of *At*SUN2-CFP + p19 + GFP-CXN images and data used in Airyscan localisation analysis. A1-3) Representative images of *At*SUN2-CFP + p19 + GFP-CXN used for localisation analyses. Nucleus – 10µm, images taken at x4.5 zoom. B1-3) Line profiles of *At*SUN2-CFP (shown in blue) + p19 + GFP-CXN (shown in black) measuring peak fluorescence intensity along a radius, originating from the centre of the nucleus to the cytosol. Red circles indicate the z-layer used in statistical analyses. C) Graphic representation of where the constructs used in these experiments are situated at the plant NE.

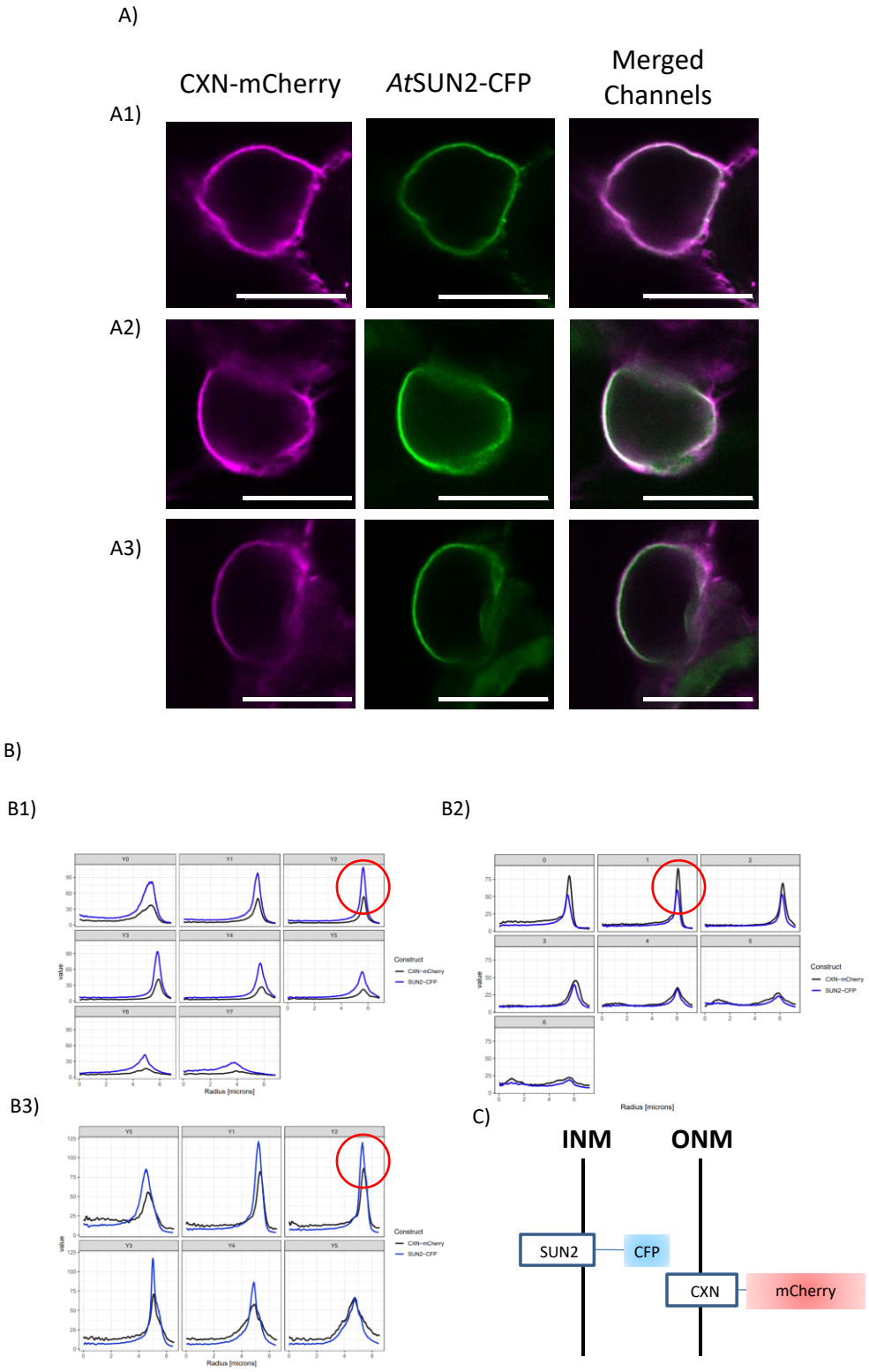

Figure 5.7. Selection of *At*SUN2-CFP + p19 + CXN-mCherry images and data used in Airyscan localisation analysis. A1-3) Representative images of *At*SUN2-CFP + p19 + CXN-mCherry used for localisation analyses. Nucleus – 10µm, images taken at x4.5 zoom. B1-3) Line profiles of *At*SUN2-CFP (shown in blue) + p19 + CXN-mCherry (shown in black) measuring peak fluorescence intensity along a radius, originating from the centre of the nucleus to the cytosol. Red circles indicate the z-layer used in statistical analyses. C) Graphic representation of where the constructs used in these experiments are situated at the plant NE.

Of all the protein combinations tested, four were identified to be suitable control marker proteins for further analysis (Fig. 5.8); GFP-CXN & CXN-mCherry, *At*SUN2-CFP & CXN-mCherry, *At*SUN2-CFP & GFP-CXN, and *At*SUN2-CFP & *At*SUN2-YFP all showed distinct and consistent expression when co-expressed (Fig. 5.4-5.7). Several other protein combinations, including the use NLS-PICL-GFP, Lamin B Receptor (LBR)-GFP and of YFP-*At*SUN2, were found to not be suitable control markers. Protein combinations were rejected on the grounds of inconsistent expression and/or mis-localisation when co-expressed with other proteins. Except for GFP-CXN & CXN-mCherry, p19 was co-expressed with each protein combination used.

The selected control markers were deemed sufficient to investigate the localisation of proteins at the NE (Fig. 5.4-5.7). The use of *At*SUN2-YFP & *At*SUN2-CFP provided a localisation profile for proteins localised to the same nuclear membrane, with their fluorescent tags located in the same sub-cellular compartment (Fig. 5.5). The inclusion of GFP-CXN + CXN-mCherry provided a localisation profile for proteins localised to the same membrane, but with their fluorescent tags located in different sub-cellular compartments (Fig. 5.4). Additionally, *At*SUN2-CFP and CXN-mCherry provided a localisation profile for proteins localised to different nuclear membranes, with their fluorescent tags also located in different sub-cellular compartments (Fig. 5.7). Conversely *At*SUN2-CFP + GFP-CXN provided a localisation profile for proteins localised to different nuclear membranes, but with their fluorescent tags located in the same sub-cellular compartment (Fig. 5.6).

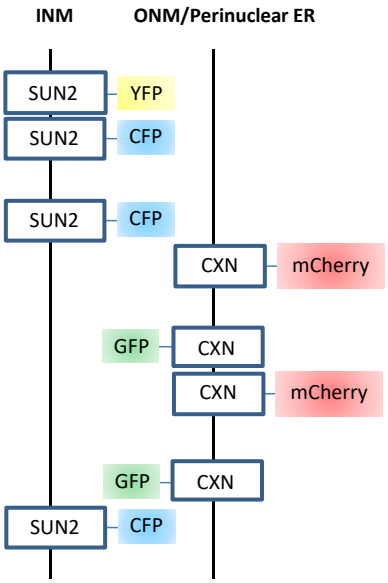

Figure 5.8. Graphic representation of protein combinations selected for use as control markers in Airyscan localisation analysis; orientation of fluorescent tags for each protein are shown. All fluorescent fusion proteins had been used in prior publications; protein topology and localisation at the NE had also been published.

5.3.2 Determining Which Numerical Value to Use for Statistical Analysis

Different numerical values representing the distance between two fluorescent proteins were calculated for the control protein combinations (Fig. 5.9). They were then compared to determine which numerical value was the most representative of this distance. The following numerical values were calculated: maximum distance, mean distance, median distance, and EMD (Fig. 5.9). Protein combinations calculated to have positive distances between each other were considered to be localised to separate membranes. Protein combinations calculated to have negative distances were considered too close in proximity to be resolved using Airyscan microscopy, and therefore localised to the same membrane.

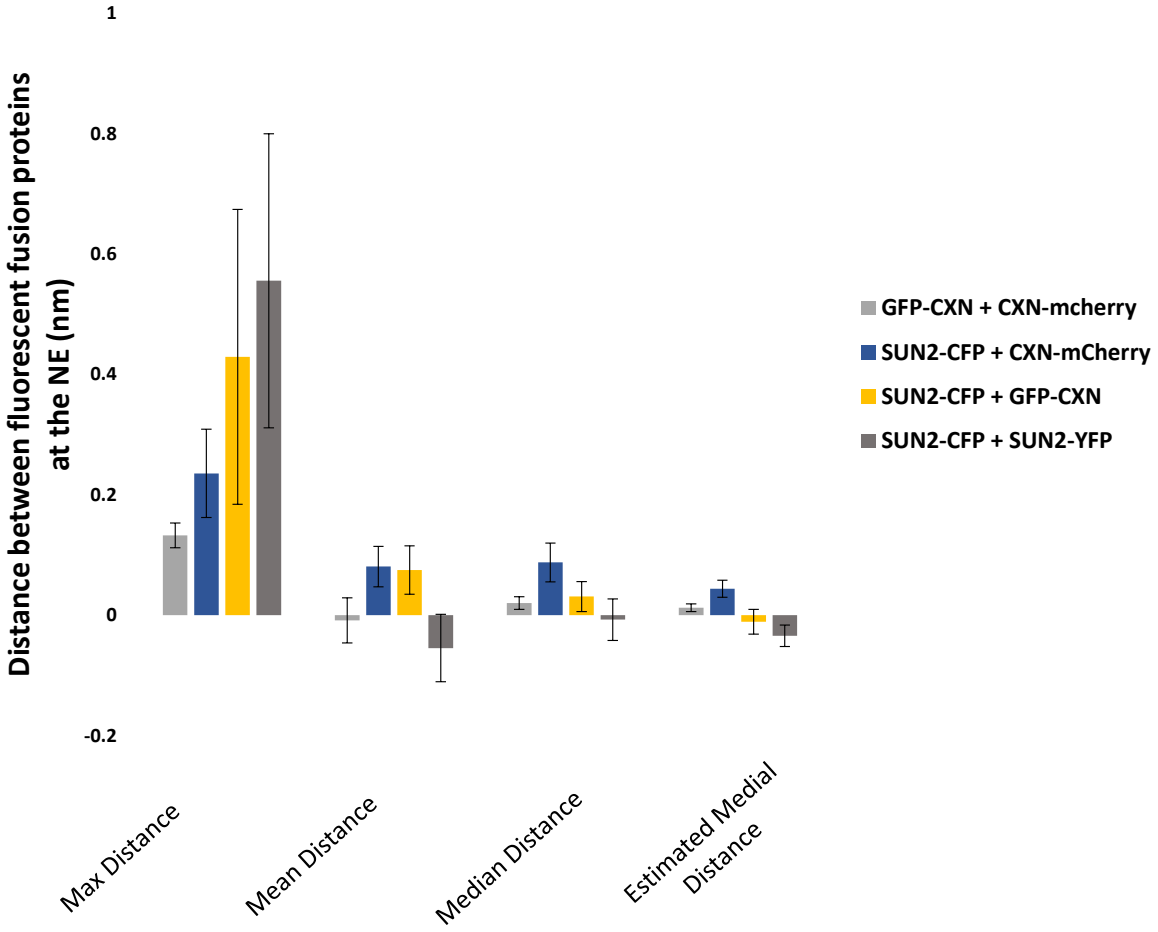

Figure 5.9. Comparison of numerical values that could be selected to represent the distance between two fluorophores at the medial plane of the NE. Max. distance (light grey), mean distance (blue), median distance (yellow), and estimated medial distance (EMD; dark grey) were calculated for each of the control protein combinations. These values were plotted as a histogram for comparison. A minimum of 20 nuclei were included in each dataset. Values shown are the median numerical value calculated for each dataset, ± standard error of the mean. A black line located at the baseline of the graph represents a value of 0.

It was found that the largest values were obtained when the maximum difference between control protein combinations were calculated (Fig. 5.9). The maximum difference in distance for each protein combination were also observed to be positive values (Fig. 5.9). Despite having overlapping error bars, the datasets calculated using either the mean or median distance showed some similarities with the EMD dataset. All three datasets showed that *At*SUN2-CFP & CXN-mCherry were the most distant from one another, whilst *At*SUN2-CFP & *At*SUN2-YFP showed the least distance from one another (Fig. 5.9). The differences in distance calculated between GFP-CXN & CXN-mCherry, as well as *At*SUN2-CFP & GFP-CXN, varied depending on which parameter was used in the

calculation. For example, there was no difference in distance between GFP-CXN & CXN-mCherry when calculated using the mean difference in distance. However, a positive distance was calculated when the median value or EMD was used (Fig. 5.9). EMD was chosen as the most representative value to measure distance between control protein combinations (Fig. 5.9). The error bars generated for this group were the smallest of each of the datasets and did not overlap (Fig. 5.9), suggesting significance between the values. Since estimating medial distance only takes data sampled from the medial planes of the nucleus into account, it is likely that variability caused by nuclear curvature is reduced.

5.3.3 Determining the Sub-Cellular Localisation of Known Proteins at the NE

Protein localisation was determined by calculating the distance of a fluorescent fusion protein from the centre of the nucleus. This was calculated for each fluorescent fusion protein used per combination, and the difference between the two values was calculated in turn. This final value represented the difference in distance between the two fluorescent fusion proteins. Line profiles were unidirectional, originating in the centre of the nucleus and terminating in the cytosol, so that measurements were consistent. The distance of the protein marker that was known to be closest to the centre of the nucleus was always subtracted from that of the protein marker known to be the furthest away. Experiments were initially focused on identifying which protein combinations could be statistically distinguished from one another, with the intent of using these results to resolve the localisation of the mid-SUN proteins.

Protein combinations that could be potentially resolved from one another were defined as those that had a positive distance between the two protein markers. Analysing the distances of all protein combinations, *At*SUN2-CFP & CXN-mCherry could potentially be resolved (0.067nm; Fig. 5.6), as could GFP-CXN & CXN-mCherry (0.012nm; Fig. 5.6). Protein combinations that were not able to be

resolved were *At*SUN2-CFP & *At*SUN2-YFP and *At*SUN2-CFP & GFP-CXN (-0.042nm and -0.01nm, respectively; Fig. 5.6).

Protein combinations that were statistically different to other combinations were considered suitable for resolving mid-SUN protein localisation. There was no significant difference in the distances measured between GFP-CXN & CXN-mCherry and *At*SUN2-CFP & GFP-CXN (p=1; data not shown). Likewise, no significant difference was found in the distances measured between GFP-CXN & CXN-mCherry and *At*SUN2-CFP & CXN-mCherry, nor GFP-CXN & CXN-mCherry and *At*SUN2-CFP & *At*SUN2-YFP (p=1 for both; Fig. 5.8). Although known to be localised to different nuclear membranes, the distance between *At*SUN2-CFP & GFP-CXN was not significantly different to the distance between any of the other protein combinations (data not shown). Further analysis of the *At*SUN2-CFP & GFP-CXN dataset showed high variability (see Appendix 6). However, the distance measured between *At*SUN2-CFP & *At*SUN2-YFP was significantly different to the distance between *At*SUN2-CFP & CXN-mCherry (p=0.00011; Fig. 5.8).

These results indicate that proteins that are localised to different nuclear membranes can be resolved from one another (Figs. 5.6&5.8). Conversely, proteins that are located on the same nuclear membrane cannot be resolved from each other, regardless of which side of the membrane that fluorophores are located. Together, these results provided localisation profiles that were then used to determine the localisation of the mid-SUN proteins. To do this, *At*SUN2-CFP & CXN-mCherry was selected as the control protein combination for comparison of novel data.

5.3.4 Determining the Sub-Cellular Localisation of the mid-SUN Proteins at the NE

Having determined the localisation of control proteins at the NE, *At*SUN3 and *At*SUN4 were subsequently tested (Figs.5.10-5.13). To see if this method could provide insight into mid-SUN topology, GFP-*At*SUN3 and *At*SUN3-GFP were used in these experiments. Only GFP-*At*SUN4 was used

to test the localisation of *At*SUN4. Each GFP-fused mid-SUN protein was co-expressed with CXN-mCherry. The distance between the two constructs were compared to those of the control dataset and used to determine if mid-SUN proteins co-localised to CXN-mCherry (Fig. 5.13).

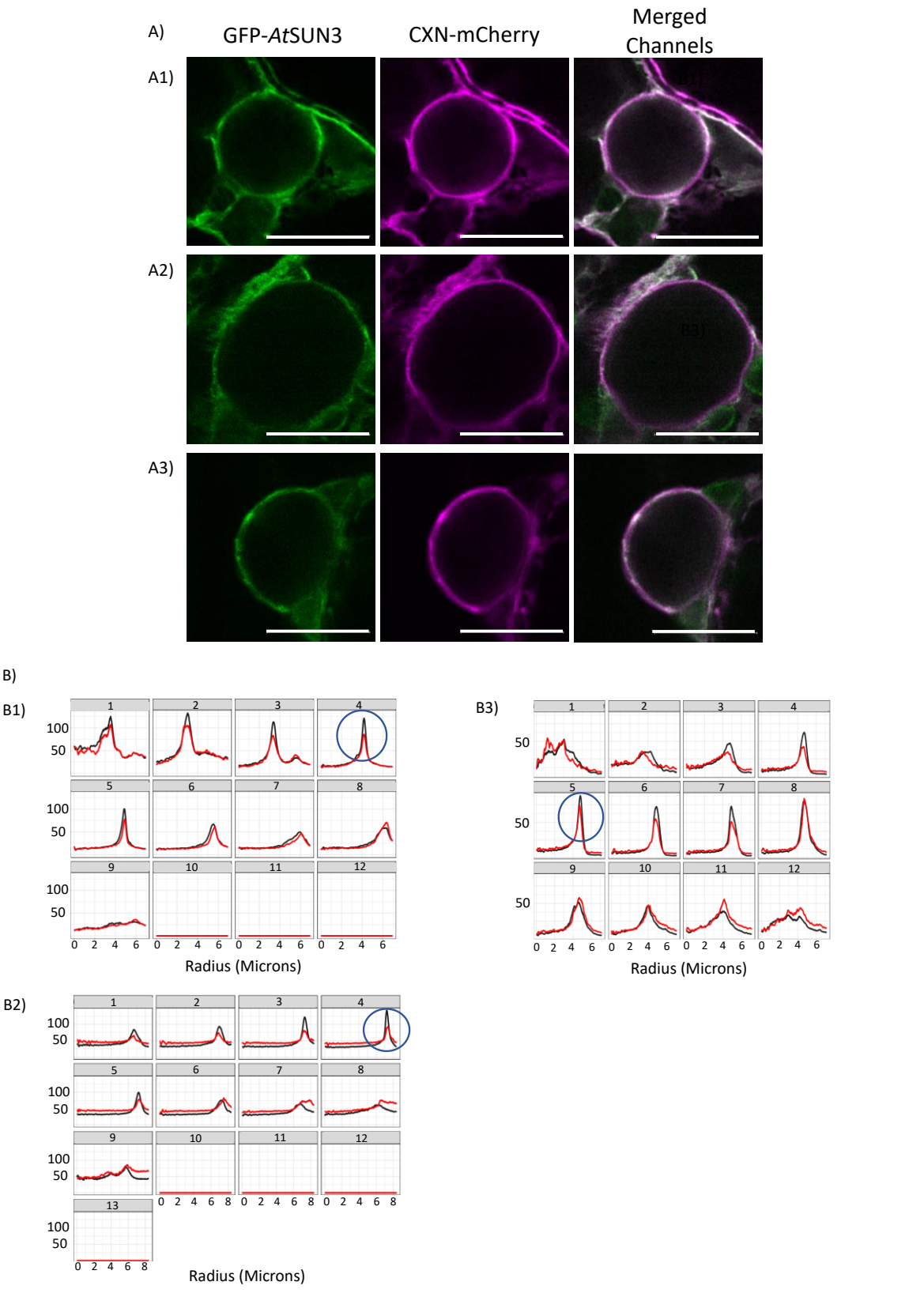

Figure 5.10. Selection of GFP-*At*SUN3 + p19 + CXN-mCherry images and data used in Airyscan localisation analysis. A1-3) Representative images of GFP-*At*SUN3 + p19 + CXN-mCherry used for localisation analyses. Nucleus – 10µm, images taken at x4.5 zoom. B1-3) Line profiles of GFP-*At*SUN3 + p19 + the ONM/PNER marker CXN-mCherry (fluorophore located in cytoplasm) measuring peak fluorescence intensity along a radius, originating from the centre of the nucleus to the cytosol. Blue circles indicate the z-layer used in statistical analyses.

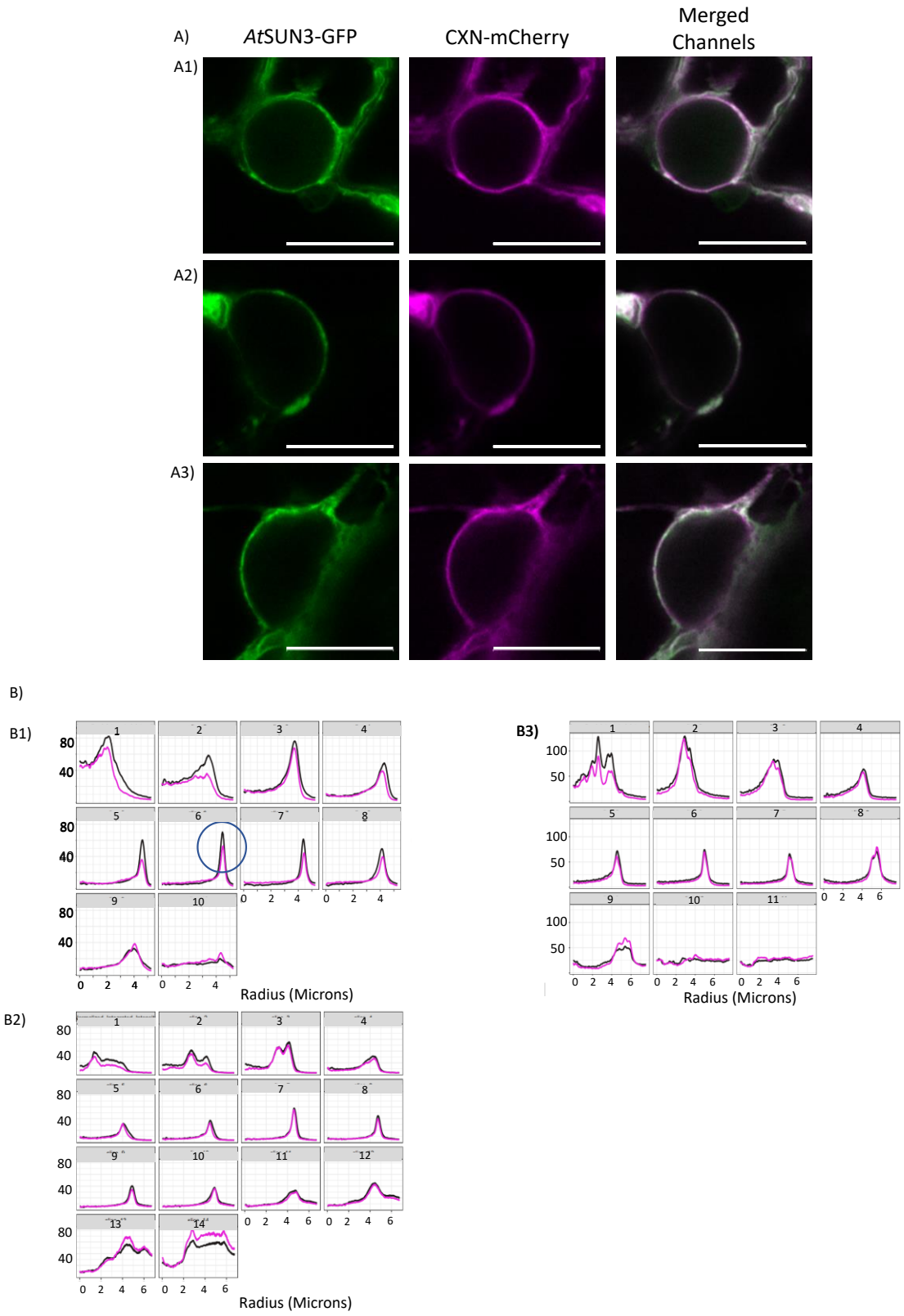

Figure 5.11. Selection of *At*SUN3-GFP + p19 + CXN-mCherry images and data used in Airyscan localisation analysis. A1-3) Representative images of *At*SUN3-GFP + p19 + CXN-mCherry used for localisation analyses. Nucleus – 10µm, images taken at x4.5 zoom. B1-3) Line profiles of *At*SUN3-GFP + p19 + the ONM/PNER marker CXN-mCherry (fluorophore located in cytoplasm) measuring peak fluorescence intensity along a radius, originating from the centre of the nucleus to the cytosol. Blue circles indicate the z-layer used in statistical analyses.

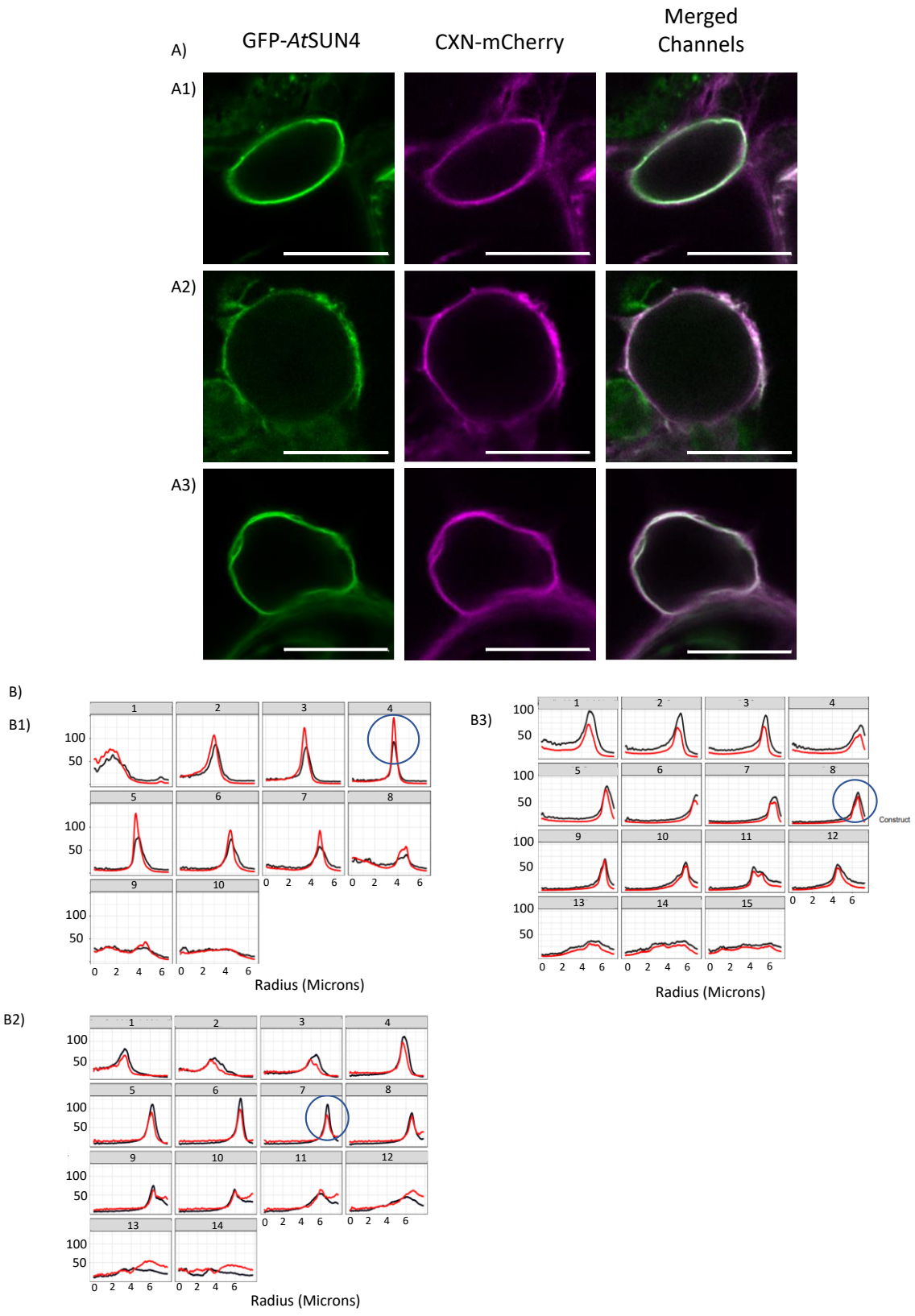

Figure 5.12. Selection of GFP-*At*SUN4 + p19 + CXN-mCherry images and data used in Airyscan localisation analysis. A1-3) Representative images of GFP-*At*SUN4 + p19 + CXN-mCherry used for localisation analyses. Nucleus – 10µm, images taken at x4.5 zoom. B1-3) Line profiles of GFP-*At*SUN4 + p19 + the ONM/PNER marker CXN-mCherry (fluorophore located in cytoplasm) measuring peak fluorescence intensity along a radius, originating from the centre of the nucleus to the cytosol. Blue circles indicate the z-layer used in statistical analyses.

The distance measured between *At*SUN2-CFP & CXN-mCherry was significantly different to that measured between GFP-*At*SUN3 & CXN-mCherry, *At*SUN3-GFP & CXN-mCherry and GFP-*At*SUN4 & CXN-mCherry (p=3.3e-06, 7.9e-05, and 0.013, respectively; Fig. 5.13A&B). The distances measured between GFP-*At*SUN3 & CXN-mCherry and GFP-CXN & CXN-mCherry (p=0.019; Fig. 5.13A&B) were also significantly different. However, the distance measured between GFP-CXN & CXN-mCherry was not significantly different to that measured for either *At*SUN3-GFP & CXN-mCherry or GFP-*At*SUN4 & CXN-mCherry (p=0.14 and 1, respectively; Fig. 5.13A&B).

The distances measured between GFP-*At*SUN3 & CXN-mCherry and *At*SUN3-GFP & CXN-mCherry were not significant from one another (p=1; Fig. 5.13A&B). The distances measured between GFP-*At*SUN3 & CXN-mCherry and GFP-*At*SUN4 & CXN-mCherry were also not significant (p=1; Fig. 5.13A&B), which was also the case when comparing the distances of *At*SUN3-GFP & CXN-mCherry and GFP-*At*SUN4 & CXN-mCherry (p=1; Fig. 5.13A&B).

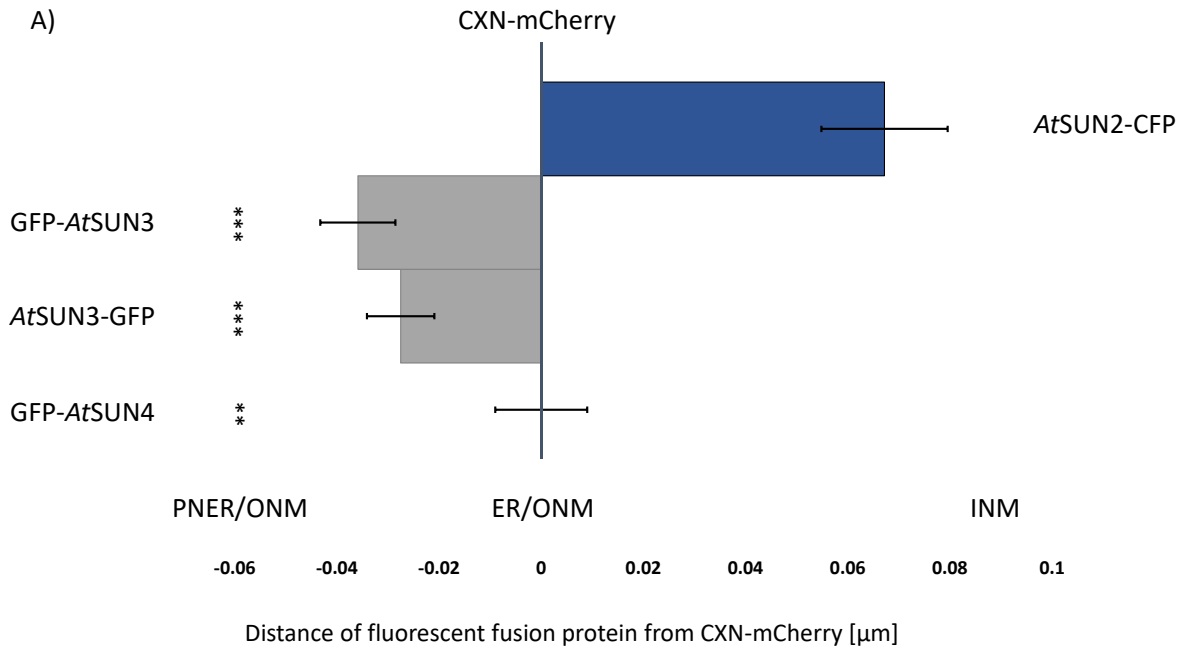

B)

Construct	Distance of construct from CXN-mCherry (µm)	S.E.M
AtSUN2-CFP	0.067	0.012
GFP-AtSUN3	-0.036	0.007
AtSUN3-GFP	-0.028	0.007
GFP-AtSUN4	0	0.009

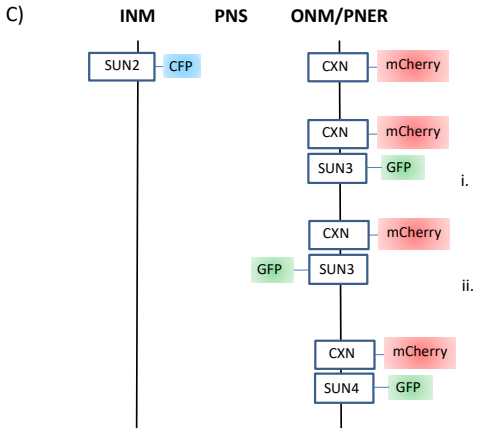

Figure 5.13. Investigation into the location of the Arabidopsis mid-SUNs using Airyscan confocal microscopy shows that *At*SUN3 and *At*SUN4 co-localise with the ER-marker Calnexin at the nuclear periphery. A) Differences in proximity (microns) of fluorescent fusion proteins to the ER membrane protein CXN-mCherry based on median EMD. A minimum of 20 nuclei collected over a minimum of 3 biological repeats were included in each dataset. There were statistically significant differences between group means as determined by a Kruskal-Wallis H test, $\chi 2(6) = 36.078$, p=2.662e-06. Proteins of known localisation in correspondence to CXN-mCherry are shown in blue; mid-SUN proteins are shown in grey (Dunn's test; ***, P < 0.0001; **, P < 0.001). B) Numerical values of median EMD for each combination used are displayed with their corresponding S.E.M. C) Graphic representation of each protein combination used and their localisation at the NE. Putative N- and C-termini of the mid-SUN proteins have been labelled based on published work on how they interact with LINC complex components (Graumann

et al., 2014); i) The N-terminus of *At*SUN3/ *At*SUN4 is located in the cytosol. ii) The C-terminus of *At*SUN3 is located in the lumen.

5.4 Discussion

This work focused on resolving the subcellular localisation of *At*SUN3 and *At*SUN4 when transiently expressed as fluorescent fusion proteins (Figs. 5.10-5.13). Proteins of known localisation and topology were transiently co-expressed *in planta* to test their suitability as control marker proteins (Figs. 5.4-5.8). Constructs that consistently co-localised at the NE were confirmed as suitable (Fig. 5.8), although several protein combinations were observed to not be NE-localised when co-expressed. It is unclear whether this could be credited to proteins being over-expressed or even interacting with one another. After comparing different numerical values, it was found that calculating EMD resulted in less variability within the dataset and therefore more likely to produce results of statistical significance (Fig. 5.8). These measurements were used to generate localisation profiles for the control marker proteins, which in turn were used to determine the localisation of *At*SUN3 and *At*SUN4 (Fig. 5.13).

It was shown that GFP-*At*SUN3, *At*SUN3-GFP and GFP-*At*SUN4 co-localise to the ER marker CXN-mCherry at the NE (-0.036nm, -0.028nm, and 0nm, respectively; Fig. 5.13). It was also found that these measurements significantly differed to the calculated proximity of *At*SUN2-CFP and CXN-mCherry (0.067nm; Fig. 5.13). As aforementioned, ROIs were selected to avoid measuring regions of the nucleus where PNER was present to avoid producing inaccurate data. However, since the PNER is closely associated with the ONM, which itself is a compartment of the ER, the data indicates that *At*SUN3 and *At*SUN4 localise to the ONM/ER.

5.4.1 Refining the Workflow

5.4.1.1 Testing of Candidate Control Protein Markers

Markers were selected that are known to be predominantly localised at the INM (*At*SUN2) or ONM/ER (Calnexin) in order to study the location of *At*SUN3 and *At*SUN4 at the NE. As stated in section 5.3.1, tests were carried out to select protein combinations that could be used as control markers. The localisation and topology of the proteins used were already established prior to testing; each of them had been demonstrated to localise to the NE when singularly expressed. Despite being published ER membrane proteins, GFP-CXN and CXN-mCherry have both been shown to localise to the NE due to the ONM being contiguous to the ER membrane (Fig. 1.1). It has been shown that *At*SUN2-CFP predominantly localises to the NE both when singularly expressed, and when co-expressed with CXN-mCherry (Fig. 5.7; Graumann, 2014; Groves et al., 2019). This protein combination was also used as a control when resolving the localisation of NLS-PICL-GFP (Groves et al., 2019). It was also found that *At*SUN2-CFP co-localised with GFP-CXN at the NE (Fig. 5.6). Lastly, *At*SUN2-YFP has been shown to localise to the NE both when singularly expressed and when co-expressed with *At*SUN2-CFP (Fig. 5.5; Graumann et al., 2010).

Each of the protein combinations listed above were selected as control protein markers due to consistently and clearly localising to the NE (Figs. 5.4-5.8). This selection of markers was necessary due to the prior report of *At*SUN3 and *At*SUN4 localising to the NE and ER when viewed using confocal microscopy (Graumann et al., 2014). Therefore, there was a requirement to test whether Arabidopsis mid-SUNs localise to either the INM or the ONM-PNER; protein markers were selected for testing accordingly.

It was also observed that proteins that only labelled the NE produced intensity profiles that showed distinct peaks of fluorescence (see Figs. 5.9-5.12 and Appendix 5). Being able to identify peak fluorescence was important since it was required to calculate protein proximity (see Figs. 5.3, 5.9-5.12 and Appendix 5) Therefore, samples were considered unsuitable for analysis if peak

fluorescence could not be easily distinguished. This in turn meant that proteins that only localised to the NE when co-expressed could be considered for use in these experiments.

Several protein combinations were found to not be considered suitable control markers when transiently co-expressed. All proteins tested have been observed to localise to the NE when transiently expressed by themselves. Some proteins, including NLS-PICL-GFP and LBR-GFP, do not consistently label the NE when co-expressed with other NE or NE-associated intrinsic membrane proteins. It is unclear as to why this is, resulting in these combinations being rejected in order to focus on refining the overall method.

5.4.1.2 Selection of EMD as Numerical Value of Distance between Fluorescent Fusion Proteins and Confirmation of Control Protein Markers

Several types of numerical values were compared to identify which could most accurately measure the relative location of proteins at the NE (see Fig. 5.8 & 5.9). It was ultimately decided that the EMD was the optimal numerical value to use for measuring the distance between fluorescent fusion proteins. Due to the way it was calculated (see section 5.2.3), an original value would more likely provide an accurate measurement of distance. This is most likely why the EMD dataset showed the lowest amount of variance compared to the other datasets (Fig. 5.9). Conversely, measurements calculated using the mean or median were still prone to being skewed despite removing inappropriate values from the original dataset. This is due to the nature by which mean or median is calculated. In addition, using the Z-layer where the maximum distance between proteins was measured resulted in a greatly skewed dataset. This was due to raw values initially being calculated using maximum FI (see Fig. 5.9).

It was decided that the only candidate protein combination that was suitable for use as a control marker when determining the localisation of unknown proteins was *At*SUN2-CFP & CXN-mCherry. It was found that the distance between *At*SUN2-CFP & *At*SUN2-YFP was significantly different from

that of *At*SUN2-CFP & CXN-mCherry, proving that proteins localised to the two nuclear membranes could be distinguished. Therefore, the optimal means of resolving the localisation of mid-SUN proteins was by calculating whether the difference in distance between them and CXN-mCherry was significantly different to that of *At*SUN2-CFP & CXN-mCherry. Although useful for developing this methodology, this resulted in the *At*SUN2-CFP & *At*SUN2-YFP protein combination not being included as a final control for comparison of the mid-SUN data (Fig. 5.13).

Despite being localised to different nuclear membranes, it was found that *At*SUN2-CFP & GFP-CXN could not be resolved from one another (Fig. 5.13). There is a possibility that there was a spectral overlap due to the fact GFP and CFP are closely located on the emission spectrum. This would account for not being able to distinguish between INM-localised *At*SUN2 and ER membrane-localised CXN, as well as the large variance within the dataset. For these reasons, this protein combination was also rejected as a control. Additionally, GFP-CXN & CXN-mCherry was not able to be resolved; this is likely due to the two proteins being too closely located to one another to be resolved using Airyscan confocal microscopy.

By using CXN-mCherry as a reference marker, and the distance between it and *At*SUN2-CFP to distinguish between ONM/ER and INM, a means of resolving the localisation of the mid-SUN proteins was provided.

5.4.2 Resolving the Localisation of the Arabidopsis mid-SUNs

These findings expand on those published by Graumann et al. (2014), which showed that fluorescent fusion proteins of *At*SUN3 and *At*SUN4 localised to the NE and ER when transiently expressed. These results however indicate that the *At*SUN3 and *At*SUN4 co-localise to an ER marker via analysis of their position at the nuclear periphery (Fig. 5.13). Due to the ER lumen being contiguous with the PNS of the NE, these results therefore be indicate ONM/ER localisation. This is the first time that this has been demonstrated in Arabidopsis. These results correlate with the protein enrichment analysis that was carried out on *At*SUN3 and *At*SUN4, which inferred that both proteins were ER-enriched

(see Chapter 4). This is also in agreement with the demonstration of the *At*SUN3-*At*maMyb interaction that was detected using apFRET (see Fig. 3.7 and Table 3.1). Therefore, the positive interactions between these two proteins provide further evidence that they are both localised to the same membrane (Fig. 5.13). The corresponding maize mid-SUNs, *Zm*SUN3 and *Zm*SUN4 have been reported to be NE-localised but it was acknowledged that 'speckles' observed in the cytoplasm may in fact show ER-localisation (Murphy et al., 2010). This was not investigated any further, however. Due to mid-SUN proteins being highly conserved throughout the plant kingdom, it is reasonable to suggest that the maize mid-SUN proteins are also localised to ONM/ER.

The localisation of *At*SUN3 and *At*SUN4 contrast to that of the Arabidopsis Cter-SUN proteins which were proved to be localised to the INM using both confocal and immunogold electron microscopy (EM; Graumann et al., 2010). Therefore, observing the sub-cellular localisation of immunogold labelled mid-SUNs could provide complimentary data to that reported in this chapter. It is interesting to note that *At*SUN2, through this work and that reported in Groves et al., (2019), has also been shown to localise to the INM using Airyscan localisation analysis. This provides further support that this method is a reliable means of investigating protein localisation at the nuclear periphery.

It is notable that mid-SUN proteins have never been reported when proteomic analyses have been conducted on plant nuclei composition (Goto et al., 2019; Tang et al., 2020). Even when using subtractive proteomics where NE proteins such as *At*SUN1 or *At*WIP1 were used as bait, *At*SUN3 and/or *At*SUN4 were not detected when probing the protein composition of the nuclear membranes (Tang et al., 2020). They were also not reported amongst candidates that were rejected due to either exhibiting dual localisation at the NE and other organelles, or non-NE localisation (Tang et al., 2020). Although this could infer that mid-SUN proteins are not localised at the NE, it should be considered that the methods of analysing plant NE composition are still being improved upon (Goto et al., 2019; Tang et al., 2020). For example, NE-associated ER proteins were detected in the work carried out by Goto et al. (2019), and both analyses detected intrinsic membrane proteins localised to the INM and ONM (Goto et al., 2019; Tang et al., 2020). It is therefore possible that many proteins, including the

Arabidopsis mid-SUNs, remain undetected when these analyses are carried out due to being lost during the fractionation process.

5.4.3 Assessing this Method's Potential to Determine mid-SUN Topology at the ER Membrane

It was also of interest to see if this method could be used to determine the topology of the mid-SUN proteins. Since GFP-*At*SUN3 and *At*SUN3-GFP were both used to determine localisation, there was potential for one of these constructs co-localise with CXN-mCherry more closely than the other. Despite being able to resolve the localisation of *At*SUN3 however (Fig. 5.13), this method was not sufficient to determine its topology. This is reflected in the localisation profiles generated for some of the control protein combinations that were used (see Figs. 5.10-5.13). Based on bioinformatic predictions, *At*SUN3 has three predicted TMDs meaning that its N- and C-terminus reside on different sides of the ER membrane. In turn, this would mean when co-expressed with CXN-mCherry that one *At*SUN3 combination would be orientated similarly to *At*SUN2-CFP & *At*SUN2-YFP. Conversely, the other *At*SUN3-CXN-mCherry combination would be orientated similarly to GFP-CXN & CXN-mCherry. Since neither of these control protein combinations could be respectively distinguished from one another, this would explain why *At*SUN3's topology could not be resolved. An alternate approach is redox-sensitive GFP (roGFP), a method specifically designed to investigate the topology of ER membrane proteins (Brach et al., 2009). Since these results infer that *At*SUN3 and *At*SUN4 would be suitable candidates for roGFP analysis, these experiments could provide crucial information regarding how mid-SUN proteins are orientated in the membrane. It would also provide further insight into how they mediate protein-protein interactions.

What has been proven however is that the method described in this chapter can indeed be used to resolve protein localisation at the nuclear periphery. Such information could be used to not only determine the localisation of novel proteins, but to further the understanding of those that have already been identified. For example, this technique could be used to investigate whether deleting

the CCD affects localisation of *At*SUN3. It would be interesting if this was affected, as *At*SUN3ΔCC was the only *At*SUN3 deletion mutant that maintained localisation to the nuclear periphery (see Chapter 3). This information would be relevant when investigating *At*SUN3's ability to form heterodimers or homodimers.

5.5 Conclusions

Overall, a refined workflow has been established to resolve the localisation of proteins at the NE using Airyscan confocal microscopy. This work provides supporting evidence that *At*SUN3 and *At*SUN4 are localised to the ONM/ER membrane, unlike the INM-localised Cter-SUN proteins. This is the first time that this been demonstrated *in planta*, but correlates to the localisation of mid-SUN proteins in other kingdoms. Although able to resolve a protein's localisation at the NE, this technique has been shown to not be able to resolve protein topology.

Chapter Six | General Discussion and Future Work

The research described in this thesis was carried out to further characterise the Arabidopsis mid-SUN proteins *At*SUN3 and *At*SUN4, focusing on their functional role. Plant mid-SUN proteins were previously described to be localised at the NE and ER of higher plants, as were maize homologs, and suggested to have a functional role in LINC complex formations (Murphy et al., 2010; Graumann et al., 2014). Additionally, work carried out on the Chickpea mid-SUN protein *Ca*SUN1 also inferred that mid-SUN proteins have a non-NE related function, and instead may be regulated by the UPR response (Jaiswal et al., 2014). Not only this, but each of the five SUN proteins have been confirmed to interact with *At*maMyb, an ER membrane-bound TF with a proposed role in root hair elongation, in MY2H screens (Slabaugh et al., 2011; Andov et al., 2014; Tatout, personal communications; see section 1.6).

6.1 Assessing Protein-Protein Interactions *in planta*

One route of investigation focused on detecting protein-protein interactions and assessing how these interactions were mediated (see Chapter 3). Particular attention was given to whether any of the SUN proteins were able to interact with *At*maMyb (see Chapter 3 & section 1.5.2.3). Overall, the findings confirm that mid-SUN proteins are able to form homomeric and heteromeric interactions *in vivo* (see Chapter 3). Following on from the confirmation in Graumann et al., (2014) that *At*SUN3 and *At*SUN4 are able to interact with each other, FRET-FLIM data showed that the N-terminus of *At*SUN3 was required to form homomeric interactions with the N-termini of other SUN proteins (see section 3.2.4 & Fig. 3.11). Homomeric interactions were only detected between *At*SUN3 proteins that were

N-terminally tagged (see section 3.2.4 & Fig. 3.11); however, both N- and C-terminally tagged *At*SUN4 proteins were detected to interact with N-terminally tagged *At*SUN3 proteins (see section 3.2.4 & Fig. 3.11). More interestingly however, *At*SUN3 was the only Arabidopsis SUN protein shown to interact with *At*maMyb, indicating a protein specific function (see section 3.2.2.1, Fig. 3.7 & Table 3.1). It currently remains unclear as to how these interactions are mediated. The only domain deletion construct used in apFRET experiments was *At*SUN3Δcoiled coil (see section 3.2.3.1, Figs. 3.9, 3.10, & Table 3.2). This construct was not detected to interact with *At*maMyb (see section 3.2.3.1, Fig. 3.10, & Table 3.2). There was an interaction detected between *A*tSUN3Δcoiled coil and full-length *At*SUN3 however, but only when testing *At*SUN3Δcoiled coil-CFP (see section 3.2.3.1, Fig. 3.10, & Table 3.2). The CCDs of Cter-SUNs have been shown to be required for mediating protein-protein interactions, both within and outside of the plant kingdom (Graumann et al., 2010; Sosa et al., 2012; Nie et al., 2016; see section 3.3.2.1). However, the results reported in this project do not yet indicate the same of mid-SUN proteins, meaning the probability for CCDs mediating protein-protein interactions is still under evaluation (see sections 3.3.2.1 and 3.3.2.2.).

6.2 Sub-Cellular Localisation of the mid-SUN Proteins

6.2.1 Sub-Cellular Localisation of the mid-SUN Proteins in Plants

The localisation of *At*SUN3 and *At*SUN4 at the NE was further investigated (see Chapter 5). To do this, a method that had been previously developed in this group, incorporating the use of Airyscan confocal microscopy to identify protein localisation at the NE, underwent further refinement (Groves et al., 2019; see section 5.2). This improved methodology was then used to determine *At*SUN3 and *At*SUN4 localisation at the nuclear periphery in relation to the ER membrane marker CXN-mCherry (see section 5.2 and Fig. 5.13). The results produced from this work showed that *At*SUN3 and *At*SUN4 GFP fusion proteins co-localised with the ER marker CXN-mCherry at the nuclear periphery

and were significantly distanced from the INM-localised *At*SUN2-CFP (see section 5.2 and Fig. 5.13). Also, the NLIs of *At*SUN3 and *At*SUN4 were calculated to determine whether these proteins were more NE- or ER-enriched; the results indicated that both mid-SUN proteins were more ER-enriched (Fig. 4.2).

Prior to this, the Arabidopsis mid-SUNs had been shown to localise to the NE and ER when observed using confocal microscopy (Graumann et al., 2014). Additionally, the maize mid-SUNs were reported to be NE-localised but were speculated to potentially be located at the ONM (Murphy et al., 2010). It was additionally noted that 'specks' were reported in the cytoplasm when mid-SUN fusion proteins were observed using fluorescence microscopy (Murphy et al., 2010). Because of this, it was suggested that they were not solely located at the NE (Murphy et al., 2010). *Ca*SUN1 was also reported to localise to the nuclear membranes and the ER (Jaiswal et al., 2014).

As previously stated, the ER membrane is contiguous with the ONM and that CXN-mCherry has been used as a marker of the ONM/ER continuum (Groves et al., 2019). Therefore, this should be taken into consideration when assessing these results. These findings add to those published by Graumann et al. (2014) by further specifying that the Arabidopsis mid-SUN proteins are localised to the ONM/PNER (Fig. 6.1). This agrees with the published localisation of *Ca*SUN1 (Jaiswal et al., 2014), as well as the confirmed interaction of *At*SUN3-*At*maMyb. These findings subsequently provide an alternative perspective regarding the putative function of the mid-SUNs, indicating that they have a role at the ER in addition to those proposed at the NE.

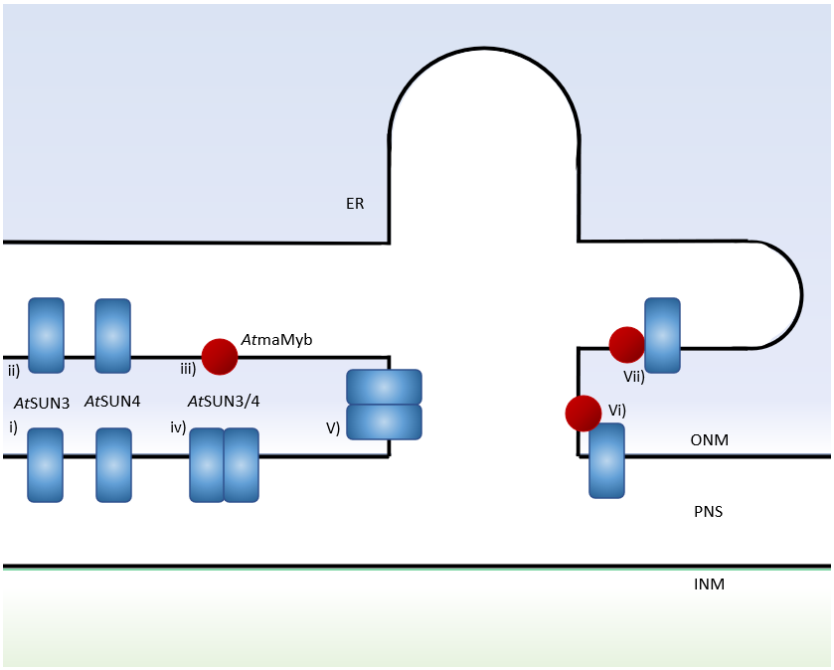

Figure 6.1 Proposed localisations of *At*SUN3 and *At*SUN4 at the nuclear periphery, and their interactions described in this thesis. i) *At*SUN3 and *At*SUN4 are localised at the ONM. ii) *At*SUN3 and *At*SUN4 are localised at the ER. iii) *At*maMyb is localised to the ER-membrane, as reported by Slabaugh et al., (2011). iv) *At*SUN3 and *At*SUN4 interact with each other at the ONM. V) *At*SUN3 and *At*SUN4 interact with each other at the ER membrane. Vi) ONM-localised *At*SUN3 interacts with ER-membrane localised *At*maMyb. Vii) *At*SUN3 and *At*maMyb interact with each other at the ER membrane.

Due to the dynamic nature of the plant ER network, its morphology (specifically the arrangement and proportions of interconnecting tubules and cisternae) varies in relation to cell type, developmental stages, and experimental treatments. Due to the recent development of the AnalyzER software package, a broad selection of parameters describing ER structure, dynamics, and persistency can be quantified (Pain et al., 2019). It would be interesting to investigate whether *At*SUN3 and/or *At*SUN4 significantly alter ER structure and assess which variables are affected by their expression. These results could subsequently contribute to studies investigating the functional role of mid-SUNs at the ER, providing quantifiable data regarding their effect on ER network dynamics.

6.2.2 Sub-Cellular Localisation of mid-SUN Proteins in Non-Plant Organisms

Mid-SUN proteins are well conserved throughout not only the plant kingdom, but also Eukaryota (Murphy et al., 2010; Graumann et al., 2014; Poulet et al., 2016). Mid-SUN proteins have previously been demonstrated to be localised to the NE and ER when transiently expressed *in planta* (Graumann et al., 2014). The work presented in this thesis furthers these findings by indicating that they are predominantly localised to the ONM and ER (see Figs 4.2 & 5.13). There is evidence that mid-SUN proteins of non-plant species are also ER-localised. For example, the murine mid-SUN protein Opt was demonstrated through sub-cellular fractionation to be an ER integral membrane protein (Sohaskey et al., 2010). It was concluded that Opt specifically localised to the rER as it fractionated with ribophorin I, an ER membrane protein known to bind ribosomes (Kreibich et al., 1978). Furthermore, ultrastructural analyses of osteoblasts lacking Opt showed a discontinuous rER that did not have well-organised cisternae (Sohaskey et al., 2010).

The yeast mid-SUN protein Slp1 was shown to be an ER integral membrane protein using co-IP and confocal microscopy (Friederichs et al., 2012). Interestingly, the Slp1 protein of the filamentous fungus *S. macrospora* was also observed to localise to both the ER and perinuclear region using fluorescence microscopy (Vasnier et al., 2014). Therefore, in this species mid-SUN proteins may be localised to the part of the ER network that is situated closest to and connects with the ONM. This would be hard to determine however without ultrastructural analysis. The mid-SUN proteins (both within and outside of the plant kingdom) discussed so far are the only examples where ER localisation are described (Murphy et al., 2010; Sohaskey et al., 2010; Friederichs et al., 2012; Graumann et al., 2014; Jaiswal et al., 2014; Vasnier et al., 2014). The only protein that has not been identified as such is SunB, the mid-SUN protein of *D. discoideum* which was reported to localise to regions surrounding nuclei (Shimada et al., 2010). A 4′,6-diamidino-2-phenylindole (DAPI) staining was used when imaging fixed cells but an ER marker was not (Shimada et al., 2010), meaning that the localisation of SunB at the ER is yet to be determined.

Interestingly, the NE-ER localisation of the mid-SUNs is observed in plants and yeast (see Fig. 5.13; Murphy et al., 2010; Friederichs et al., 2012; Graumann et al., 2014; Jaiswal et al., 2014; Vasnier et al., 2014), but not in animals (Sohaskey et al., 2010). While this is surprising due to the high conservation of mid-SUNs throughout Eukaryota (Murphy et al., 2010; Graumann et al., 2014; Vasnier et al., 2014), it should be noted that the localisation of Opt1 at the NE was not investigated (Sohaskey et al., 2010). Therefore, it is still possible that Opt1 localises to this compartment in addition to the ER due to the ER membrane and ONM being contiguous with one another. This is also the only recorded characterisation of a mid-SUN protein in mammals (Sohaskey et al., 2010), meaning that these findings may not be entirely representative of mid-SUNs in that kingdom. If, however, future work does show that mammalian mid-SUN proteins do only localise to the ER, then this may indicate that there is a functional divergence between kingdoms.

6.3 Putative Functions of mid-SUN Proteins

6.3.1 Putative Functions of mid-SUNs at the ER Membrane

The INM-localisation of the Cter-SUNs is pertinent to their function, the formation of LINC complexes, via interactions with ONM-localised KASH proteins. This raises questions about the putative functions of the Arabidopsis mid-SUN proteins. As aforementioned, Arabidopsis mid-SUN proteins were found to interact with Cter-SUNs, in addition to the plant KASH proteins *At*WIP1 and *At*TIK (Graumann et al., 2014). Previously to this, mid-SUN proteins had only been shown to interact with Cter-SUNs in yeast and fungi (Friederichs et al., 2012; Vasnier et al., 2014). The conservation of these interactions throughout multiple kingdoms suggest that they have a functional importance. Additional to this, the observation that mid-SUN proteins can interact with the KASH domain of *At*WIP1 further suggests that they have an active role in LINC complex formation (Graumann et al.,

2014). Their localisation to the ONM/ER infers however that they have a functional role in addition to LINC complex formation, but further work is required to determine if they have multiple roles.

Sohaskey et al. (2010) proposed that ER membrane-localised Opt is required to interact with ONM-localised KASH proteins via its SUN domain to connect the rER lumen to the cytoskeleton. It was hypothesised that such an interaction would help the rER maintain its structure and position within the cell, as well as facilitate intracellular communication (Sohaskey et al., 2010). If this were so, then that would mean that the functional role of the mid-SUN proteins may have a similar role to that of Cter-SUNs, in that they are required to form structural bridging complexes. This could be investigated by conducting ultrastructural analyses of plants are either single or double *At*SUN3/*At*SUN4 knockout mutants. If there were any changes in ER organisation, this could infer that mid-SUNs indeed have a biomechanical purpose. Similar experiments could also be carried out using the *At*SUN3 domain deletion mutants described in Chapter 3 to see if they also affect ER organisation.

6.3.1.1 Putative Role of mid-SUN Proteins in Unfolded Protein Response Signalling

Slp1 has been demonstrated to form a complex with the ER membrane protein Emp65 (Friederichs et al., 2012). These two proteins were initially detected in a screen used to identify genes involved in the Unfolded Protein Response (UPR; Jonikas et al., 2009), a highly complex signal transduction pathway that maintains protein homeostasis in response to ER stress in Eukaryotes, including plants (Angelos et al., 2017; Srivastava et al., 2018; Mitra and Ryoo, 2019; Fun and Thibault, 2020). Work into understanding the complexity of the UPR has focused largely on resolving ER stress, which is caused by an accumulation of un- or mis-folded proteins. It has been additionally shown that UPR components are involved in regulating physiological processes such as pollen development and pollen tube growth, as well as root hair development (Deng et al., 2016; Fragkostefanakis et al., 2016; Bao et al., 2019). These proteins were subsequently demonstrated to form a guardian complex

that protects partially-folded proteins from undergoing degradation (Zhang et al., 2017). Protein folding is a process that is currently not associated with LINC complex formation. This suggests a new avenue to explore for determining the function of plant mid-SUN proteins in addition to the structural role suggested in the work carried out on Opt1 at the rER (Sohaskey et al., 2010). Like Slp1, the ER membrane protein Emp65 is conserved throughout Eukaryota; its homolog in plants is called pollen defective in guidance1 (POD1). POD1 has already been shown to be an ER resident protein that interacts with the ER chaperone protein Calreticulin3 (CRT3; Li et al., 2011), which itself has been observed to mediate folding of membrane receptors. It has also been reported to be involved in ER protein retention (Li et al., 2011). It has been proposed that POD1 regulates CRT3 to control protein folding in the ER, specifically to regulate pollen tube guidance and early embryo patterning in response to female tissue signalling (Li et al., 2011).

POD1 has not yet been shown to interact with either *At*SUN3 or *At*SUN4, but this could be investigated to see if this ER membrane complex is formed in plants as well as in yeast. The observed activity of POD1 in ER protein retention and the formation of CRT3 complex would suggest that it plays a role in protein folding regulation. If interactions between POD1 and mid-SUN proteins were detected, it could be further suggested that this complex serves a similar purpose to that of the EMP65/Slp1 complex in *S. cerevisiae*. Promisingly, both *At*SUN3 and *At*SUN4 are predicted to interact with POD1 *in silico* according to the protein-protein interaction prediction software, STRING (Snel et al., 2000). Such interactions can be established using techniques that have already been used to identify interaction partners of AtSUN3 and AtSUN4, namely apFRET and/or FRET-FLIM (see Chapter 3). It would be highly interesting if POD1 was demonstrated to interact with the mid-SUN proteins, as this would provide further evidence that they have a functional role at the ER. This would particularly suggest that they have a role in protein-folding and would provide a novel avenue of research for future work to follow.

Empirical evidence that supports this hypothesis can be found in work conducted on *Cicer arietinum*, the Chickpea mid-SUN protein *Ca*SUN1 (Jaiswal et al., 2014). Mass spectrometry was used to identify *Ca*SUN1 as a component of dehydration response and was subsequently proposed to be regulated by

UPR signalling after carrying out stress-response assays (Jaiswal et al., 2014). Due to the sensitive nature of the ER, dehydration is just one of the environmental cues that can result in increased protein misfolding, triggering the UPR pathway. It has been shown that genes associated with the UPR signalling pathway are also involved in the osmotic stress pathway in plants, indicating that there is crosstalk between the two (Alvim et al., 2001; Koiwa et al., 2003; Irsigler et al., 2007; Valente et al., 2009; Zhang et al., 2017). For example, a salt stress response pathway was identified in Arabidopsis that resembled an ER stress response pathway (Liu et al., 2007).

*Ca*SUN1 was the first NE-associated protein that had been reported to be involved in dehydration pathway in plants (Jaiswal et al., 2014). Further work showed that *Ca*SUN1 was involved in UPR signalling by showing that, when subjected to dithiothreitol (DTT) treatment could complement the growth defect phenotype of the *S. cerevisiae* Slp1 mutant (Jaiswal et al., 2014), which is hypersensitive to UPR stress (Jonikas et al., 2009). Additionally, stably transformed seedlings overexpressing *Ca*SUN1 were found to have higher tolerance to dehydration, as well as other forms of stress (Jaiswal et al., 2014). Notably, phenotypic screenings of these mutants already presented a significantly shorter root length than wild-type plants prior to stress treatments (Jaiswal et al., 2014). Interestingly, the same study revealed that *At*SUN3 homozygous mutant seedlings subjected to the same stress treatments were found to be hypersensitive, resulting in decreased root length (Jaiswal et al., 2014). Overall, these findings suggest that the Arabidopsis mid-SUN proteins could have a functional role in stress response pathways that are regulated by UPR signalling.

6.3.1.2 A Potential Function for the AtSUN3-AtmaMyb Interaction?

Although this project has confirmed an interaction between *At*SUN3 and *At*maMyb, the function of this interaction remains unclear. If indeed *At*SUN3 has a role in UPR signalling however, then this potentially would provide further understanding. *At*maMyb is an ER membrane bound TF (see section 1.6; Slabaugh et al., 2011). Membrane bound TFs function when the active component is released from the membrane by proteolysis and is trafficked to the nucleus (see section 1.6; Liu et

al., 2018); *At*maMyb has been shown to be involved in root hair development and linked to auxin signalling (Slabaugh et al., 2011). Therefore, if *At*SUN3 was associated with UPR signalling, it could be suggested that its interaction with *At*maMyb may have a role in plant responses to stress.

It would therefore be useful to investigate whether the *At*SUN3-*At*maMyb interaction is related to ER stress response pathways. The production of transgenic Arabidopsis plants transformed with either *At*SUN3 or *At*maMyb under a 35S promoter, or use of existing *At*SUN3 or *At*maMyb knockout lines, could be used for investigating their potential role in the osmotic stress response (Jaiswal et al., 2014). Such experiments could assess whether their expression is upregulated in response to osmotic stress treatments and provide an indication as to whether *At*SUN3 is involved in plant stress responses.

6.3.2 Putative Functions of mid-SUNs at the NE

In addition to their putative roles at the ER membrane, mid-SUN localisation in plants also places them in prime position to interact with NE proteins. This is supported by the findings that *At*SUN3 and *At*SUN4 have been found to interact with both INM and ONM-localised proteins using apFRET (Graumann et al., 2014).

Such interactions have also been observed in organisms other than plants. For example, Slp1 in *S.cerevisiae* has been found to be required for localising Mps3, a Cter-SUN, to the NE (Friedrichs et al., 2012). It could be suggested that Slp1 is required to interact with Mps3 in order to tether it to the NE. Alternatively, it could also be suggested that this interaction is required for Mps3's translocation to the NE post-synthesis. In addition, Slp1 in *S. macrospora* has been shown to be required for nuclear fusion during meiosis, but not for any events proceeding this (Vasnier et al., 2014). It has been proposed that Slp1 acts in conjunction with SUN1, the Sordaria Cter-SUN protein whh localises to the SPB before, throughout, and following karyogamy. This hypothesis suggests that the two SUN

proteins transduce signals activated by nucleo-cytoskeletal dynamics to initiate nuclear fusion between homologous chromosomes (Vasnier et al., 2014). Interestingly SUN1 was observed to still localise to the spindle pole body during meiosis in an Slp1 null mutant line (Vasnier et al., 2014). Although not included in the work carried out in this thesis *At*SUN5, as well as *Zm*SUN5 and *Gb*SUN5, has been reported to be highly expressed in pollen, indicating a meiotic function for this mid-SUN protein (Murphy et al., 2010; Graumann et al., 2014; Yuan et al., 2021).

Despite not having yet been shown to form LINC complexes in plants, there is still a possibility that mid-SUN proteins do have a functional role in their formation. Arabidopsis mid-SUNs interact with Cter-SUNs and KASH proteins *in planta* (Graumann et al., 2014). Due to their ONM/ER localisation, if they do contribute to LINC complex formation then they might form bridging complexes from the ONM rather than INM. In turn, this would produce further interest in identifying which components they bind to whilst forming LINC complexes. For example, it would be of interest to observe whether mid-SUN proteins interact with any previously reported cytoskeletal LINC complex components, or if they interact with novel components. Alternatively, the potential formation of a mid-SUN-Cter-SUN-KASH domain protein complex could also be investigated. The localisation of the mid-SUN proteins also broadens the binding diversity of LINC complexes at the plant NE, which is already varied due to the presence of multiple KASH protein families: *At*WIPs, SINE proteins as well as *At*TIK (Xu et al., 2007; Graumann et al., 2014; Zhou et al., 2014).

Confirmation of mid-SUN protein interactions with plant KASH proteins provided evidence that the KASH domain is required for mid-SUN-KASH protein interactions (Graumann et al., 2014). It is still yet to be confirmed however whether mid-SUNs mediate this interaction via their SUN domain as Cter-SUNs do (Zhou et al., 2012). This is essential information as the domains that mediate this interaction determine whether mid-SUN-KASH protein complexes can be defined as LINC complexes. This could be determined by using techniques used previously in this thesis, such as MY2H, apFRET or FRET-FLIM (see Chapter 3), to test for interactions between KASH proteins and specific domains of the mid-SUN proteins. If the SUN domain of mid-SUN proteins is required for this interaction, then this will confirm that they form LINC complexes at the NE. This would provide an avenue for future

work to explore regarding the specific events required for mid-SUN-KASH LINC complexes in place of Cter-SUN-KASH LINC complexes. If these interactions are mediated via another domain of the mid-SUN protein however, then this would provide evidence that mid-SUN proteins have a functional role at the NE outside of LINC complex formation.

The above observations indicate that even if the Arabidopsis mid-SUN proteins do not contribute to LINC-complex formation, that they still interact with LINC complex components for other reasons. Further work would be required to determine this, but different functions for mid-SUN proteins at the NE could potentially include a biomechanical purpose, as proposed in other organisms (Sohaskey et al., 2010; Friedrichs et al., 2012). Alternatively, or in addition to this, mid-SUN proteins may form part of an additional network at the nuclear periphery. Due to the nature of their localisation, mid-SUN proteins may provide an interface through which they can interact with NE and ER components in tandem to transduce signals across the nuclear periphery. By facilitating this, mid-SUN proteins may contribute to the regulation of vital signalling pathways. The means by which mid-SUNs may facilitate signal transduction between these two organelles remains unclear, although it is likely that these events are related to multiple signalling pathways.

The broad variety of roles reported from previous work however shows that mid-SUNs are involved in cellular processes linked to both organelles (Murphy et al., 2010; Sohaskey et al., 2010; Friederichs et al., 2012; Graumann et al., 2014; Jaiswal et al., 2014; Vasnier et al., 2014). Therefore, it can be suggested that mid-SUN proteins contribute to a network that facilitates a functional relationship between the NE and ER. Mid-SUN localisation at the ONM/ER discussed previously (see Figs 4.2 & 5.13) supports this, as does their interactions with both NE- and ER-localised proteins (see Figs 3.7 & 3.11; Graumann et al., 2014). A significant amount of work would need to be carried out however to provide evidence for this hypothesis.

6.4 Insights into mid-SUN Topology

The orientation of the mid-SUN proteins is still unconfirmed. Whilst there is a predicted topology based on the amino acid sequence (see sections 1.5.2.2; Fig. 1.2), this has yet to be verified. There are several predictions that have already been published regarding the topology of mid-SUN proteins in *Z. mays* (Murphy et al., 2010). What is unclear from bioinformatic predictions is which protein terminus is located on which side of the membrane, and whether the topology is consistent for both mid-SUN proteins. Despite this however the work described in thesis, as well as previous work, has offered an insight as to the orientation of mid-SUN proteins. With three predicted TMDs, it is likely that the N- and C- termini of the Arabidopsis mid-SUN proteins are located on different sides of the membrane (see Fig. 1.2), with the main binding domains located in the luminal space.

The results from previous findings indicate that a large proportion of a mid-SUN protein extends into the PNS (Graumann et al., 2014). This is because they have been shown to interact with plant Cter-AtSUNs and KASH proteins (Graumann et al., 2014). The domains required of both to interact with mid-SUN proteins (the CCD and KASH domain, respectively) are located within the PNS (Graumann et al., 2010; Murphy et al., 2010; Zhou et al., 2012; see Fig. 1.2).

For these published interactions to take place, the domains of the mid-SUN proteins responsible for these interactions have to be located within the same sub-cellular compartment as their interaction partners. For example, apFRET has demonstrated that *At*SUN3 and *At*SUN4 are able to interact with *At*TIK via its KASH domain (Graumann et al., 2014). Since this domain is located in the PNS, this suggests that the interacting domain of the mid-SUN proteins is also located in the same sub-cellular compartment. It has not yet been determined which domain of the mid-SUN proteins is required for this interaction, but it can be hypothesised that the SUN domain mediates the binding of the two proteins.

Results from the work described in this thesis provide further insight regarding the orientation of mid-SUNs. As well as showing that *At*maMyb and *At*SUN3 interact with each other, its notable that the results from Table 2 show YFP-*At*SUN3 can interact with *At*maMyb regardless of which terminus

the fluorophore is fused to. The topology of *At*maMyb has already been established (Slabaugh et al., 2011), with both termini located in the cytosol. A detected interaction between it and *At*SUN3 using apFRET indicates that the N-terminus is also cytosol-facing. As an interaction between YFP-*At*SUN3 and CFP-*At*SUN4 was previously shown (Graumann et al., 2014), it can be further implied that the N-terminus of *At*SUN4 is also cytosolic-facing.

Due to *At*SUN3 and *At*SUN4 being indicated to localise to the ONM/PNER (see Chapters 4&5), roGFP can be used to confirm whether this model is correct (Brach et al., 2009). Determining the orientation of the mid-SUNs is crucial to understanding how they interact with both NE and ER proteins. It would provide information as to which domains, if any in particular, are required to mediate these interactions. This would provide novel insight into mid-SUN function at the nuclear periphery, particularly in regard to facilitating ER-NE signalling.

6.6 Conclusions

To summarise, the main findings presented in this thesis indicate that the Arabidopsis mid-SUN proteins have a different localisation at the nuclear periphery compared to Cter-SUNs. In turn, this has led to the conclusions that they potentially have a very different functional role. Not only have *At*SUN3 and *At*SUN4 been shown to form protein complexes within the mid-SUN sub-class, but the *At*SUN3- *At*maMyb indicates that mid-SUNs have functions that are not directly related to LINC complexes. Work investigating the functional roles of non-Arabidopsis mid-SUNs support this, indicating that they potentially have a role related to UPR signalling. The emerging work showing how UPR components are utilised in physiological processes provide an avenue to further investigating the *At*SUN3-AtmaMyb interaction. The observed localisation of *At*SUN3 and *At*SUN4 at the ONM/PNER support the hypotheses for their functional roles in both organelles. Although the mid-SUN proteins have yet to be shown to have a role in LINC complex formation, they potentially have alternate functions at the NE. The results produced using apFRET provide insight into mid-SUN

topology, indicating that the N-terminus is located in the cytosol whilst the C-terminus is located in the PNS/lumen. Collectively, this raises new questions regarding the character and function of *At*SUN3 and *At*SUN4, including whether they have protein-specific functions.

References

Aebi U, Cohn J, Buhle L, Gerace L. 1986. The nuclear lamina is a meshwork of intermediate-type filaments. Nature 323: 560–564.

Akhtar W, de Jong J, Pindyurin AV, Pagie L, Meuleman W, de Ridder J, Berns A, Wessels LFA, van Lohuizen M, van Steensel B. 2013. Chromatin Position Effects Assayed by Thousands of Reporters Integrated in Parallel. Cell 154: 914–927.

Al-Bassam J, Cui Y, Klopfenstein D, Carragher BO, Vale RD, Milligan RA. 2003. Distinct conformations of the kinesin Unc104 neck regulate a monomer to dimer motor transition. J. Cell Biol. 163: 743–753.

Alvim FC, Carolino SMB, Cascardo JCM, Nunes CC, Martinez CA, Otoni WC, Fontes EPB. 2001. Enhanced Accumulation of BiP in Transgenic Plants Confers Tolerance to Water Stress. Plant Physiol. 126: 1042 LP – 1054.

Anderson DJ, Hetzer MW. 2008. Shaping the endoplasmic reticulum into the nuclear envelope. J. Cell Sci. 121: 137 LP – 142.

Anderson DJ, Hetzer MW. 2007. Nuclear envelope formation by chromatin-mediated reorganization of the endoplasmic reticulum. Nat. Cell Biol. 9: 1160–1166.

Andov, B. 2014. 'Characterisation of the mid-SUN3 protein of *Arabidopsis thaliana*', undergraduate dissertation, Oxford Brookes University.

Anelli T, Sitia R. 2008. Protein quality control in the early secretory pathway. EMBO J. 27: 315–327.

Angelos E, Ruberti C, Kim S-J, Brandizzi F. 2017. Maintaining the factory: the roles of the unfolded protein response in cellular homeostasis in plants. Plant J. 90: 671–682.

Apel ED, Lewis RM, Grady RM, Sanes JR. 2000. Syne-1, a dystrophin- and Klarsicht-related protein associated with synaptic nuclei at the neuromuscular junction. J. Biol. Chem. 275: 31986–31995.

Ariotti N, Rae J, Giles N, Martel N, Sierecki E, Gambin Y, Hall TE, Parton RG. 2018. Ultrastructural localisation of protein interactions using conditionally stable nanobodies. PLOS Biol. 16: e2005473.

Armstrong MR, Boyden K, Browning ND, Campbell GH, Colvin JD, DeHope WJ, Frank AM, Gibson DJ, Hartemann F, Kim JS, King WE, LaGrange TB, Pyke BJ, Reed BW, Shuttlesworth RM, Stuart BC, Torralva BR. 2007. Practical considerations for high spatial and temporal resolution dynamic transmission electron microscopy. Ultramicroscopy 107: 356–367.

Bahmanyar S, Schlieker C. 2020. Lipid and protein dynamics that shape nuclear envelope identity. Mol. Biol. Cell 31: 1315–1323.

Bao Y, Bassham DC, Howell SH. 2019. A Functional Unfolded Protein Response Is Required for Normal Vegetative Development. Plant Physiol. 179: 1834 LP – 1843.

Bass HW, Bordoli SJ, Foss EM. 2003. The desynaptic (dy) and desynaptic1 (dsy1) mutations in maize (Zea mays L.) cause distinct telomere-misplacement phenotypes during meiotic prophase. J. Exp. Bot. 54: 39–46.

Bateman A, Finn RD, Sims PJ, Wiedmer T, Biegert A, Söding J. 2009. Phospholipid scramblases and Tubby-like proteins belong to a new superfamily of membrane tethered transcription factors. Bioinformatics 25: 159–162.

Baumann O, Walz BBT-IR of C. 2001. Endoplasmic reticulum of animal cells and its organization into structural and functional domains. Academic Press, p 149–214.

Becker W. 2012. Fluorescence lifetime imaging – techniques and applications. J. Microsc. 247: 119–136.

Biel A, Moser M, Meier I. 2020. Arabidopsis KASH Proteins SINE1 and SINE2 Are Involved in Microtubule Reorganization During ABA-Induced Stomatal Closure. Front. Plant Sci. 11: 575573.

Borg M, Brownfield L, Khatab H, Sidorova A, Lingaya M, Twell D. 2011. The R2R3 MYB Transcription Factor DUO1 Activates a Male Germline-Specific Regulon Essential for Sperm Cell Differentiation in Arabidopsis Plant Cell 23: 534 LP – 549.

Brach T, Soyk S, Müller C, Hinz G, Hell R, Brandizzi F, Meyer AJ. 2009. Non-invasive topology analysis of membrane proteins in the secretory pathway. Plant J. 57: 534–541.

Breeze E, Dzimitrowicz N, Kriechbaumer V, Brooks R, Botchway SW, Brady JP, Hawes C, Dixon AM, Schnell JR, Fricker MD, Frigerio L. 2016. A C-terminal amphipathic helix is necessary for the in vivo tubule-shaping function of a plant reticulon. Proc. Natl. Acad. Sci. 113: 10902 LP – 10907.

Bronshtein I, Kepten E, Kanter I, Berezin S, Lindner M, Redwood AB, Mai S, Gonzalo S, Foisner R, Shav-Tal Y, Garini Y. 2015. Loss of lamin A function increases chromatin dynamics in the nuclear interior. Nat. Commun. 6: 8044.

Brown D, Feeney M, Ahmadi M, Lonoce C, Sajari R, Di Cola A, Frigerio L. 2017. Subcellular localization and interactions among rubber particle proteins from Hevea brasiliensis. J. Exp. Bot. 68: 5045–5055.

Brunet A, Forsberg F, Fan Q, Sæther T, Collas P. 2019. Nuclear Lamin B1 Interactions With Chromatin During the Circadian Cycle Are Uncoupled From Periodic Gene Expression . Front. Genet. 10: 917.

Bücherl CA, Bader A, Westphal AH, Laptenok SP, Borst JW. 2014. FRET-FLIM applications in plant systems. Protoplasma 251: 383–394.

Burdakov D, Verkhratsky A. 2006. Biophysical re-equilibration of Ca2+ fluxes as a simple biologically plausible explanation for complex intracellular Ca2+ release patterns. FEBS Lett. 580: 463–468.

Burke B. 2018. LINC complexes as regulators of meiosis. Curr. Opin. Cell Biol. 52: 22–29.

Burke B, Stewart CL. 2013. The nuclear lamins: flexibility in function. Nat. Rev. Mol. Cell Biol. 14: 13–24.

Cain NE, Jahed Z, Schoenhofen A, Valdez VA, Elkin B, Hao H, Harris NJ, Herrera LA, Woolums BM, Mofrad MRK, Luxton GWG, Starr DA. 2018. Conserved SUN-KASH Interfaces Mediate LINC Complex-Dependent Nuclear Movement and Positioning. Curr. Biol. 28: 3086-3097.e4.

Camborde L, Jauneau A, Brière C, Deslandes L, Dumas B, Gaulin E. 2017. Detection of nucleic acid-protein interactions in plant leaves using fluorescence lifetime imaging microscopy. Nat. Protoc. 12: 1933–1950.

Caron NS, Munsie LN, Keillor JW, Truant R. 2012. Using FLIM-FRET to Measure Conformational Changes of Transglutaminase Type 2 in Live Cells. PLoS One 7: e44159.

Casolari JM, Brown CR, Komili S, West J, Hieronymus H, Silver PA. 2004. Genome-Wide Localization of the Nuclear Transport Machinery Couples Transcriptional Status and Nuclear Organization. Cell 117: 427–439.

Chabaud M, Genre A, Sieberer BJ, Faccio A, Fournier J, Novero M, Barker DG, Bonfante P. 2011. Arbuscular mycorrhizal hyphopodia and germinated spore exudates trigger Ca2+ spiking in the legume and nonlegume root epidermis. New Phytol. 189: 347–355.

Chang Y, Kim D-H, Zhou K, Jeong MG, Park S, Kwon Y, Hong TM, Noh J, Ryu SH. 2021. Improved resolution in single-molecule localization microscopy using QD-PAINT. Exp. Mol. Med. 53: 384–392.

Chen P, Takatsuka H, Takahashi N, Kurata R, Fukao Y, Kobayashi K, Ito M, Umeda M. 2017. Arabidopsis R1R2R3-Myb proteins are essential for inhibiting cell division in response to DNA damage. Nat. Commun. 8: 635.

Chen Y, Mills JD, Periasamy A. 2003. Protein localization in living cells and tissues using FRET and FLIM. Differentiation 71: 528–541.

Chi Y-H, Haller K, Peloponese J-M, Jeang K-T. 2007. Histone acetyltransferase hALP and nuclear membrane protein hsSUN1 function in de-condensation of mitotic chromosomes. J. Biol. Chem. 282: 27447–27458.

Ciska M, Hikida R, Masuda K, Moreno Díaz de la Espina S. 2019. Evolutionary history and structure of nuclear matrix constituent proteins, the plant analogues of lamins. J. Exp. Bot. 70: 2651–2664.

Ciska M, Moreno DÃ-az de la Espina S. 2014. The intriguing plant nuclear lamina. Front. Plant Sci. 5: 166.

Coffinier C, Jung H-J, Nobumori C, Chang S, Tu Y, Barnes RH, Yoshinaga Y, de Jong PJ, Vergnes L, Reue K, Fong LG, Young SG. 2011. Deficiencies in lamin B1 and lamin B2 cause neurodevelopmental defects and distinct nuclear shape abnormalities in neurons. Mol. Biol. Cell 22: 4683–4693.

Colcombet J, Lopez-Obando M, Heurtevin L, Bernard C, Martin K, Berthomé R, Lurin C. 2013. Systematic study of subcellular localization of Arabidopsis PPR proteins confirms a massive targeting to organelles. RNA Biol. 10: 1557–1575.

Conchello J-A, Lichtman JW. 2005. Optical sectioning microscopy. Nat. Methods 2: 920–931.

Conrad MN, Lee C-Y, Chao G, Shinohara M, Kosaka H, Shinohara A, Conchello J-A, Dresser ME. 2008. Rapid Telomere Movement in Meiotic Prophase Is Promoted By NDJ1, MPS3, and CSM4 and Is Modulated by Recombination. Cell 133: 1175–1187.

Cox G, Sheppard CJR. 2004. Practical limits of resolution in confocal and non-linear microscopy. Microsc. Res. Tech. 63: 18–22.

Craig S, Staehelin LA. 1988. High pressure freezing of intact plant tissues. Evaluation and characterization of novel features of the endoplasmic reticulum and associated membrane systems. Eur. J. Cell Biol. 46: 81–93.

Cremazy FGE, Manders EMM, Bastiaens PIH, Kramer G, Hager GL, van Munster EB, Verschure PJ, Gadella TJ, van Driel R. 2005. Imaging in situ protein–DNA interactions in the cell nucleus using FRET–FLIM. Exp. Cell Res. 309: 390–396.

Crisp M, Liu Q, Roux K, Rattner JB, Shanahan C, Burke B, Stahl PD, Hodzic D. 2006. Coupling of the nucleus and cytoplasm: role of the LINC complex. J. Cell Biol. 172: 41–53.

Cronshaw JM, Krutchinsky AN, Zhang W, Chait BT, Matunis MJ. 2002. Proteomic analysis of the mammalian nuclear pore complex . J. Cell Biol. 158: 915–927.

DeGrasse JA, DuBois KN, Devos D, Siegel TN, Sali A, Field MC, Rout MP, Chait BT. 2009. Evidence for a Shared Nuclear Pore Complex Architecture That Is Conserved from the Last Common Eukaryotic Ancestor*,. Mol. Cell. Proteomics 8: 2119–2130.

Deng Y, Humbert S, Liu J-X, Srivastava R, Rothstein SJ, Howell SH. 2011. Heat induces the splicing by IRE1 of a mRNA encoding a transcription factor involved in the unfolded protein response in Arabidopsis. Proc. Natl. Acad. Sci. 108: 7247 LP – 7252.

Deng Y, Srivastava R, Quilichini TD, Dong H, Bao Y, Horner HT, Howell SH. 2016. IRE1, a component of the unfolded protein response signaling pathway, protects pollen development in Arabidopsis from heat stress. Plant J. 88: 193–204.

Dennison SR, Harris F, Brandenburg K, Phoenix DA. 2007. Characterization of the N-terminal segment used by the barley yellow dwarf virus movement protein to promote interaction with the nuclear membrane of host plant cells. Peptides 28: 2091–2097.

Devos D, Dokudovskaya S, Williams R, Alber F, Eswar N, Chait BT, Rout MP, Sali A. 2006. Simple fold composition and modular architecture of the nuclear pore complex. Proc. Natl. Acad. Sci. 103: 2172 LP – 2177.

Dikovskaya D, Dinkova-Kostova AT. 2020. Measuring Changes in Keap1-Nrf2 Protein Complex Conformation in Individual Cells by FLIM-FRET. Curr. Protoc. Toxicol. 85: e96.

Dilworth DJ, Tackett AJ, Rogers RS, Yi EC, Christmas RH, Smith JJ, Siegel AF, Chait BT, Wozniak RW, Aitchison JD. 2005. The mobile nucleoporin Nup2p and chromatin-bound Prp20p function in endogenous NPC-mediated transcriptional control . J. Cell Biol. 171: 955–965.

Ding X, Xu R, Yu J, Xu T, Zhuang Y, Han M. 2007. SUN1 is required for telomere attachment to nuclear envelope and gametogenesis in mice. Dev. Cell 12: 863–872.

Dittmer TA, Stacey NJ, Sugimoto-Shirasu K, Richards EJ. 2007. LITTLE NUCLEI Genes Affecting Nuclear Morphology in Arabidopsis thaliana Plant Cell 19: 2793 LP – 2803.

Doré K, Labrecque S, Tardif C, De Koninck P. 2014. FRET-FLIM Investigation of PSD95-NMDA Receptor Interaction in Dendritic Spines; Control by Calpain, CaMKII and Src Family Kinase. PLoS One 9: e112170.

Downie L, Priddle J, Hawes C, Evans DE. 1998. A calcium pump at the higher plant nuclear envelope? FEBS Lett. 429: 44–48.

Du H, Liang Z, Zhao S, Nan M-G, Tran L-SP, Lu K, Huang Y-B, Li J-N. 2015. The Evolutionary History of R2R3-MYB Proteins Across 50 Eukaryotes: New Insights Into Subfamily Classification and Expansion. Sci. Rep. 5: 11037.

Dubos C, Stracke R, Grotewold E, Weisshaar B, Martin C, Lepiniec L. 2010. MYB transcription factors in Arabidopsis. Trends Plant Sci. 15: 573–581.

Dufrêne YF, Ando T, Garcia R, Alsteens D, Martinez-Martin D, Engel A, Gerber C, Müller DJ. 2017. Imaging modes of atomic force microscopy for application in molecular and cell biology. Nat. Nanotechnol. 12: 295–307.

Dvořák Tomaštíková E, Rutten T, Dvořák P, Tugai A, Ptošková K, Petrovská B, van Damme D, Houben A, Doležel J, Demidov D. 2020. Functional Divergence of Microtubule-Associated TPX2 Family Members in Arabidopsis thaliana. Int. J. Mol. Sci. 21.

Ehrhardt DW, Wais R, Long SR. 1996. Calcium Spiking in Plant Root Hairs Responding to Rhizobium Nodulation Signals. Cell 85: 673–681.

Elhanany-Tamir H, Yu Y V, Shnayder M, Jain A, Welte M, Volk T. 2012. Organelle positioning in muscles requires cooperation between two KASH proteins and microtubules. J. Cell Biol. 198: 833–846.

Ellenberg J, Siggia ED, Moreira JE, Smith CL, Presley JF, Worman HJ, Lippincott-Schwartz J. 1997. Nuclear Membrane Dynamics and Reassembly in Living Cells: Targeting of an Inner Nuclear Membrane Protein in Interphase and Mitosis . J. Cell Biol. 138: 1193–1206.

Elmore SP, Nishimura Y, Qian T, Herman B, Lemasters JJ. 2004. Discrimination of depolarized from polarized mitochondria by confocal fluorescence resonance energy transfer. Arch. Biochem. Biophys. 422: 145–152.

Fava F, Raynaud-Messina B, Leung-Tack J, Mazzolini L, Li M, Guillemot JC, Cachot D, Tollon Y, Ferrara P, Wright M. 1999. Human 76p: A New Member of the γ-Tubulin–Associated Protein Family. J. Cell Biol. 147: 857–868.

Ferrol N, Bennett AB. 1996. A Single Gene May Encode Differentially Localized Ca2+-ATPases in Tomato. Plant Cell 8: 1159 LP – 1169.

Field MC, Koreny L, Rout MP. 2014. Enriching the Pore: Splendid Complexity from Humble Origins. Traffic 15: 141–156.

Fiserova J, Kiseleva E, Goldberg MW. 2009. Nuclear envelope and nuclear pore complex structure and organization in tobacco BY-2 cells. Plant J. 59: 243–255.

Fragkostefanakis S, Mesihovic A, Hu Y, Schleiff E. 2016. Unfolded protein response in pollen development and heat stress tolerance. Plant Reprod. 29: 81–91.

Fridolfsson HN, Ly N, Meyerzon M, Starr DA. 2010. UNC-83 coordinates kinesin-1 and dynein activities at the nuclear envelope during nuclear migration. Dev. Biol. 338: 237–250.

Friederichs JM, Gardner JM, Smoyer CJ, Whetstine CR, Gogol M, Slaughter BD, Jaspersen SL. 2012. Genetic analysis of Mps3 SUN domain mutants in Saccharomyces cerevisiae reveals an interaction with the SUN-like protein Slp1. G3 (Bethesda). 2: 1703–18.

Fu S, Yang L, Li P, Hofmann O, Dicker L, Hide W, Lin X, Watkins SM, Ivanov AR, Hotamisligil GS. 2011. Aberrant lipid metabolism disrupts calcium homeostasis causing liver endoplasmic reticulum stress in obesity. Nature 473: 528–531.

Fu X, Liao Y, Cheng S, Xu X, Grierson D, Yang Z. 2021. Nonaqueous fractionation and overexpression of fluorescent-tagged enzymes reveals the subcellular sites of L-theanine biosynthesis in tea. Plant Biotechnol. J. 19: 98–108.

Fun XH, Thibault G. 2020. Lipid bilayer stress and proteotoxic stress-induced unfolded protein response deploy divergent transcriptional and non-transcriptional programmes. Biochim. Biophys. Acta - Mol. Cell Biol. Lipids 1865: 158449.

Funakoshi T, Maeshima K, Yahata K, Sugano S, Imamoto F, Imamoto N. 2007. Two distinct human POM121 genes: Requirement for the formation of nuclear pore complexes. FEBS Lett. 581: 4910–4916.

Gerace L, Tapia O. 2018. Messages from the voices within: regulation of signaling by proteins of the nuclear lamina. Curr. Opin. Cell Biol. 52: 14–21.

Göb E, Schmitt J, Benavente R, Alsheimer M. 2010. Mammalian Sperm Head Formation Involves Different Polarization of Two Novel LINC Complexes. PLoS One 5: e12072.

Golden A, Liu J, Cohen-Fix O. 2009. Inactivation of the C. elegans lipin homolog leads to ER disorganization and to defects in the breakdown and reassembly of the nuclear envelope. J. Cell Sci. 122: 1970 LP – 1978.

Gomez-Cavazos JS, Hetzer MW. 2012. Outfits for different occasions: tissue-specific roles of Nuclear Envelope proteins. Curr. Opin. Cell Biol. 24: 775–783.

Goodin MM, Chakrabarty R, Yelton S, Martin K, Clark A, Brooks R. 2007. Membrane and protein dynamics in live plant nuclei infected with Sonchus yellow net virus, a plant-adapted rhabdovirus. J. Gen. Virol. 88: 1810–1820.

Goto C, Hashizume S, Fukao Y, Hara-Nishimura I, Tamura K. 2019. Comprehensive nuclear proteome of Arabidopsis obtained by sequential extraction. Nucleus 10: 81–92.

Goto C, Tamura K, Fukao Y, Shimada T, Hara-Nishimura I. 2014. The novel nuclear envelope protein KAKU4 modulates nuclear morphology in Arabidopsis. Plant Cell 26: 2143–2155.

Graumann K. 2014. Evidence for LINC1-SUN associations at the plant nuclear periphery. PLoS One 9: e93406.

Graumann K, Evans DE. 2011. Nuclear envelope dynamics during plant cell division suggest common mechanisms between kingdoms. Biochem. J. 435: 661–7.

Graumann K, Runions J, Evans DE. 2010. Characterization of SUN-domain proteins at the higher plant nuclear envelope. Plant J. 61: 134–144.

Graumann K, Vanrobays E, Tutois S, Probst A V, Evans DE, Tatout C. 2014. Characterization of two distinct subfamilies of SUN-domain proteins in Arabidopsis and their interactions with the novel KASH-domain protein AtTIK. J. Exp. Bot. 65: 6499–6512.

Groves NR, McKenna JF, Evans DE, Graumann K, Meier I. 2019. A nuclear localization signal targets tail-anchored membrane proteins to the inner nuclear envelope in plants. J. Cell Sci. 132: jcs226134.

Gruenbaum Y, Medalia O. 2015. Lamins: the structure and protein complexes. Curr. Opin. Cell Biol. 32: 7–12.

Gueth-Hallonet C, Wang J, Harborth J, Weber K, Osborn M. 1998. Induction of a Regular Nuclear Lattice by Overexpression of NuMA. Exp. Cell Res. 243: 434–452.

Gumber HK, McKenna JF, Estrada AL, Tolmie AF, Graumann K, Bass HW. 2019. Identification and characterization of genes encoding the nuclear envelope LINC complex in the monocot species Zea mays J. Cell Sci. 132: jcs221390.

Gundersen GG, Worman HJ. 2013. Nuclear positioning. Cell 152: 1376–89.

Gundersen GG, Worman HJ. 2013. Nuclear Positioning. Cell 152: 1376–1389.

Guo T, Mao X, Zhang H, Zhang Y, Fu M, Sun Z, Kuai P, Lou Y, Fang Y. 2017. Lamin-like Proteins Negatively Regulate Plant Immunity through NAC WITH TRANSMEMBRANE MOTIF1-LIKE9 and NONEXPRESSOR OF PR GENES1 in Arabidopsis thaliana. Mol. Plant 10: 1334–1348.

Hagan I, Yanagida M. 1995. The product of the spindle formation gene sad1+ associates with the fission yeast spindle pole body and is essential for viability. J. Cell Biol. 129: 1033–47.

Haque F, Lloyd DJ, Smallwood DT, Dent CL, Shanahan CM, Fry AM, Trembath RC, Shackleton S. 2006. SUN1 interacts with nuclear lamin A and cytoplasmic nesprins to provide a physical connection between the nuclear lamina and the cytoskeleton. Mol. Cell. Biol. 26: 3738–3751.

Henderson MJ, Wires ES, Trychta KA, Richie CT, Harvey BK. 2014. SERCaMP: a carboxy-terminal protein modification that enables monitoring of ER calcium homeostasis. Mol. Biol. Cell 25: 2828–2839.

Hermann R, Walther P, Müller M. 1996. Immunogold labeling in scanning electron microscopy. Histochem. Cell Biol. 106: 31–39.

Hetzer MW. 2010. The nuclear envelope. Cold Spring Harb. Perspect. Biol. 2: a000539–a000539.

Hodzic DM, Yeater DB, Bengtsson L, Otto H, Stahl PD. 2004. Sun2 is a novel mammalian inner nuclear membrane protein. J. Biol. Chem. 279: 25805–12.

Horn HF, Kim DI, Wright GD, Wong ESM, Stewart CL, Burke B, Roux KJ. 2013. A mammalian KASH domain protein coupling meiotic chromosomes to the cytoskeleton. J. Cell Biol. 202: 1023–1039.

Hu B, Wang N, Bi X, Karaaslan ES, Weber A-L, Zhu W, Berendzen KW, Liu C. 2019. Plant lamin-like proteins mediate chromatin tethering at the nuclear periphery. Genome Biol. 20: 87.

Huang W, Miao M, Kud J, Niu X, Ouyang B, Zhang J, Ye Z, Kuhl JC, Liu Y, Xiao F. 2013. SlNAC1, a stress-related transcription factor, is fine-tuned on both the transcriptional and the post-translational level. New Phytol. 197: 1214–1224.

Huber MD, Guan T, Gerace L. 2009. Overlapping Functions of Nuclear Envelope Proteins NET25 (Lem2) and Emerin in Regulation of Extracellular Signal-Regulated Kinase Signaling in Myoblast Differentiation. Mol. Cell. Biol. 29: 5718 LP – 5728.

Huff J, Bergter A, Birkenbeil J, Kleppe I, Engelmann R, Krzic U. 2017. The new 2D Superresolution mode for ZEISS Airyscan. Nat. Methods 14: 1223.

Hurt E, Beck M. 2015. Towards understanding nuclear pore complex architecture and dynamics in the age of integrative structural analysis. Curr. Opin. Cell Biol. 34: 31–38.

Irons SL, Evans DE, Brandizzi F. 2003. The ® rst 238 amino acids of the human lamin B receptor are targeted to the nuclear envelope in plants. 54: 943–950.

Irsigler AST, Costa MDL, Zhang P, Reis PAB, Dewey RE, Boston RS, Fontes EPB. 2007. Expression profiling on soybean leaves reveals integration of ER- and osmotic-stress pathways. BMC Genomics 8: 431.

Iwabuchi K, Minamino R, Takagi S. 2010. Actin Reorganization Underlies Phototropin-Dependent Positioning of Nuclei in Arabidopsis Leaf Cells. Plant Physiol. 152: 1309 LP – 1319.

Iwabuchi K, Sakai T, Takagi S. 2007. Blue Light-Dependent Nuclear Positioning in Arabidopsis thaliana Leaf Cells. Plant Cell Physiol. 48: 1291–1298.

Jackson AO, Dietzgen RG, Goodin MM, Bragg JN, Deng M. 2005. Biology of Plant Rhabdoviruses. Annu. Rev. Phytopathol. 43: 623–660.

Jahed Z, Hao H, Thakkar V, Vu UT, Valdez VA, Rathish A, Tolentino C, Kim SCJ, Fadavi D, Starr DA, Mofrad MRK. 2019. Role of KASH domain lengths in the regulation of LINC complexes. Mol. Biol. Cell 30: 2076–2086.

Jahed Z, Shams H, Mofrad MRK. 2015. A Disulfide Bond Is Required for the Transmission of Forces through SUN-KASH Complexes. Biophys. J. 109: 501–509.

Jaiswal DK, Mishra P, Subba P, Rathi D, Chakraborty S, Chakraborty N. 2014. Membrane-associated proteomics of chickpea identifies Sad1/UNC-84 protein (CaSUN1), a novel component of dehydration signaling. Sci. Rep. 4: 4177.

Jalbert I, Stapleton F, Papas E, Sweeney DF, Coroneo M. 2003. In vivo confocal microscopy of the human cornea. Br. J. Ophthalmol. 87: 225–236.

Jevtić P, Mukherjee RN, Chen P, Levy DL. 2019. Altering the levels of nuclear import factors in early Xenopus laevis embryos affects later development. PLoS One 14: e0215740.

Jonikas MC, Collins SR, Denic V, Oh E, Quan EM, Schmid V, Weibezahn J, Schwappach B, Walter P, Weissman JS, Schuldiner M. 2009. Comprehensive characterization of genes required for protein folding in the endoplasmic reticulum. Science 323: 1693–1697.

Kalab P, Weis K, Heald R. 2002. Visualization of a Ran-GTP gradient in interphase and mitotic Xenopus egg extracts. Science 295: 2452–2456.

Karpova TS, Baumann CT, He L, Wu X, Grammer A, Lipsky P, Hager GL, McNally JG. 2003. Fluorescence resonance energy transfer from cyan to yellow fluorescent protein detected by acceptor photobleaching using confocal microscopy and a single laser. J. Microsc. 209: 56–70.

Kim DI, KC B, Roux KJ. 2015. Making the LINC: SUN and KASH protein interactions. Biol. Chem. 396: 295–310.

Kim J-K, Louhghalam A, Lee G, Schafer BW, Wirtz D, Kim D-H. 2017. Nuclear lamin A/C harnesses the perinuclear apical actin cables to protect nuclear morphology. Nat. Commun. 8: 2123.

Kim S-G, Lee S, Seo PJ, Kim S-K, Kim J-K, Park C-M. 2010. Genome-scale screening and molecular characterization of membrane-bound transcription factors in Arabidopsis and rice. Genomics 95: 56–65.

Kim Y-S, Kim S-G, Park J-E, Park H-Y, Lim M-H, Chua N-H, Park C-M. 2006. A membrane-bound NAC transcription factor regulates cell division in Arabidopsis. Plant Cell 18: 3132–3144.

Klüsener B, Boheim G, Liss H, Engelberth J, Weiler EW. 1995. Gadolinium-sensitive, voltage-dependent calcium release channels in the endoplasmic reticulum of a higher plant mechanoreceptor organ. EMBO J. 14: 2708–2714.

Knockenhauer KE, Schwartz TU. 2016. The Nuclear Pore Complex as a Flexible and Dynamic Gate. Cell 164: 1162–1171.

Koiwa H, Li F, McCully MG, Mendoza I, Koizumi N, Manabe Y, Nakagawa Y, Zhu J, Rus A, Pardo JM, Bressan RA, Hasegawa PM. 2003. The STT3a Subunit Isoform of the Arabidopsis Oligosaccharyltransferase Controls Adaptive Responses to Salt/Osmotic Stress. Plant Cell 15: 2273 LP – 2284.

Kon T, Imamula K, Roberts AJ, Ohkura R, Knight PJ, Gibbons IR, Burgess SA, Sutoh K. 2009. Helix sliding in the stalk coiled coil of dynein couples ATPase and microtubule binding. Nat. Struct. Mol. Biol. 16: 325–333.

Kornblihtt AR, Schor IE, Alló M, Dujardin G, Petrillo E, Muñoz MJ. 2013. Alternative splicing: a pivotal step between eukaryotic transcription and translation. Nat. Rev. Mol. Cell Biol. 14: 153–165.

Korobchevskaya K, Lagerholm BC, Colin-York H, Fritzsche M. 2017. Exploring the Potential of Airyscan Microscopy for Live Cell Imaging. Photonics 4.

Koszul R, Kim KP, Prentiss M, Kleckner N, Kameoka S. 2008. Meiotic Chromosomes Move by Linkage to Dynamic Actin Cables with Transduction of Force through the Nuclear Envelope. Cell 133: 1188–1201.

Kreibich G, Czakó-Graham M, Grebenau R, Mok W, Rodriguez-Boulan E, Sabatini DD. 1978. Characterization of the ribosomal binding site in rat liver rough microsomes: Ribophorins I and II, two integral membrane proteins related to ribosome binding. J. Supramol. Struct. 8: 279–302.

Kriechbaumer V, Botchway SW, Hawes C. 2017. Localization and interactions between Arabidopsis auxin biosynthetic enzymes in the TAA/YUC-dependent pathway. J. Exp. Bot. 68: 4195–4207.

Kriechbaumer V, Botchway SW, Slade SE, Knox K, Frigerio L, Oparka K, Hawes C. 2015. Reticulomics: Protein-Protein Interaction Studies with Two Plasmodesmata-Localized Reticulon Family Proteins Identify Binding Partners Enriched at Plasmodesmata, Endoplasmic Reticulum, and the Plasma Membrane. Plant Physiol. 169: 1933 LP – 1945.

Kriechbaumer V, Breeze E, Pain C, Tolmie F, Frigerio L, Hawes C. 2018. Arabidopsis Lunapark proteins are involved in ER cisternae formation. New Phytol. 219: 990–1004.

Kumaran RI, Thakar R, Spector DL. 2008. Chromatin Dynamics and Gene Positioning. Cell 132: 929–934.

Kylberg K, Björk P, Fomproix N, Ivarsson B, Wieslander L, Daneholt B. 2010. Exclusion of mRNPs and ribosomal particles from a thin zone beneath the nuclear envelope revealed upon inhibition of transport. Exp. Cell Res. 316: 1028–1038.

Lei K, Zhang X, Ding X, Guo X, Chen M, Zhu B, Xu T, Zhuang Y, Xu R, Han M. 2009. SUN1 and SUN2 play critical but partially redundant roles in anchoring nuclei in skeletal muscle cells in mice. Proc. Natl. Acad. Sci. 106: 10207 LP – 10212.

Lei K, Zhu X, Xu R, Shao C, Xu T, Zhuang Y, Han M. 2012. Inner Nuclear Envelope Proteins SUN1 and SUN2 Play a Prominent Role in the DNA Damage Response. Curr. Biol. 22: 1609–1615.

Li H-J, Xue Y, Jia D-J, Wang T, hi D-Q, Liu J, Cui F, Xie Q, Ye D, Yang W-C. 2011. POD1 Regulates Pollen Tube Guidance in Response to Micropylar Female Signaling and Acts in Early Embryo Patterning in Arabidopsis Plant Cell 23: 3288 LP – 3302.

Lin-Wang K, Bolitho K, Grafton K, Kortstee A, Karunairetnam S, McGhie TK, Espley R V, Hellens RP, Allan AC. 2010. An R2R3 MYB transcription factor associated with regulation of the anthocyanin biosynthetic pathway in Rosaceae. BMC Plant Biol. 10: 50.

Liu B-F, Anbarasu K, Liang JJ-N. 2007. Confocal fluorescence resonance energy transfer microscopy study of protein-protein interactions of lens crystallins in living cells. Mol. Vis. 13: 854–861.

Liu DYT, Smith PMC, Barton DA, Day DA, Overall RL. 2017. Characterisation of Arabidopsis calnexin 1 and calnexin 2 in the endoplasmic reticulum and at plasmodesmata. Protoplasma 254: 125–136.

Liu Y, Li P, Fan L, Wu M. 2018. The nuclear transportation routes of membrane-bound transcription factors. Cell Commun. Signal. 16: 12.

Liu Y, Salter HK, Holding AN, Johnson CM, Stephens E, Lukavsky PJ, Walshaw J, Bullock SL. 2013. Bicaudal-D uses a parallel, homodimeric coiled coil with heterotypic registry to coordinate recruitment of cargos to dynein. Genes Dev. 27: 1233–1246.

Long Y, Stahl Y, Weidtkamp-Peters S, Postma M, Zhou W, Goedhart J, Sánchez-Pérez M-I, Gadella TWJ, Simon R, Scheres B, Blilou I. 2017. In vivo FRET–FLIM reveals cell-type-specific protein interactions in Arabidopsis roots. Nature 548: 97–102.

Long Y, Stahl Y, Weidtkamp-Peters S, Smet W, Du Y, Gadella TWJ, Goedhart J, Scheres B, Blilou I. 2018. Optimizing FRET-FLIM Labeling Conditions to Detect Nuclear Protein Interactions at Native Expression Levels in Living Arabidopsis Roots . Front. Plant Sci. 9: 639.

Malone CJ, Fixsen WD, Horvitz HR, Han M. 1999. UNC-84 localizes to the nuclear envelope and is required for nuclear migration and anchoring during C. elegans development. Development 126: 3171 LP – 3181.

Marques PE, Antunes MM, David BA, Pereira R V., Teixeira MM, Menezes GB. 2015. Imaging liver biology in vivo using conventional confocal microscopy. Nat. Protoc. 10: 258–268.

Mason JM, Arndt KM. 2004. Coiled coil domains: stability, specificity, and biological implications. Chembiochem 5: 170–176.

Matzke M, Weiger TM, Papp I, Matzke AJM. 2009. Nuclear membrane ion channels mediate root nodule development. Trends Plant Sci. 14: 295–298.

McAlinden A, Smith TA, Sandell LJ, Ficheux D, Parry DAD, Hulmes DJS. 2003. α-Helical Coiled-coil Oligomerization Domains Are Almost Ubiquitous in the Collagen Superfamily*. J. Biol. Chem. 278: 42200–42207.

Meinema AC, Laba JK, Hapsari RA, Otten R, Mulder FAA, Kralt A, van den Bogaart G, Lusk CP, Poolman B, Veenhoff LM. 2011. Long Unfolded Linkers Facilitate Membrane Protein Import Through the Nuclear Pore Complex. Science (80-.). 333: 90 LP – 93.

Meinke P, Schirmer EC. 2015. LINC'ing form and function at the nuclear envelope. FEBS Lett. 589: 2514–2521.

Mermet, S. 2018. 'Investigating functional domains of mid-SUN proteins in plants'. Université Clermont Auvergne.

Meyerzon M, Fridolfsson HN, Ly N, McNally FJ, Starr DA. 2009. UNC-83 is a nuclear-specific cargo adaptor for kinesin-1-mediated nuclear migration. Development 136: 2725 LP – 2733.

Miserey-Lenkei S, Waharte F, Boulet A, Cuif M-H, Tenza D, El Marjou A, Raposo G, Salamero J, Héliot L, Goud B, Monier S. 2007. Rab6-interacting Protein 1 Links Rab6 and Rab11 Function. Traffic 8: 1385–1403.

Mitchell JM, Mansfeld J, Capitanio J, Kutay U, Wozniak RW. 2010. Pom121 links two essential subcomplexes of the nuclear pore complex core to the membrane. J. Cell Biol. 191: 505–521.

Mitra S, Ryoo HD. 2019. The unfolded protein response in metazoan development. J. Cell Sci. 132: jcs217216.

Moreno JE, Shyu C, Campos ML, Patel LC, Chung HS, Yao J, He SY, Howe GA. 2013. Negative Feedback Control of Jasmonate Signaling by an Alternative Splice Variant of JAZ10. Plant Physiol. 162: 1006 LP – 1017.

Morimoto A, Shibuya H, Zhu X, Kim J, Ishiguro K, Han M, Watanabe Y. 2012. A conserved KASH domain protein associates with telomeres, SUN1, and dynactin during mammalian meiosis. J. Cell Biol. 198: 165–72.

Mukherjee RN, Sallé J, Dmitrieff S, Nelson KM, Oakey J, Minc N, Levy DL. 2020. The Perinuclear ER Scales Nuclear Size Independently of Cell Size in Early Embryos. Dev. Cell 54: 395-409.e7.

Murphy SP, Gumber HK, Mao Y, Bass HW. 2014. A dynamic meiotic SUN belt includes the zygotene-stage telomere bouquet and is disrupted in chromosome segregation mutants of maize (Zea mays L.) . Front. Plant Sci. 5: 314.

Murphy SP, Simmons CR, Bass HW. 2010. Structure and expression of the maize (Zea mays L.) SUN-domain protein gene family: evidence for the existence of two divergent classes of SUN proteins in plants. BMC Plant Biol. 10: 269.

Murphy SM, Preble AM, Patel UK, O'Connell KL, Dias DP, Moritz M, Agard D, Stults JT, Stearns T. 2001. GCP5 and GCP6: Two New Members of the Human γ-Tubulin Complex. Mol. Biol. Cell 12: 3340–3352.

Nagashima Y, von Schaewen A, Koiwa H. 2018. Function of N-glycosylation in plants. Plant Sci. 274: 70–79.

Narayan K, Danielson CM, Lagarec K, Lowekamp BC, Coffman P, Laquerre A, Phaneuf MW, Hope TJ, Subramaniam S. 2014. Multi-resolution correlative focused ion beam scanning electron microscopy: Applications to cell biology. J. Struct. Biol. 185: 278–284.

Noel DK, J.S. RA, Jan L. 2008. Nuclear Shape, Mechanics, and Mechanotransduction. Circ. Res. 102: 1307–1318.

Obado SO, Brillantes M, Uryu K, Zhang W, Ketaren NE, Chait BT, Field MC, Rout MP. 2016. Interactome Mapping Reveals the Evolutionary History of the Nuclear Pore Complex. PLOS Biol. 14: e1002365.

Oda Y, Fukuda H. 2011. Dynamics of Arabidopsis SUN proteins during mitosis and their involvement in nuclear shaping. Plant J. 66: 629–641.

Oliver C, Sánchez P, Valenzuela K, Hernández M, Pontigo JP, Rauch MC, Garduño RA, Avendaño-Herrera R, Yáñez AJ. 2020. Subcellular Location of Piscirickettsia salmonis Heat Shock Protein 60 (Hsp60) Chaperone by Using Immunogold Labeling and Proteomic Analysis. Microorg. 8.

Onischenko EA, Crafoord E, Hallberg E. 2007. Phosphomimetic mutation of the mitotically phosphorylated serine 1880 compromises the interaction of the transmembrane nucleoporin gp210 with the nuclear pore complex. Exp. Cell Res. 313: 2744–2751.

Osterrieder A, Carvalho CM, Latijnhouwers M, Johansen JN, Stubbs C, Botchway S, Hawes C. 2009. Fluorescence Lifetime Imaging of Interactions between Golgi Tethering Factors and Small GTPases in Plants. Traffic 10: 1034–1046.

Östlund C, Folker ES, Choi JC, Gomes ER, Gundersen GG, Worman HJ. 2009. Dynamics and molecular interactions of linker of nucleoskeleton and cytoskeleton (LINC) complex proteins. J. Cell Sci. 122: 4099 LP – 4108.

Pain C, Kriechbaumer V, Kittelmann M, Hawes C, Fricker M. 2019. Quantitative analysis of plant ER architecture and dynamics. Nat. Commun. 10: 984.

Park J, Kim Y-S, Kim S-G, Jung J-H, Woo J-C, Park C-M. 2011. Integration of auxin and salt signals by the NAC transcription factor NTM2 during seed germination in Arabidopsis. Plant Physiol. 156: 537–549.

Pawar V, Poulet A, Détourné G, Tatout C, Vanrobays E, Evans DE, Graumann K. 2016. A novel family of plant nuclear envelope-associated proteins. J. Exp. Bot. 67: 5699–5710.

Peddie CJ, Domart M-C, Snetkov X, O'Toole P, Larijani B, Way M, Cox S, Collinson LM. 2017. Correlative super-resolution fluorescence and electron microscopy using conventional fluorescent proteins in vacuo. J. Struct. Biol. 199: 120–131.

Peiter E, Sun J, Heckmann AB, Venkateshwaran M, Riely BK, Otegui MS, Edwards A, Freshour G, Hahn MG, Cook DR, Sanders D, Oldroyd GED, Downie JA, Ané J-M. 2007. The Medicago truncatula DMI1 Protein Modulates Cytosolic Calcium Signaling. Plant Physiol. 145: 192 LP – 203.

Poulet A, Probst A V., Graumann K, Tatout C, Evans D. 2017. Exploring the evolution of the proteins of the plant nuclear envelope. Nucleus 8: 46–59.

Ramsay NA, Glover BJ. 2005. MYB–bHLH–WD40 protein complex and the evolution of cellular diversity. Trends Plant Sci. 10: 63–70.

Razafsky D, Wirtz D, Hodzic D. 2014. Nuclear envelope in nuclear positioning and cell migration. Adv. Exp. Med. Biol. 773: 471–90.

Reddy KL, Zullo JM, Bertolino E, Singh H. 2008. Transcriptional repression mediated by repositioning of genes to the nuclear lamina. Nature 452: 243–247.

Redmond JW, Batley M, Djordjevic MA, Innes RW, Kuempel PL, Rolfe BG. 1986. Flavones induce expression of nodulation genes in Rhizobium. Nature 323: 632–635.

Relić B, Perret X, Estrada-García MT, Kopcinska J, Golinowski W, Krishnan HB, Pueppke SG, Broughton WJ. 1994. Nod factors of Rhizobium are a key to the legume door. Mol. Microbiol. 13: 171–179.

Riely BK, Lougnon G, Ané J-M, Cook DR. 2007. The symbiotic ion channel homolog DMI1 is localized in the nuclear membrane of Medicago truncatula roots. Plant J. 49: 208–216.

Rolls MM, Hall DH, Victor M, Stelzer EHK, Rapoport TA. 2002. Targeting of rough endoplasmic reticulum membrane proteins and ribosomes in invertebrate neurons. Mol. Biol. Cell 13: 1778–1791.

Rout MP, Aitchison JD, Suprapto A, Hjertaas K, Zhao Y, Chait BT. 2000. The yeast nuclear pore complex: Composition, architecture, transport mechanism. J. Cell Biol. 148: 635–651.

Roux KJ, Crisp ML, Liu Q, Kim D, Kozlov S, Stewart CL, Burke B. 2009. Nesprin 4 is an outer nuclear membrane protein that can induce kinesin-mediated cell polarization. Proc. Natl. Acad. Sci. 106: 2194 LP – 2199.

Sakamoto Y, Takagi S. 2013. LITTLE NUCLEI 1 and 4 Regulate Nuclear Morphology in Arabidopsis thaliana. Plant Cell Physiol. 54: 622–633.

Sanchez WY, Prow TW, Sanchez WH, Grice J, Roberts MS. 2010. Analysis of the metabolic deterioration of ex vivo skin from ischemic necrosis through the imaging of intracellular NAD(P)H by multiphoton tomography and fluorescence lifetime imaging microscopy. J. Biomed. Opt. 15: 1–11.

Santana I, Wu H, Hu P, Giraldo JP. 2020. Targeted delivery of nanomaterials with chemical cargoes in plants enabled by a biorecognition motif. Nat. Commun. 11: 2045.

Schneider M, Lu W, Neumann S, Brachner A, Gotzmann J, Noegel AA, Karakesisoglou I. 2011. Molecular mechanisms of centrosome and cytoskeleton anchorage at the nuclear envelope. Cell. Mol. Life Sci. 68: 1593–1610.

Schoberer J, Botchway SW. 2014. Investigating Protein–Protein Interactions in the Plant Endomembrane System Using Multiphoton-Induced FRET-FLIM BT - Plant Endosomes: Methods and Protocols. In: Otegui MS, editor. New York, NY: Springer New York, p 81–95.

Schwartz TU. 2016. The Structure Inventory of the Nuclear Pore Complex. J. Mol. Biol. 428: 1986–2000.

Seltzer V, Janski N, Canaday J, Herzog E, Erhardt M, Evrard J-L, Schmit A-C. 2007. Arabidopsis GCP2 and GCP3 are part of a soluble γ-tubulin complex and have nuclear envelope targeting domains. Plant J. 52: 322–331.

Shao X, Tarnasky HA, Lee JP, Oko R, van der Hoorn FA. 1999. Spag4, a Novel Sperm Protein, Binds Outer Dense-Fiber Protein Odf1 and Localizes to Microtubules of Manchette and Axoneme. Dev. Biol. 211: 109–123.

Shimada N, Inouye K, Sawai S, Kawata T. 2010. SunB, a novel Sad1 and UNC-84 domain-containing protein required for development of Dictyostelium discoideum. Dev. Growth Differ. 52: 577–590.

Shimamura M, Brown RC, Lemmon BE, Akashi T, Mizuno K, Nishihara N, Tomizawa K-I, Yoshimoto K, Deguchi H, Hosoya H, Horio T, Mineyuki Y. 2004. γ-Tubulin in Basal Land Plants: Characterization, Localization, and Implication in the Evolution of Acentriolar Microtubule Organizing Centers. Plant Cell 16: 45 LP – 59.

Šimková E, Staněk D. 2012. Probing Nucleic Acid Interactions and Pre-mRNA Splicing by Förster Resonance Energy Transfer (FRET) Microscopy. Int. J. Mol. Sci. 13.

Slabaugh, E. (2011) PhD thesis: CHARACTERIZATION OF A PLANT-SPECIFIC MEMBRANE-TETHERED MYB TRANSCRIPTION FACTOR IN ARABIDOPSIS THALIANA. Michigan State University.

Slabaugh E, Held M, Brandizzi F. 2011. Control of root hair development in Arabidopsis thaliana by an endoplasmic reticulum anchored member of the R2R3-MYB transcription factor family.

Snel B, Lehmann G, Bork P, Huynen MA. 2000. STRING: a web-server to retrieve and display the repeatedly occurring neighbourhood of a gene. Nucleic Acids Res. 28: 3442–3444.

Sohaskey ML, Jiang Y, Zhao JJ, Mohr A, Roemer F, Harland RM. 2010. Osteopotentia regulates osteoblast maturation, bone formation, and skeletal integrity in mice. J. Cell Biol. 189: 511–25.

Solovei I, Wang AS, Thanisch K, Schmidt CS, Krebs S, Zwerger M, Cohen T V., Devys D, Foisner R, Peichl L, Herrmann H, Blum H, Engelkamp D, Stewart CL, Leonhardt H, Joffe B. 2013. LBR and Lamin A/C sequentially tether peripheral heterochromatin and inversely regulate differentiation. Cell 152: 584–598.

Song S, Qi T, Huang H, Ren Q, Wu D, Chang C, Peng W, Liu Y, Peng J, Xie D. 2011. The Jasmonate-ZIM Domain Proteins Interact with the R2R3-MYB Transcription Factors MYB21 and MYB24 to Affect

Jasmonate-Regulated Stamen Development in Arabidopsis Plant Cell 23: 1000 LP – 1013.

Sosa BA, Rothballer A, Kutay U, Schwartz TU. 2012. LINC complexes form by binding of three KASH peptides to domain interfaces of trimeric SUN proteins. Cell 149: 1035–1047.

Sparkes I, Tolley N, Aller I, Svozil J, Osterrieder A, Botchway S, Mueller C, Frigerio L, Hawes C. 2010. Five Arabidopsis Reticulon Isoforms Share Endoplasmic Reticulum Location, Topology, and Membrane-Shaping Properties. Plant Cell 22: 1333 LP – 1343.

Srivastava R, Li Z, Russo G, Tang J, Bi R, Muppirala U, Chudalayandi S, Severin A, He M, Vaitkevicius SI, Lawrence-Dill CJ, Liu P, Stapleton AE, Bassham DC, Brandizzi F, Howell SH. 2018. Response to Persistent ER Stress in Plants: A Multiphasic Process That Transitions Cells from Prosurvival Activities to Cell Death. Plant Cell 30: 1220 LP – 1242.

Staehelin LA. 1997. The plant ER: a dynamic organelle composed of a large number of discrete functional domains. Plant J. 11: 1151–1165.

Stagljar I, Korostensky C, Johnsson N, te Heesen S. 1998. A genetic system based on split-ubiquitin for the analysis of interactions between membrane proteins in vivo. Proc. Natl. Acad. Sci. U. S. A. 95: 5187–5192.

Starr DA, Han M. 2002. Role of ANC-1 in tethering nuclei to the actin cytoskeleton. Science 298: 406–9.

Starr DA, Hermann GJ, Malone CJ, Fixsen W, Priess JR, Horvitz HR, Han M. 2001. unc-83 encodes a novel component of the nuclear envelope and is essential for proper nuclear migration. Development 128: 5039 LP – 5050.

Stewart-Hutchinson PJ, Hale CM, Wirtz D, Hodzic D. 2008. Structural requirements for the assembly of LINC complexes and their function in cellular mechanical stiffness. Exp. Cell Res. 314: 1892–1905.

Stracke R, Werber M, Weisshaar B. 2001. The R2R3-MYB gene family in Arabidopsis thaliana. Curr. Opin. Plant Biol. 4: 447–456.

Strambio-De-Castillia C, Niepel M, Rout MP. 2010. The nuclear pore complex: bridging nuclear transport and gene regulation. Nat. Rev. Mol. Cell Biol. 11: 490–501.

Stricker SA, Centonze VE, Paddock SW, Schatten G. 1992. Confocal microscopy of fertilization-induced calcium dynamics in sea urchin eggs. Dev. Biol. 149: 370–380.

Stubbs CD, Botchway SW, Slater SJ, Parker AW. 2005. The use of time-resolved fluorescence imaging in the study of protein kinase C localisation in cells. BMC Cell Biol. 6: 22.

Tamura K, Fukao Y, Iwamoto M, Haraguchi T, Hara-Nishimura I. 2010. Identification and Characterization of Nuclear Pore Complex Components in Arabidopsis thaliana Plant Cell 22: 4084 LP – 4097.

Tamura K, Iwabuchi K, Fukao Y, Kondo M, Okamoto K, Ueda H, Nishimura M, Hara-Nishimura I. 2013. Myosin XI-i links the nuclear membrane to the cytoskeleton to control nuclear movement and shape in Arabidopsis. Curr. Biol. 23: 1776–1781.

Tan BL, Sarafis V, Beattie GAC, White R, Darley EM, Spooner-Hart R. 2005. Localization and movement of mineral oil in plants by fluorescence and confocal microscopy. J. Exp. Bot. 56: 2755–2763.

Tang Y, Huang A, Gu Y. 2020. Global profiling of plant nuclear membrane proteome in Arabidopsis. Nat. Plants 6: 838–847.

Terry LJ, Shows EB, Wente SR. 2007. Crossing the Nuclear Envelope: Hierarchical Regulation of Nucleocytoplasmic Transport. Science (80-.). 318: 1412 LP – 1416.

Thakar K, May CK, Rogers A, Carroll CW. 2017. Opposing roles for distinct LINC complexes in regulation of the small GTPase RhoA. Mol. Biol. Cell 28: 182–191.

Truebestein L, Leonard TA. 2016. Coiled-coils: The long and short of it. BioEssays 38: 903–916.

Tuijtel MW, Koster AJ, Jakobs S, Faas FGA, Sharp TH. 2019. Correlative cryo super-resolution light and electron microscopy on mammalian cells using fluorescent proteins. Sci. Rep. 9: 1369.

Tulgren ED, Turgeon SM, Opperman KJ, Grill B. 2014. The Nesprin Family Member ANC-1 Regulates Synapse Formation and Axon Termination by Functioning in a Pathway with RPM-1 and β-Catenin. PLOS Genet. 10: e1004481.

Tzur YB, Wilson KL, Gruenbaum Y. 2006. SUN-domain proteins: “Velcro” that links the nucleoskeleton to the cytoskeleton. Nat. Rev. Mol. Cell Biol. 7: 782–788.

Valente MAS, Faria JAQA, Soares-Ramos JRL, Reis PAB, Pinheiro GL, Piovesan ND, Morais AT, Menezes CC, Cano MAO, Fietto LG, Loureiro ME, Aragão FJL, Fontes EPB. 2009. The ER luminal binding protein (BiP) mediates an increase in drought tolerance in soybean and delays drought-induced leaf senescence in soybean and tobacco. J. Exp. Bot. 60: 533–546.

Varas J, Graumann K, Osman K, Pradillo M, Evans DE, Santos JL, Armstrong SJ. 2015. Absence of SUN1 and SUN2 proteins in Arabidopsis thaliana leads to a delay in meiotic progression and defects in synapsis and recombination. Plant J. 81: 329–346.

Vasnier C, de Muyt A, Zhang L, Tessé S, Kleckner NE, Zickler D, Espagne E. 2014. Absence of SUN-domain protein Slp1 blocks karyogamy and switches meiotic recombination and synapsis from homologs to sister chromatids. Proc. Natl. Acad. Sci. 111: E4015 LP-E4023.

Venditti R, Rega LR, Masone MC, Santoro M, Polishchuk E, Sarnataro D, Paladino S, D’Auria S, Varriale A, Olkkonen VM, Di Tullio G, Polishchuk R, De Matteis MA. 2019. Molecular determinants of ER–Golgi contacts identified through a new FRET–FLIM system. J. Cell Biol. 218: 1055–1065.

Versari C, Stoma S, Batmanov K, Llamosi A, Mroz F, Kaczmarek A, Deyell M, Lhoussaine C, Hersen P, Batt G. 2017. Long-term tracking of budding yeast cells in brightfield microscopy: CellStar and the Evaluation Platform. J. R. Soc. Interface 14: 20160705.

Vladar EK, Antic D, Axelrod JD. 2009. Planar cell polarity signaling: the developing cell's compass. Cold Spring Harb. Perspect. Biol. 1: a002964.

Voeltz GK, Rolls MM, Rapoport TA. 2002. Structural organization of the endoplasmic reticulum. EMBO Rep. 3: 944–950.

Wandke C, Kutay U. 2013. Enclosing chromatin: Reassembly of the nucleus after open mitosis. Cell 152: 1222–1225.

Wang H, Dittmer TA, Richards EJ. 2013. Arabidopsis CROWDED NUCLEI (CRWN) proteins are required for nuclear size control and heterochromatin organization. BMC Plant Biol. 13: 200.

Wang Y, Zhang X, Zhang H, Lu Y, Huang H, Dong X, Chen J, Dong J, Yang X, Hang H, Jiang T. 2012. Coiled-coil networking shapes cell molecular machinery. Mol. Biol. Cell 23: 3911–3922.

WATSON ML. 1955. The nuclear envelope; its structure and relation to cytoplasmic membranes. J. Biophys. Biochem. Cytol. 1: 257–270.

Webster M, Witkin KL, Cohen-Fix O. 2009. Sizing up the nucleus: nuclear shape, size and nuclear-envelope assembly. J. Cell Sci. 122: 1477 LP – 1486.

Weems JC, Slaughter BD, Unruh JR, Boeing S, Hall SM, Mclaird MB, Yasukawa T, Aso T, Svejstrup JQ, Conaway XJW, Conaway RC. 2017. Cockayne syndrome B protein regulates recruitment of the Elongin A ubiquitin ligase to sites of DNA damage. 292: 6431–6437.

West JA, Mito M, Kurosaka S, Takumi T, Tanegashima C, Chujo T, Yanaka K, Kingston RE, Hirose T, Bond C, Fox A, Nakagawa S. 2016. Structural, super-resolution microscopy analysis of paraspeckle nuclear body organization. J. Cell Biol. 214: 817–830.

Wiese AJ, Steinbachová L, Timofejeva L, Čermák V, Klodová B, Ganji RS, Limones-Mendez M, Bokvaj P, Hafidh S, Potěšil D, Honys D. 2021. Arabidopsis bZIP18 and bZIP52 Accumulate in Nuclei Following Heat Stress where They Regulate the Expression of a Similar Set of Genes. Int. J. Mol. Sci. 22.

Wilhelmsen K, Litjens SHM, Kuikman I, Tshimbalanga N, Janssen H, van den Bout I, Raymond K, Sonnenberg A. 2005. Nesprin-3, a novel outer nuclear membrane protein, associates with the cytoskeletal linker protein plectin . J. Cell Biol. 171: 799–810.

Wimmers LE, Ewing NN, Bennett AB. 1992. Higher plant Ca(2+)-ATPase: primary structure and regulation of mRNA abundance by salt. Proc. Natl. Acad. Sci. 89: 9205 LP – 9209.

Wong X, Luperchio TR, Reddy KL. 2014. NET gains and losses: the role of changing nuclear envelope proteomes in genome regulation. Curr. Opin. Cell Biol. 28: 105–120.

Wyatt SE, Tsou P-L, Robertson D. 2002. Expression of the high capacity calcium-binding domain of calreticulin increases bioavailable calcium stores in plants. Transgenic Res. 11: 1–10.

Xu XM, Meulia T, Meier I. 2007. Anchorage of plant RanGAP to the nuclear envelope involves novel nuclear-pore-sssociated proteins. Curr. Biol. 17: 1157–1163.

Yang J, Chang Y, Qin Y, Chen D, Zhu T, Peng K, Wang H, Tang N, Li X, Wang Y, Liu Y, Li X, Xie W, Xiong L. 2020. A lamin-like protein OsNMCP1 regulates drought resistance and root growth through chromatin accessibility modulation by interacting with a chromatin remodeller OsSWI3C in rice. New Phytol. 227: 65–83.

Yu J, Lei K, Zhou M, Craft CM, Xu G, Xu T, Zhuang Y, Xu R, Han M. 2011. KASH protein Syne-2/Nesprin-2 and SUN proteins SUN1/2 mediate nuclear migration during mammalian retinal development. Hum. Mol. Genet. 20: 1061–1073.

Yuan L, Pan J, Zhu S, Li Y, Yao J, Li Q, Fang S, Liu C, Wang X, Li B, Chen W, Zhang Y. 2021. Evolution and Functional Divergence of SUN Genes in Plants. Front. Plant Sci. 12: 646622.

Zeitler B, Weis K. 2004. The FG-repeat asymmetry of the nuclear pore complex is dispensable for bulk nucleocytoplasmic transport in vivo . J. Cell Biol. 167: 583–590.

Zhang F, Ma L, Zhang C, Du G, Shen Y, Tang D, Li Y, Yu H, Ma B, Cheng Z. 2020. The SUN Domain Proteins OsSUN1 and OsSUN2 Play Critical but Partially Redundant Roles in Meiosis. Plant Physiol. 183: 1517 LP – 1530.

Zhang Q, Skepper JN, Yang F, Davies JD, Hegyi L, Roberts RG, Weissberg PL, Ellis JA, Shanahan CM. 2001. Nesprins: a novel family of spectrin-repeat-containing proteins that localize to the nuclear membrane in multiple tissues. J. Cell Sci. 114: 4485 LP – 4498.

Zhang Q, Wang F, Zhang H, Zhang Y, Liu M, Liu Y. 2018. Universal Ti3C2 MXenes Based Self-Standard Ratiometric Fluorescence Resonance Energy Transfer Platform for Highly Sensitive Detection of Exosomes. Anal. Chem. 90: 12737–12744.

Zhang S, Xu C, Larrimore KE, Ng DTW. 2017. Slp1-Emp65: a guardian factor that protects folding polypeptides from promiscuous degradation. Cell 171: 346-357.e12.

Zhang X, Lei K, Yuan X, Wu X, Zhuang Y, Xu T, Xu R, Han M. 2009. SUN1/2 and Syne/Nesprin-1/2 Complexes Connect Centrosome to the Nucleus during Neurogenesis and Neuronal Migration in Mice. Neuron 64: 173–187.

Zhen Y-Y, Libotte T, Munck M, Noegel AA, Korenbaum E. 2002. NUANCE, a giant protein connecting the nucleus and actin cytoskeleton. J. Cell Sci. 115: 3207 LP – 3222.

Zhou X, Graumann K, Evans DE, Meier I. 2012. Novel plant SUN-KASH bridges are involved in RanGAP anchoring and nuclear shape determination. J. Cell Biol. 196: 203–11.

Zhou X, Graumann K, Meier I. 2015. The plant nuclear envelope as a multifunctional platform LINCed by SUN and KASH. J. Exp. Bot. 66: 1649–1659.

Zhou X, Graumann K, Wirthmueller L, Jones JDG, Meier I. 2014. Identification of unique SUN-interacting nuclear envelope proteins with diverse functions in plants. J. Cell Biol. 205: 677–92.

Zhou X, Meier I. 2013. How plants LINC the SUN to KASH. Nucleus 4: 206–215.

Zuleger N, Boyle S, Kelly DA, de las Heras JI, Lazou V, Korfali N, Batrakou DG, Randles KN, Morris GE, Harrison DJ, Bickmore WA, Schirmer EC. 2013. Specific nuclear envelope transmembrane proteins can promote the location of chromosomes to and from the nuclear periphery. Genome Biol. 14: R14.

Appendices

Appendix 1. List of transformed plasmids generated

Plasmid Name	Selection antibiotic	Constructed by
pDONR221-SUN3	Kanamycin	Bisa Andov
pDONR221-SUN4	Kanamycin	Bisa Andov
pDONR207-SUN3 del. Nter	Gentamicin	Sarah Mermet
pDONR207-SUN3 del. SUN	Gentamicin	Sarah Mermet
pDONR207-SUN3 del. CC	Gentamicin	Sarah Mermet

Appendix 2. Table of primers used to generate constructs used

Name of Primer	Direction	Description	DNA sequence (aa)
KSF2	Forward	binds to first 20bp of *At*SUN4	ATGCAAAGATCACGGAGAGC
BA1	Reverse	binds to the last 26bp of *At*SUN4 minus STOP codon	aagtgacaaaatgaacataacgaatg
BA2	forward	binds to bp 61-82 of *At*SUN4 (for N-terminal deletion)	Ggaaggaatcgcttctacaaag
BA3	forward	same as BA2 with TOPO-cloning sequence (for N-terminal deletion)	caccGgaaggaatcgcttctacaaag
BA4	reverse	binds bp 514-534 of *At*SUN4 (for larger SUN domain deletion)	cgctctgctcttgaactcatc

BA5	Forward	binds bp 1030 - 1048 of *At*SUN4 (for larger SUN domain deletion)	gtggagcgaatgctggagg
BA6	reverse	overlapping primer binds bp 514 -534 to bp1030 - 1048 (for larger SUN domain deletion)	cctccagcattcgctccaccgctctgctcttgaactcatc
BA7	forward	overlapping primer binds bp 1030 - 1048 to bp 514 - 534 (for larger SUN domain deletion)	gatgagttcaagagcagagcggtggagcgaatgctggagg
BA8	reverse	binds bp 634-654 of *At*SUN4 (for putative shortened SUN domain deletion)	gataagacctttgcacctttg
BA9	reverse	binds bp 1383 - 1408 of *At*SUN4 (for CC domain deletion)	ccttgaatatcatcccgtatttcaag
BA10	forward	binds bp 1636 - 1658 of *At*SUN4 (for CC domain deletion)	gtggttgtgttcacaatctgtg
BA11	reverse	overlapping primer binds bp 1383 - 1408 to bp 1636 - 1658 (for CC domain deletion)	cacagattgtgaacacaaccacccttgaatatcatcccgtatttcaag
BA12	forward	overlapping primer binds bp 1636 - 1658 to	cttgaaatacgggatgatattcaagggtggttgtgttcacaatctgtg

		bp1383 - 1408 (for CC domain deletion)	
BA13	reverse	overlapping primer binds bp643 - 654 to bp1030 - 1048 of *At*SUN4 (for putative shortened SUN domain deletion)	cctccagcattcgctccacgataagacctttgcacctttg
BA14	forward	overlapping primer binds bp1030 - 1048 to bp643 - 654 of *At*SUN4 (for putative shortened SUN domain deletion)	caaaaggtgcaaaggtcttatcgtggagcgaatgctggagg
BA15	forward	same as KSF2 with TOPO-cloning sequence	CACC ATG
BA16	Forward	Gateway primer for *At*SUN4, and is the same as KSF2 with attB1 sequence	GGGGACAAGTTTGTACAAAAAAGCAGGCTTCCCGCCA CAA AGA TCA CGG AGA GC
BA17	Forward	Gateway primer for *At*SUN4, and is the same as BA2 with attB1 sequence	GGGGACAAGTTTGTACAAAAAAGCAGGCTTCCCGCCA Ggaaggaatcgcttctacaaag
BA18	Reverse	Gateway primer for *At*SUN4, has attB2 sequence and binds to the last 26bp of SUN4 minus STOP codon	GGGGACCACTTTGTACAAGAAAGCTGGGTCaagtgaca aaatgaacataacgaatg
SM1	forward	22 bp binds to bp 64-88 of	ttttacaaagtctctttgtctc

		*At*SUN3 (Nter deletion)	
SM2	reverse	21 bp binds to bp 691 - 711 of *At*SUN3 (for SUN domain deletion)	cgctctgctcttgaactcatc
SM3	Forward	19 bp binds to bp 1207 - 1225 of *At*SUN3 (for SUN domain deletion)	gtagaacgaatgctggagg
SM4	reverse	21bp binds to bp 1498 - 1518 of *At*SUN3 (for CC deletion)	cttctgcatcagtatcttcag
SM5	forward	24 bp binds to bp 1831 - 1854 of *At*SUN3 (for CC deletion)	acggttttcaccgtatgtctaggg
SM6	reverse	overlapping primer binds to bp 691 - 711 to 1207 - 1226 for SUN domain deletion	tcctccagcattcgttctac cgctctgctcttgaactcatc
SM7	forward	overlapping primer binds to bp 692 - 711 to 1207 - 1225 for SUN domain deletion	atgagttcaagagcagagcg gtagaacgaatgctggagg
SM8	reverse	overlapping primer binds to bp 1498 - 1518 to 1831 - 1850 for CC deletion	agacatacggtgaaaaccgt cttctgcatcagtatcttcag
SM9	forward	overlapping primer binds to bp 1499 - 1518 to 1831 - 1854 for CC deletion	tgaagatactgatgcagaag acggttttcaccgtatgtctaggg
SM1GW	forward	gateway primers for *At*SUN3	ggggacaagtttgtacaaaaaagcaggcttcccgcca ttttacaaagtctctttgtctc

		deleted of N terminal same sequence of SM1 with additional attB1 sequence	

Appendix 3. Donor and Expression Vector maps

i) pDONR221

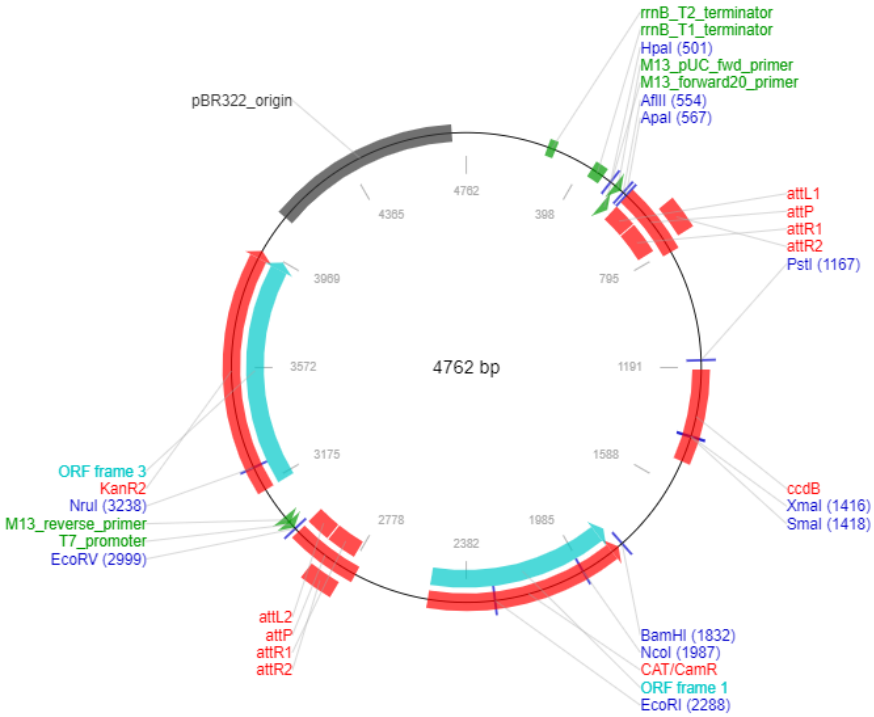

ii) pDONR207

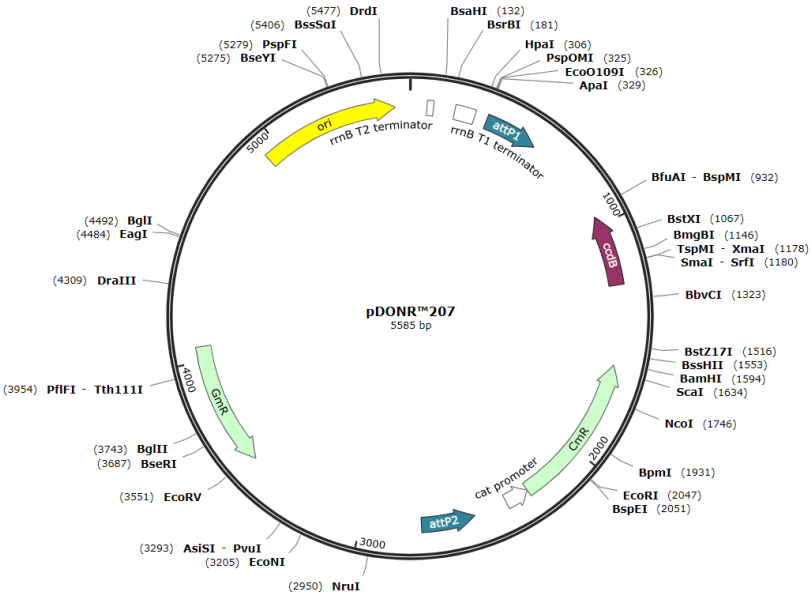

iii) pK7WGR2 – N-terminal RFP

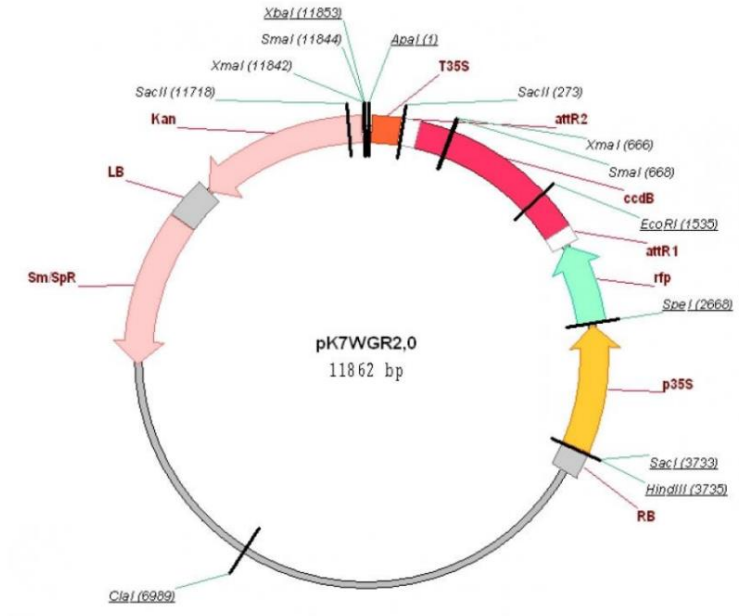

IV) pK7RWG2 – C-terminal RFP

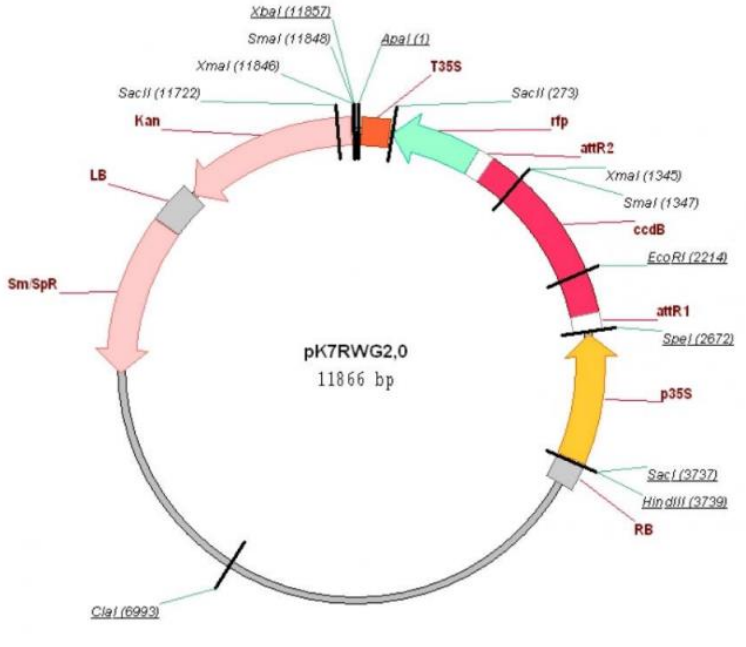

V) pCambia1300- Binary Vector to produce YFP-tagged proteins (N- and C-terminal)

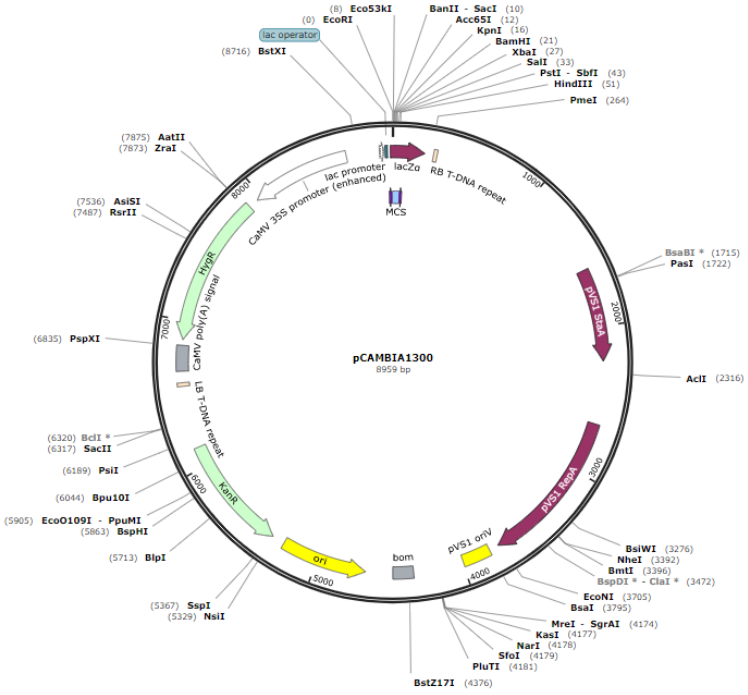

Vi) pK7CWG2 – C-terminal CFP

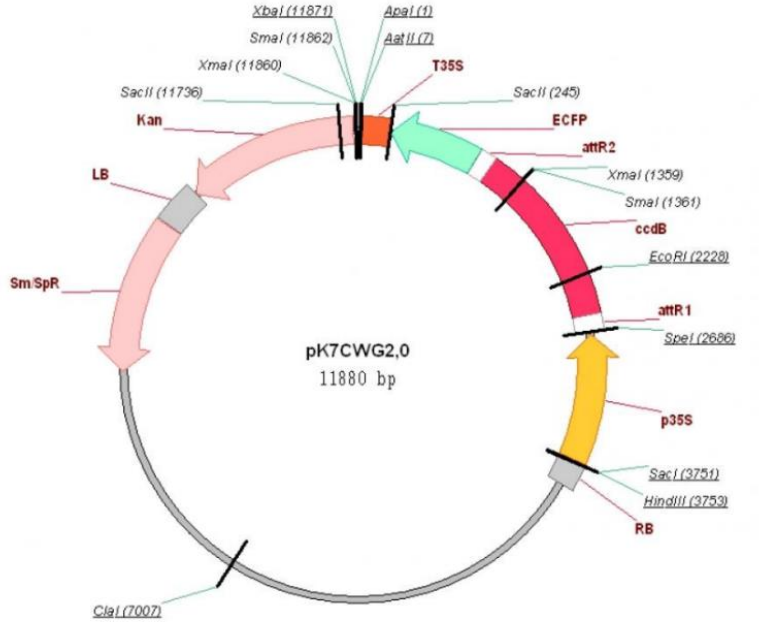

Vii) pB7WGC2 - N-terminal CFP

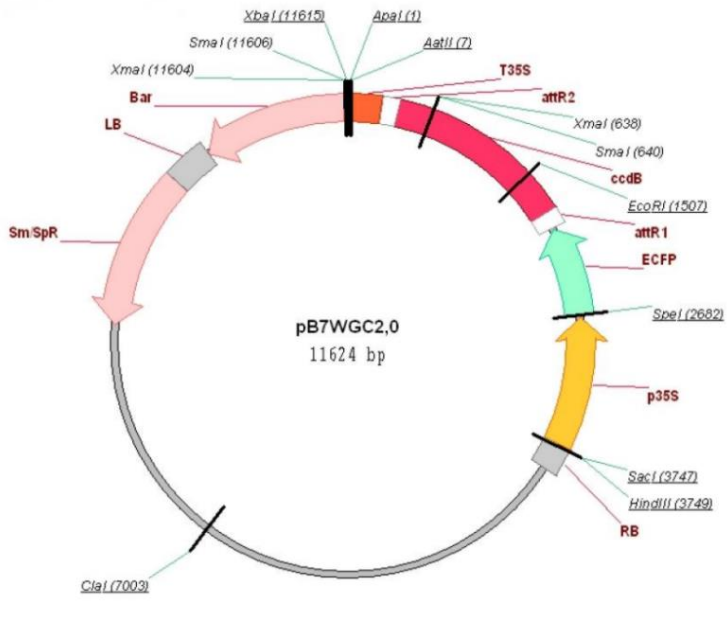

Viii) pB7FWG2 - C-terminal GFP

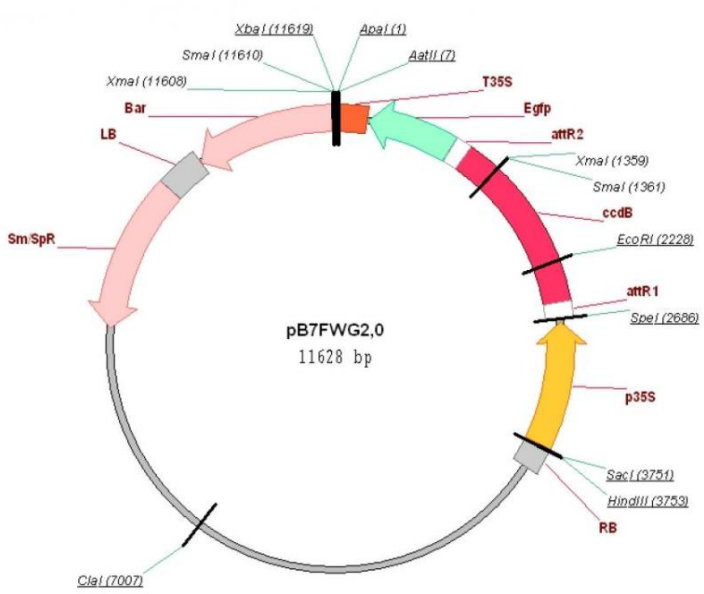

ix) PB7WGF2 - N-terminal GFP

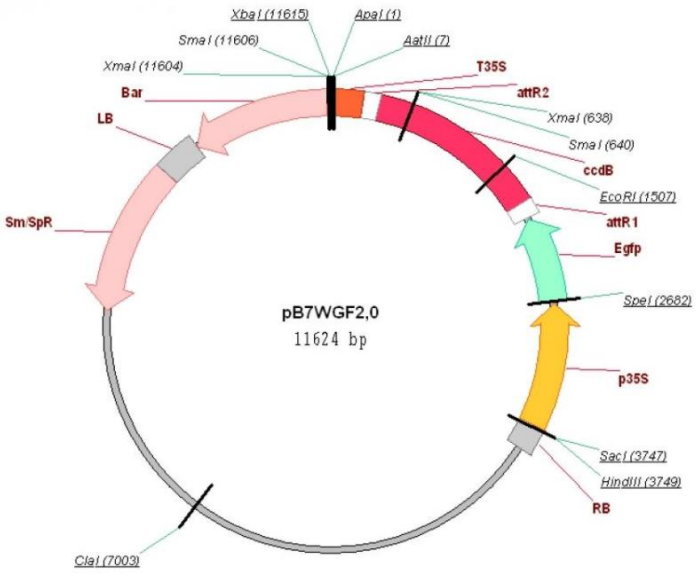

Appendix 4. Maximum integrated average of FI per protein measured is displayed as a line profile. This distribution provides information as to how the nucleus was orientated throughout the Z-stack and supports the idea that the Z-plane selected for analysis is extremely important.

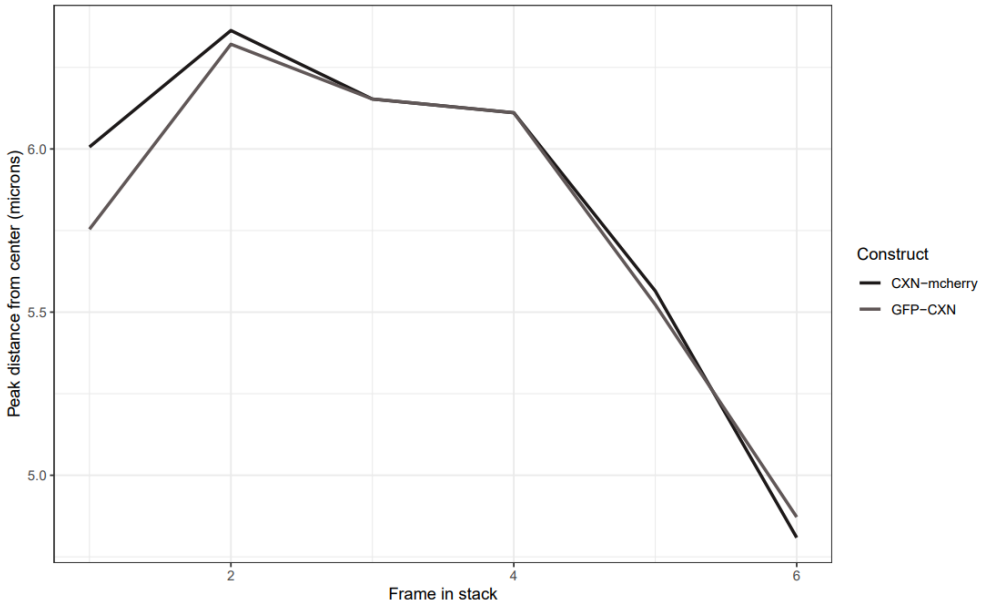

Appendix 5. Intensity profiles shows how fluorescence is distributed along the line profiles measured for each protein, with maximum FI displayed a peak. These are used to determine sample quality and calculate EMD values.

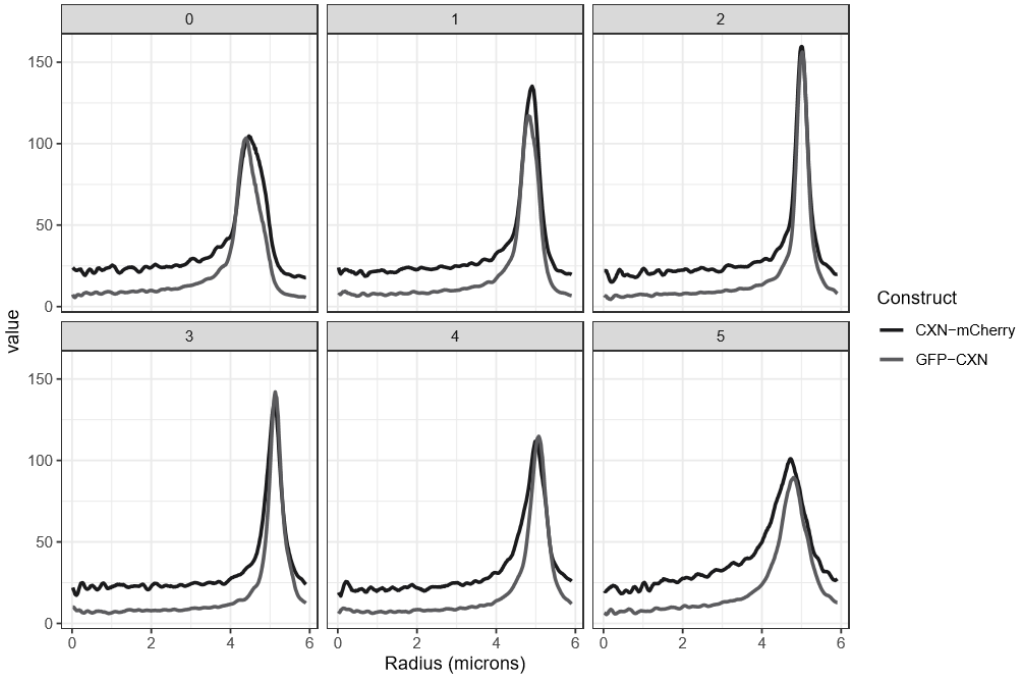

Appendix 6. Histogram displaying the distribution of EMD values for each protein combination analysed. The distribution of data for each protein combination was a factor in deciding which are suitable for use in resolving protein localisation at the NE. For example, the *At*SUN2-CFP + GFP-CXN dataset is much broader than the rest, indicating that it is irregular.